Hypothalamic Neuron Circuits Underlying Interplay Between Biological Clock and Metabolism

Qijun Tang

Chuxiong, Yunnan, China

B.S., Fuday University, Shanghai, China, 2016

A Dissertation presented to the Graduate Faculty of the University of Virginia in Candidacy for the Degree of Doctor of Philosophy

Department of Biology

University of Virginia

December 2022

Committee Members:
Ali Güler
Ignacio Provencio
Jay Hirsh
Jianhua Cang
Christopher Deppmann

Abstract

Generally all creatures on this planet attain a circadian system, which impacts almost all aspects of living by regulating daily rhythmic physical processes and behaviors. In mammals, the central pacemaker, suprachiasmatic nucleus (SCN), is located in the hypothalamus, right above optic chiasm. Receiving light information from the environment from the retina, SCN synchronizes the circadian rhythms of the entire body in coordination to the sunrise and sunset cycle, to maximize survival. While light entrained circadian clocks regulate daily behavioral patterns of feeding, availability of food is also an important salient environmental cue that is able to alter the circadian machinery. However, less is known about the mechanism of how food alters the biological clock. In this dissertation, using mouse (*mus musculus*) as model organism, with a focus in the hypothalamus, we investigated the mechanisms of the interplay between biological clock and metabolism. We demonstrated that dopamine signaling in the SCN enables energy-dense food induced alteration of the daily eating pattern and consequential obesity. We also identified a leptin responsive neuron circuit from dorsal medial hypothalamus (DMH) to the SCN that behaves as an integration hub for food to entrain the circadian system.

Table of contents

Chapter 1 Introduction

The contents and ideas in this chapter were partially published in July, 2022, on *Frontiers in Integrative Neuroscience*. DOI: 10.3389/fnint.2022.957193. [1].

c1.1 Circadian system

c1.1.1 Molecular circadian oscillators

The revolution of Earth on its axis generates the daily light-dark (LD) cycle. Basically all the life forms take advantage of this temporal niche and have evolved internal timekeeping systems, and hence fine-tune their physiological responses across different time of day to ensure optimal survival. This internal timekeeping system is named circadian system, in which the term “circadian” derives from the Latin phrase “circa diem,” which means “about a day”.

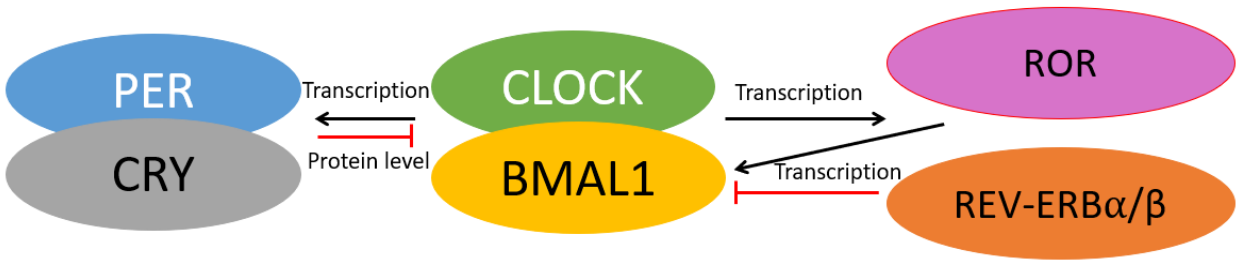

Figure 1. Simplified schematic illustrating the molecular transcription-translation feedback loop (TTFL) governing the circadian system.

It was initially revealed in flies and plants that there is a molecular transcription-translation feedback loop (TTFL) governing the organismal circadian clock to coordinate behavior and metabolism according to the daily light-dark cycle (Figure 1) [2–4]. The conservation of this internal clock mechanism extends to mammals [4–7]. In

mammals, the core circadian proteins are CLOCK and BMAL1, which form a dimer and trigger the transcription and translation of repressor proteins PER (-1,-2, and -3) and CRY (-1 and -2). PER and CRY will then dimerize and interact with CLOCK-BMAL1 to suppress their own expression. In addition to the loop through PERs and CRYs, CLOCK-BMAL1 also induces the expression of ROR and REV-ERBα/β. ROR enhances the expression of *Bmal1* gene, whereas REV-ERBα/β compete with ROR to suppress the expression of *Bmal1* (Figure 1) [8]. Together, the repression loops among these core circadian proteins generate a rhythmic pattern of the expression of these proteins with a period of about 24 hours. In addition to generating the circadian expression of themselves, these core circadian proteins are all transcriptional factors and can modulate the expression of various genes in a circadian mannar, hence relay rhythmic outputs [8–11].

c1.1.2 SCN is the master synchronizer coordinating body rhythm with environmental cues

Notably, the circadian oscillators are widely expressed in most, if not all, cells, and are cell-autonomous in a period of approximately 24 hours in the absence of external time cues [6]. In mammals, a brain area in the hypothalamus, suprachiasmatic nucleus (SCN) is known to be the central synchronizer that receives circadian timing cues from environment and coordinates the clock of the whole body, and then coordinates a variety of physiological, psychological, and behavioral processes [12–14]. Lesion and transplant studies have demonstrated that the SCN is the principal regulator of all light entrained rhythms [12,15–18], but there are some exceptions such as photoreceptors in

skin cells that can drive local circadian rhythms in subpopulations of tissues [19]. Remarkably, the SCN maintains rhythmic activity even when explanted from a rodent's brain and maintained in vitro [20,21].

Light and other external factors (e.g. food availability) called "zeitgebers", or time-givers, modulate the expression of clock genes to reset and entrain the timing of the circadian clock in the SCN, other brain regions or peripheral tissues [22,23]. Interestingly, mice with SCN lesions still maintain circadian rhythms in their peripheral tissues but the rhythms between tissues are desynchronized, showing that the SCN is vital for synchronization [21]. There is emerging interest in elucidating biological clocks outside of the SCN and determining how non-photic stimuli such as exercise, mating, fear and feeding compete and collaborate with the SCN to regulate circadian cycles [24–26].

c1.1.3 Food as Zeitgeber

Several brain regions and many peripheral tissues can be entrained by daily cycles of feeding [27,28]. In rodents, this is readily demonstrated by restricting food access to the middle of the light period when nocturnal rodents normally eat little and are inactive [29]. Food restriction induces a pronounced shift of organ physiology and animal behavior to align with the new daily feeding time, while the activity of the SCN remains coupled to light cycles [30]. This is also associated with the emergence of a daily burst of motor activity that anticipates mealtime by 1-3h and an increase in core body temperature [31]. Remarkably, this "food anticipatory activity" (FAA) persists robustly after removal of

the SCN [32]. The underlying neuronal systems and/or circuitry responsible for mediating FAA have been contested, with very few studies showing reproducible effects of genetic mutations or lesions to the brain [32,33]. At present, nuclei as diverse as the cerebellum [34], hypothalamic areas including dorsomedial hypothalamus [35,36] and arcuate nucleus [37]; and striatum [38,39], have been implicated in promoting FAA. The only area of consistent agreement is that the SCN is not required for FAA [32,40–43], although it might modulate the amplitude of food rhythms in some contexts [44,45]. Since there has been so much difficulty in isolating the neural constituent(s) of FAA, it has been suggested that such a region, referred to as a food entrainable oscillator (FEO), may not exist as a singular entity; therefore lesioning studies may be too narrow of an approach, and the molecular tagging or systems based approaches may offer higher potential in locating multiple FEOs distributed across the brain and body [27,32,43,46]. The ability of rodents to have multiple bouts of FAA entrained to multiple food deliveries with same or different cycle period further provided evidence that food entrainment is regulated by a multi-core network [47].

By analogy to studies of light entrainment, researchers initially focused on using mouse mutants in known molecular components of the core clock TTFL to map the brain region(s) responsible for FAA, yet these experiments have yielded mixed results. For example, mutations of *Bmal1* and double/triple deletions of *Per* genes did not reveal effects on FAA in mice [48,49]. However, this is not to say that clock genes are completely uninvolved in food entrainment, for example, BMAL1 and CRY KO mice could be entrained to shorter feeding cycles that are outside of circadian range and can

not entrain WT animals [40]. Moreover, Mendoza and colleagues report several studies of PER and CRY mutants also had diminished/unstable FAA and desynchronized expectations of mealtimes [34]. Interestingly, mice with global and brain-specific deletion of *Nr1d1*, which encodes for REV-ERBα, an inhibitor of BMAL1 transcription, showed neither light nor food entrainment [50]. A surprising experiment demonstrated that conditional deletion of PER2 in the liver nearly abolished FAA whereas deletion of PER2 in the brain had no impact, leading the authors to conclude that the liver is the long sought after FEO [51]. Interestingly, mice with liver-specific deletion of PER2 were observed to have a reduction in enzymes associated with β-oxidation, suggesting that ketone body production was important for mediating FAA. In support of this, time-specific application of β-hydroxybutyrate in the PER2 liver conditional knockout mice rescued FAA modestly [51].

c1.2 Feeding behavior regulation

c1.2.1 Homeostatic and hedonic feeding behavior

Feeding behavior is commonly thought to be divided into two complementary and interacting types: homeostatic and non-homeostatic. The homeostatic control of feeding responds to energy needs and sustains metabolic homeostasis. The non-homeostatic aspect of feeding regulation includes cognition, pre-learned experiences and hedonic factors, and non-homeostatic drive can override the inhibitory homeostatic mechanisms that dysregulate energy balance [52].

The arcuate nucleus (ARC) in the hypothalamus is the main homeostatic feeding regulator of the brain [52,53]. There are two major populations of neurons embedded in

ARC, agouti-related peptide (AgRP) and pro-opiomelanocortin (POMC) neurons [53]. AgRP neurons express AgRP and neuropeptide-Y (NPY) and release GABA. Activation of AgRP neurons leads to increased food intake [54–57]. In contrast, POMC neurons co-express POMC with cocaine- and amphetamine-regulated transcript (CART), and release a-melanocyte stimulating hormone (a-MSH) which will reduce food intake, in contrast to AgRP [58] [59]. These two groups of neurons play an important role in sensing the internal energy states and relaying information to control food intake. For example, ghrelin, which is mainly produced by the stomach as a hunger cue [60], activates AgRP-neurons but inhibits POMC-neurons. In contrast, leptin, which is mainly produced by adipose tissue as a satiation cue [61], inhibits AgRP-neurons and activates POMC-neurons [53]. Interestingly, insulin, another satiation hormone, inhibits the activity of both types of neurons [53]. The expression level of those four hypothalamic neuropeptides (AgRP, NPY, POMC, CART) was reported to have circadian oscillation, and amplitude of the oscillation is attenuated in high-fat diet (HFD) fed mice [62].

Hedonic, or reward-based feeding, occurs when highly palatable foods are consumed even during periods of energy surplus [52,53,63]. It mainly arises from the ventral tegmental area (VTA) to the nucleus accumbens (NAc). Upon the presence of palatable food, these neurons are activated and release dopamine (DA) in proportion to the reward value of food which encodes the appropriate level of motivation for food consumption[63,64]. It has been demonstrated that elimination of AgRP neurons in the ARC causes feeding deficit and hence lethal, but the DA neurons can take over and drive the feeding behavior, which emphasizes the ability of hedonic feeding pathways to override the homeostatic pathways [65,66] . On the other hand, ARC to VTA

communication has been revealed by recent work suggesting it is a bridge between homeostatic and hedonic feeding pathways. For example, ARC POMC neurons send direct projections to the VTA and the NAc[67,68], while the activity of ARC AgRP neurons and dopaminergic VTA neurons are reciprocally regulated during feeding[69]. The activation of ARC AgRP neurons in well fed animals induces, although not direct electrophysiological change of neuron activity, acute elevation of neuron activity to food present in the VTA, akin the fasting-refeed response [45]. Delineating the homeostatic and hedonic feeding pathways and how they interact will surely randor fruitful insights for therapeutic treatment for eating behavior and metabolic disorders.

c1.2.2 Circadian regulation of feeding

Foraging and feeding is essential for all animals. The feeding behavior is under circadian regulation and shows a daily rhythmic pattern. Normally, the window of animals' food intake is in coordination with the active phase of the animals. However, when the food availability is shifted to abnormal time, animals are able to readjust their clock and show anticipatory behavior to the food access time, including increased locomotor activity prior to food, increased body temperature and plasma glucocorticoid, without changing the regular light entrained locomotor activity [22]. Additionally, the animals that are entrained to scheduled food access show higher drive to consume the food when the food is delivered (see Chapter 3), indicating that not only the locomotor behavior, but the timing control of feeding behavior itself can be entrained by scheduled food access.

To regulate the timing of the feeding behavior, the hedonic and homeostatic neuron circuits discussed above have to be tuned to function in a circadian mannar. However, the mechanisms modulating the circadian pattern of neuron activity in these circuits, hence circadian pattern of feeding behavior are investigated but yet clear. On the circuit level, the master clock SCN makes direct or indirect connections to the areas that regulate feeding behavior. For example, ARC is one of the output targets of SCN and also potentially projects back to the SCN [70,71]. Surgical elimination of the reciprocal connection between the SCN and ARC results in deficits of circadian homeostasis control [72]. On the other hand, the feeding regulating neurons expresses various receptors of feeding related hormones, of which many show rhythmic patterns. Hunger hormones such as glucocorticoids, ghrelin and glucagon secreted before meal time serve as pre-meal timer to initiate feeding, and satiation cues such as insulin and leptin can be post-feeding timers to define the offset of feeding [73]. In addition to hormonal cues, nutrients and microbiota also contribute to the circadian tuning of the feeding regulating neuron circuits[73].

In summary, the fact that feeding behavior is normally synchronized to sleep-wake cycle, and losses rhythmicity together with sleep-wake cycle in SCN lesioned animals [74], suggests the ability of the light entrained master clock on defining the timing of food intake. On the other hand, if the food is provided repetitively, SCN lesioned animals can still emerge food anticipatory activity, even when the rhythmicity of locomotor activity is generally lost [41,42]. The capability for the food anticipation to decouple from the light entrained clock indicates that there is a “food clock” system that can be isolated from the “light clock” when necessary. To better understand the regulation of the timing

of feeding behavior, the anatomical location and molecular mechanism of “food clock”, and its relationship with “light clock” remain to be further discovered.

c1.3 Dopamine system

c.1.3.1 Role of dopamine in regulation circadian rhythms

Dopamine system is known for reward processing and is required for sustained motivation and execution of goal-directed behaviors [75–77]. In addition to the important role of the dopamine system in feeding regulation (discussed in section c.1.2.1), the dopamine system was also implicated to play a significant role in the circadian system. Around 60% of SCN neurons express dopamine 1 receptor (Drd1) [78]. During the development, while the eyes of the animals are not open to be able to receive light cue from the environment, Drd1 signaling in the SCN is essential for the synchronization of SCN during development [79]. In the adult animals, an intact dopamine system is required for the speed of phase shift of the circadian entrainment [80], and a rewarding food potentially increases the speed of circadian re-entrainment to a shift of light cycle [81]. The dopamine circuit from substantia nigra (SN) to dorsal striatum, specially, Drd1 dependent signaling is necessary for proper food entrainment [39]. Besides regular scheduled food access, other “rewarding” based environmental stimuli can also entrain the circadian behavior of animals, including scheduled rewarding food or receptive mate [24,82,83]. Methamphetamine exposure studies revealed other dopamine related circadian systems described as methamphetamine-sensitive circadian oscillator (MASCO) and dopamine ultradian oscillator (DUO). These systems are able to alter or entrain the circadian behavior of animals lacking SCN or with circadian gene knockout

[84–86]. In summary, the dopamine system plays a significant role in the orchestration of circadian systems hence circadian behavior.

c.1.4 Eating disorder and obesity

In the United States, over a third of the population is obese, which is the greatest risk factor for chronic disorders such as diabetes, cardiovascular and kidney diseases[87–93]. However, on the other hand, anorexia nervosa remains the most fatal of all psychiatric diseases [94,95]. Therefore, it is necessary to investigate the mechanisms underpinning the regulation of feeding behavior and how the defects of these systems lead to disorder of food intake.

It has been growing acknowledged that not only what and how much are are eating, but also the time of eating play a critical role in the maintenance of metabolic homeostasis and general health [96–99]. Human study demonstrating that disruption of metabolism by meal time emphasizes the important role of circadian food consumption [100]. In animal models, surprisingly, even during conditions of daily isocaloric intake, restricting the food consumption to only the active phase can rescue the metabolic disorders caused by energy-rich food consumption [98,101,102]. In addition to these forced feeding time designs in laboratory conditions, disruption of the circadian system also results in disrupted timing regulation of voluntary food intake, which also usually leads to metabolic disorders. Transgenic deletion of circadian genes in mice leads to a disrupted nocturnal food intake pattern and weight gain [103]. Abnormal light cycles, for example constant light (LL), or dim light at night cause interruption of circadian rhythms

in the SCN, and lead to interrupted nocturnal feeding pattern and obesity [104,105]. When supplied with *ad libitum* access to energy-dense diets, which is similar to modern diets availability in current human society, mice switch their voluntary feeding pattern from nocturnal (~80% at night) to low rhythmicity constant snacking (~60% at night), which results in obesity [62,98].

In summary the internal circadian system regulates voluntary feeding behavior and hence energy homeostasis. In turn, interrupted energy homeostasis influences the orchestration of the circadian system which further destroys the metabolic system. Therefore, delineating the mechanism underlying the interplay between circadian system and feeding behavior is necessary, and will provide insights for new therapeutic strategies against the growing global pandemic of metabolic syndromes. In this dissertation, (1) I demonstrate that dopamine signaling in the SCN is sufficient to enable energy-dense food induced overeating and obesity, in collaboration with Ryan Grippo *et. al.* (Chapter 2); (2) I delineate a circadian neuron circuit from DMH to SCN that regulates the entrainment to scheduled feeding, in collaboration with Brandon Podyma *et. al.* (Chapter 3); (3) I develop an open-source, budget-efficient rodent locomotor behavior monitoring system to enhance our capability to study circadian behavior (Addendum 1).

Chapter 2 Dopamine Signaling in the Suprachiasmatic Nucleus Enables Weight Gain Associated with Hedonic Feeding

Ryan M. Grippo[1†], Qijun Tang[1†], Qi Zhang[1], Sean R. Chadwick[1], Yingnan Gao[1], Everett B. Altherr[1], Laura Sipe[1,2], Aarti M. Purohit[1,3], Nidhi M. Purohit[1], Meghana D. Sunkara[1], Krystyna J. Cios[1], Michael Sidikpramana[4], Anthony J. Spano[1], John N. Campbell[1], Andrew D. Steele[4], Jay Hirsh[1], Christopher D. Deppmann[1,5], Martin Wu[1], Michael M. Scott[6], Ali D. Güler[1,5*].

[1]Department of Biology, University of Virginia, Charlottesville, VA 22904, USA.
[2]The University of Tennessee Health Science Center, Memphis, TN 38163, USA.
[3]Department of Medicine, Johns Hopkins University School of Medicine, Baltimore, MD 21205, USA.
[4]Department of Biological Sciences, California State Polytechnic University Pomona, Pomona, CA 91768, USA.
[5]Department of Neuroscience, School of Medicine, University of Virginia, Charlottesville, VA 22908, USA.
[6]Department of Pharmacology, University of Virginia, Charlottesville, VA 22908, USA.
[†]Co-first authors

Correspondence

*To whom correspondence should be sent:
Ali D. Güler
Departments of Biology and Neuroscience
University of Virginia
Charlottesville, VA 22904-4328
Email: aguler@virginia.edu

This chapter was published in January, 2020, in *Current Biology*. PMID: 31902720, PMCID: PMC6981074, DOI: 10.1016/j.cub.2019.11.029. This work was in close collaboration with Ryan Grippo *et al.*; results presented here may also be included in the Ph.D. dissertation thesis of Dr. Ryan Grippo, Dr. Sean Chadwick, Dr. Qi Zhang, and the graduation thesis of other co-authors. Major contributors to each work are indicated in the figure legend.

c2.1 Abstract

Currently, the availability of energy-dense, rewarding foods is widely spread both spatially and temporally. This leads to overeating both during and outside of regular mealtimes which correlates with a globally increased incidence of obesity. It has been observed that consumption of energy-dense food restructures the timing of voluntary food intake, with unclear understanding of the neuronal mechanisms behind such modulation. Here, we demonstrate that dopaminergic signaling within the suprachiasmatic nucleus (SCN), the central circadian pacemaker, disrupts the timing of feeding, resulting in overconsumption of food. D1 dopamine receptor (Drd1) null mice are resistant to diet-induced obesity, metabolic disease, and circadian disruption associated with energy-dense diets. Conversely, genetic rescue of Drd1 expression within the SCN restores diet-induced overconsumption, weight gain, and obesogenic symptoms. Access to rewarding food increases SCN dopamine tone, and dampens the amplitude of SCN rhythmicity via elevated Drd1 signaling which disinhibits downstream orexigenic responses. These findings define a connection between the reward and circadian pathways in the regulation of pathological calorie consumption.

c2.2 Main

Over a third of the U.S. population is obese, which is the greatest risk factor for chronic disorders such as diabetes, cardiovascular and kidney diseases[87–93]. In 2016, obesity and being overweight cost the nation $1.72 trillion in healthcare costs and lost economic productivity[88]. Weight gain occurs when energy intake is greater than expenditure. However, diets that restrict calorie intake and increase exercise are only

partially effective in preventing obesity[106–108]. This is because, in addition to their calorie rich content, availability of rewarding foods reduces “diet adherence” and their consumption outside of regular meal times diminish “metabolic efficiency”[98,103,106–113]. The precise mechanism by which these energy-rich foods promote consumption beyond energy needs remains obscure. Determining the neural mechanisms by which palatable foods alter feeding amount and meal-timing is a necessary step toward developing effective therapies against obesity.

Proper maintenance of energy homeostasis requires the synchronization of meals with daily metabolic rhythms [103]. Surprisingly, even during conditions of isocaloric energy intake, high-fat food consumption out of phase with rhythmic metabolic processes leads to obesity through altered energy utilization and increased energy storage in mice [98,114]. Consistent with these observations, late-night eaters tend to be refractory to weight-loss therapy [96], while temporal restriction of meal timing improves the metabolic profiles of pre-diabetic men [97]. These findings emphasize the importance of both the amount and timing of calorie intake on metabolic health. While becoming recognized as critically important for well-being, the precise mechanisms by which energy-dense, rewarding foods alter food intake and feeding patterns remain unknown.

Dopamine (DA) is known for reward processing and is required for sustained motivation and execution of goal-directed behaviors [75,76]. Genetic ablation of DA production leads to hypophagia and eventual death by starvation in mice [115]. Modulation of DA-dependent neural activity and behavior is mediated by a group of G protein-coupled receptors expressed in anatomically distinct regions throughout the central and

peripheral nervous systems. Both D1-like (G_s-coupled) and D2-like (G_i-coupled) receptors have been implicated in non-homeostatic consumption of palatable foods and obesity [116–118]. Selective activation of D1 dopamine receptor (Drd1) expressing neurons in the prefrontal cortex induces food intake [119] and prolonged access to a high-fat diet alters Drd1 expression within the reward centers of the brain [120,121]. Additionally, treatment with a Drd1 antagonist reduces food intake in rodents and causes weight loss in humans [122,123]. Given the importance of DA signaling in food reward response and feeding regulation, we sought to determine the role of this neuromodulatory system in diet-induced obesity.

In this study, we show that Drd1 expression is necessary for overconsumption of a high-fat, high-sugar (HFD) diet. Moreover, Drd1 signaling in response to HFD perturbs circadian feeding and activity rhythms. Unlike wild-type mice, Drd1-knockout mice provided *ad libitum* access to palatable foods are resistant to weight gain. Most strikingly, Drd1-knockout mice on a HFD maintain robust daily rhythms of food consumption, foraging, and fuel utilization, while wild-type mice on a HFD demonstrate altered circadian regulation of metabolism. Selective restoration of Drd1 expression within the nucleus accumbens (NAc), the predominant reward processing center of the brain, fails to rescue the overconsumption of energy-rich food and attendant weight gain observed in wild-type mice. However, Drd1 rescue specifically within the central circadian clock, the SCN, of Drd1-knockout mice completely restores the obesogenic phenotype. The overall excitability of the SCN is reduced in response to Drd1 agonist treatment likely due to the increased activity of GABAergic Drd1-expressing-SCN

neurons inhibiting the local post-synaptic cells. Therefore, we posit that in response to rewarding foods, the increased dopaminergic tone on the circadian pacemaker dampens SCN neuronal activity, disinhibiting downstream orexigenic targets and promoting out-of-phase foraging.

c2.2.1 Drd1-KO Mice are Protected from High-Fat Diet-Induced Obesity

Mice with *ad libitum* access to rewarding, calorically dense food rapidly develop obesity, diabetes, and metabolic disease [124,125]. To explore the potential relationship between Drd1 signaling and obesity, we monitored responses to dietary challenge using *Drd1a*$^{Cre/Cre}$ (KO) mice, in which both *Drd1a* alleles were replaced by an open reading frame encoding Cre recombinase (Cre) [126]. We monitored weekly changes in body weight (BW) between adult male wild-type (WT) and KO mice during *ad libitum* access to either standard chow diet (SCD; 19% fat, 0% sucrose) or high-fat, high-sugar diet (HFD; 45% fat, 17% sucrose) (Figure 1A and S1A-B). Percent and total BW change was indistinguishable between adult male WT and KO mice on SCD (WT-SCD: 5.0±2.6% increase; KO-SCD: 5.9±1.1% increase; Student's two-tailed t-test, p=0.8). As expected, WT mice on HFD (WT-HFD) significantly increased BW (Figure 1B and S1C), however, KO mice fed the same diet (KO-HFD) were resistant to diet-induced weight gain (WT-HFD: 29.5±3.1% increase; KO-HFD: 5.4±1.6% increase; Student's two-tailed t-test, p<0.001; Figure 1B-C, and S1C). We also observed resistance to obesity in a separate *Drd1a* null (*Drd1*$^{-/-}$) mouse model [127], following twelve-week access to a palatable high-fat, low sugar diet (60% fat, 10.7% sucrose) (Figure S1D). These data

indicate that Drd1 signaling is necessary for weight gain on a variety of calorically dense food sources in a strain independent manner.

Paralleling their weight gain, daily HFD consumption of WT mice was significantly increased compared to all other groups (Figure S1E-F). Diets rich in fat not only increase food consumption, but also alter feeding patterns resulting in food intake that extends into the rest phase [114,128]. This disruption in feeding rhythms induces weight gain independent of overconsumption, highlighting the importance of maintaining robust feeding rhythms for proper metabolic regulation [98]. While caloric intake of either diet was equivalent between genotypes during the active (night) phase (Figure 1D), WT mice exhibited a significant increase in rest (day) phase HFD consumption that was nearly absent in KO-HFD mice (Figure 1D-E, and S1E). Attenuated daytime consummatory behavior in KO animals was also present during access to a highly palatable liquid diet (Ensure), demonstrating that this phenotype is observed in response to a variety of hypercaloric food sources (Figure S1G).

The inhibitory effects of light on general activity and feeding (masking) have been well documented [129]. However, when placed into constant dark conditions (DD), KO mice still consumed significantly less during the subjective day (DD-day) compared to WT-HFD controls (WT-HFD: 42.8±2.9%; KO-HFD: 27.8±3.9%; Student's two-tailed t-test, $p=0.009$; Figure S1H-I). Furthermore, KO mice remained resistant to weight gain following ten days of HFD access in DD, indicating that light exposure is not the primary determinant of reduced HFD consumption in KO mice (WT-HFD: 17.3±2.1%; KO-HFD: -0.4±1.8% BW change; Student's two-tailed t-test, $p<0.001$; Figure S1J). Next, we

ascertained whether the reduced daytime food intake in KO mice was a result of diurnally regulated motivation for rewarding foods. Although progressive ratio breakpoint analysis is the standard test for motivation, because of the deficit in operant conditioning performance in KO mice during both phases of the day (Figures S1K-M) [130], we designed a simpler foraging assay, which more closely mimics *ad libitum* food access conditions. In this assay, habituated mice are placed into an arena with a HFD pellet buried under the bedding at one end. The latency for the mice to find and consume food is recorded. Consistent with reduced daytime food intake, KO mice exhibited an increased latency to food during the day compared to WT controls (ZT8; WT: 21.9±4.2s; KO: 58.6±12.9s). However, no detectable differences in foraging latency were observed at night (ZT15; WT: 32.9±12.2s; KO: 38.4±8.5s) demonstrating that Drd1 is important for out-of-phase palatable food-seeking, and the observed daytime reduction of food intake in KO mice is not a generalized impairment in olfaction or locomotion (Figure 1F) [131]. Taken together, these data suggest that Drd1-dependent overconsumption of palatable food, predominantly during the light phase, leads to obesity and metabolic disease. These findings not only reaffirm the importance of circadian regulation in energy balance [132], but also implicate an essential role for the Drd1-dependent DA-signaling in this process.

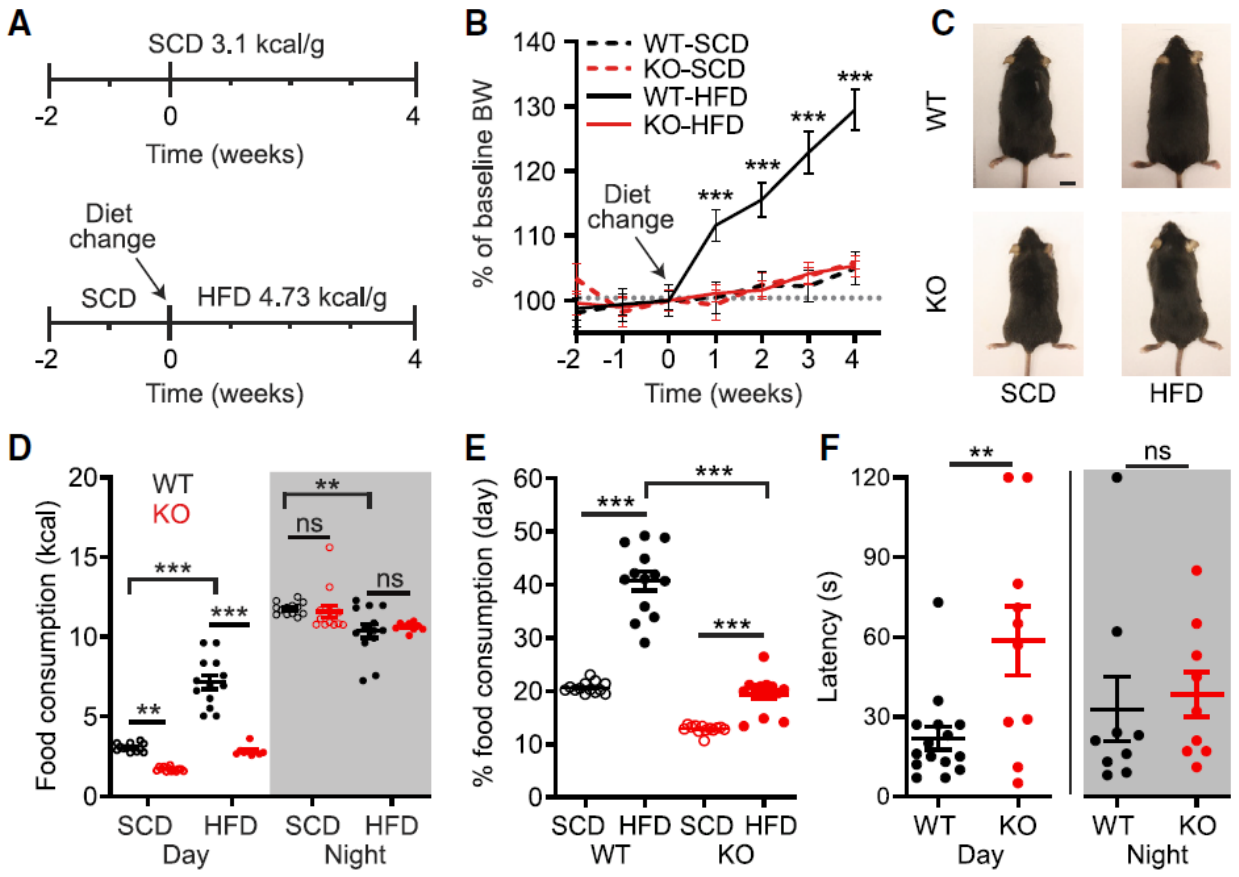

Figure 1. Drd1-KO Mice Are Protected from HFD-Induced Obesity

A.(Ryan Grippo) Food access paradigm. Diet switch from SCD to HFD (week 0) is shown.

B.(Ryan Grippo, Qijun Tang) Percent BW change relative to week 0 for WT and KO mice on SCD or HFD. Repeated measures three-way ANOVA with Bonferroni post hoc comparison; n = 7–13/group; $F_{genotype}(1,37) = 4.8$, $p = 0.03$; $F_{diet}(1,37) = 5.9$, $p = 0.02$. Arrow marks diet switch from SCD to HFD. Statistical significance between WT-HFD and KO-HFD is depicted.

C.(Ryan Grippo, Qijun Tang, Qi Zhang) Representative images of WT or KO mice from (A) and (B). Scale bar represents 1 cm.

D.(Ryan Grippo, Qijun Tang) Calorie intake during the 12-h light (day) or dark phases (night) for WT and KO mice on SCD or HFD. Repeated-measures three-way ANOVA with Bonferroni post hoc comparison; n = 13/group; $F_{time}(1,96) = 1,544$, $p < 0.001$; $F_{genotype}(1,96) = 57.1$, $p < 0.001$; Fdiet(1,96) = 12.6, $p < 0.001$.

E.(Ryan Grippo, Qijun Tang) Percent of total daily food intake during the day for WT and KO mice on SCD or HFD. Two-way ANOVA with Bonferroni post hoc comparison; n = 13/group; $F_{genotype}(1,48) = 203.2$, $p < 0.001$; $F_{diet}(1,48) = 170.2$, $p < 0.001$.
F.(Qijun Tang) Latency to retrieve a HFD pellet, day or night, for WT and KO mice. Student's two-tailed t test; n = 9–15/group.
Data are represented as mean ± SEM. **p < 0.01; ***p < 0.001; ns, not significant. See also Figure S1.

c2.2.2 Drd1-KO Mice Are Resistant to Dampening of Metabolic Rhythms and Metabolic Disease

One consequence of *ad libitum* calorie-rich food consumption is the adaptation of metabolic processes, which switch from a high amplitude circadian oscillation between carbohydrate utilization (during the active phase) and lipid oxidation (during the rest phase) to a low amplitude oscillation reflective of metabolic shunting towards energy storage [62,101,133]. While WT-SCD and KO-SCD mice exhibited robust circadian rhythms of respiratory exchange ratio (RER) (Figures 2A-B) indicating efficient energy source cycling between predominantly carbohydrates (RER of ~1) or fats (RER of ~0.7), the circadian amplitude of RER in WT-HFD mice was significantly dampened (Figures 2D-E, and S2A). Interestingly, nighttime RER values were reduced in both WT-HFD and KO-HFD mice likely due to the elevated fat/carbohydrate ratio of the diet (Figures 2B and 2D). However, KO-HFD mice sustained higher-amplitude RER rhythms reflecting increased fat utilization during the rest phase (Figure 2D). Consistent with a lower RER value and adipocyte lipolysis, KO-HFD mice had elevated activated phosphorylated hormone sensitive lipase (pHSL) levels during the rest phase (ZT 6) (Figures S2B and S2C) [134,135]. These data reveal that KO-HFD mice maintain SCD-like metabolic

rhythms compared to WT-HFD animals, which is favorable for metabolic well-being and protection from weight gain.

It has been reported that Drd1 expression within the nucleus accumbens (NAc) is involved in the maintenance of wakefulness [136], which could interfere with time spent foraging. Both WT and KO mice exhibited similar hourly putative sleep duration during the day on HFD (WT-HFD: 42.0±5.1 min/hour; KO-HFD: 48.5±1.8 min/hour; Student's two-tailed t-test, p=0.4) suggesting that the observed feeding phenotype is unlikely to be caused by increased sleep bouts in KO mice. In fact, KO-HFD mice exhibit marginal hyperactivity at night, however, this does not translate to a difference in twenty-four hour energy expenditure (EE), resting metabolic rate (RMR) or excess energy lost to heat compared to WT-HFD mice (Figure 2C, 2F, and S2D-G) [137,138]. Lastly, while there was no difference in fecal energy density between all groups (Figure S2H), KO-HFD mice show diminished daily energy assimilation and hence the reduced BW in these animals is not due to increased energy excretion (Figure S2I).

Obesity from HFD consumption also results in increased fat mass, adipocyte hypertrophy, hepatic steatosis, glucose intolerance, and insulin resistance [125,139]. As expected, WT-HFD mice accumulated significant total body adiposity, while KO-HFD animals, maintained similar body fat composition to SCD controls (WT-SCD: 12.5±5.1%; KO-SCD: 10.8±1.5%; WT-HFD: 27.7±6.1%; KO-HFD: 11.4±1.5%; Figure 2G and S2L). Additionally, adipocyte cell hypertrophy in gonadal white adipose tissue (GWAT) and posterior subcutaneous adipose tissue (SCAT) were reduced, and hepatic lipid accumulation was diminished in KO-HFD mice compared to WT-HFD animals (Figures

2H-J, S2J-K). Most strikingly, KO-HFD mice were protected from glucose intolerance and insulin resistance, two hallmarks of obesity-induced metabolic disease (Figures 2K-L, and S2M-N) [140,141]. Taken together, these data demonstrate that unlike WT mice, KO mice on HFD maintain high amplitude rhythms in activity, temperature, and energy source, as well as reduced adiposity and robust responsiveness to glucose and insulin fluctuations.

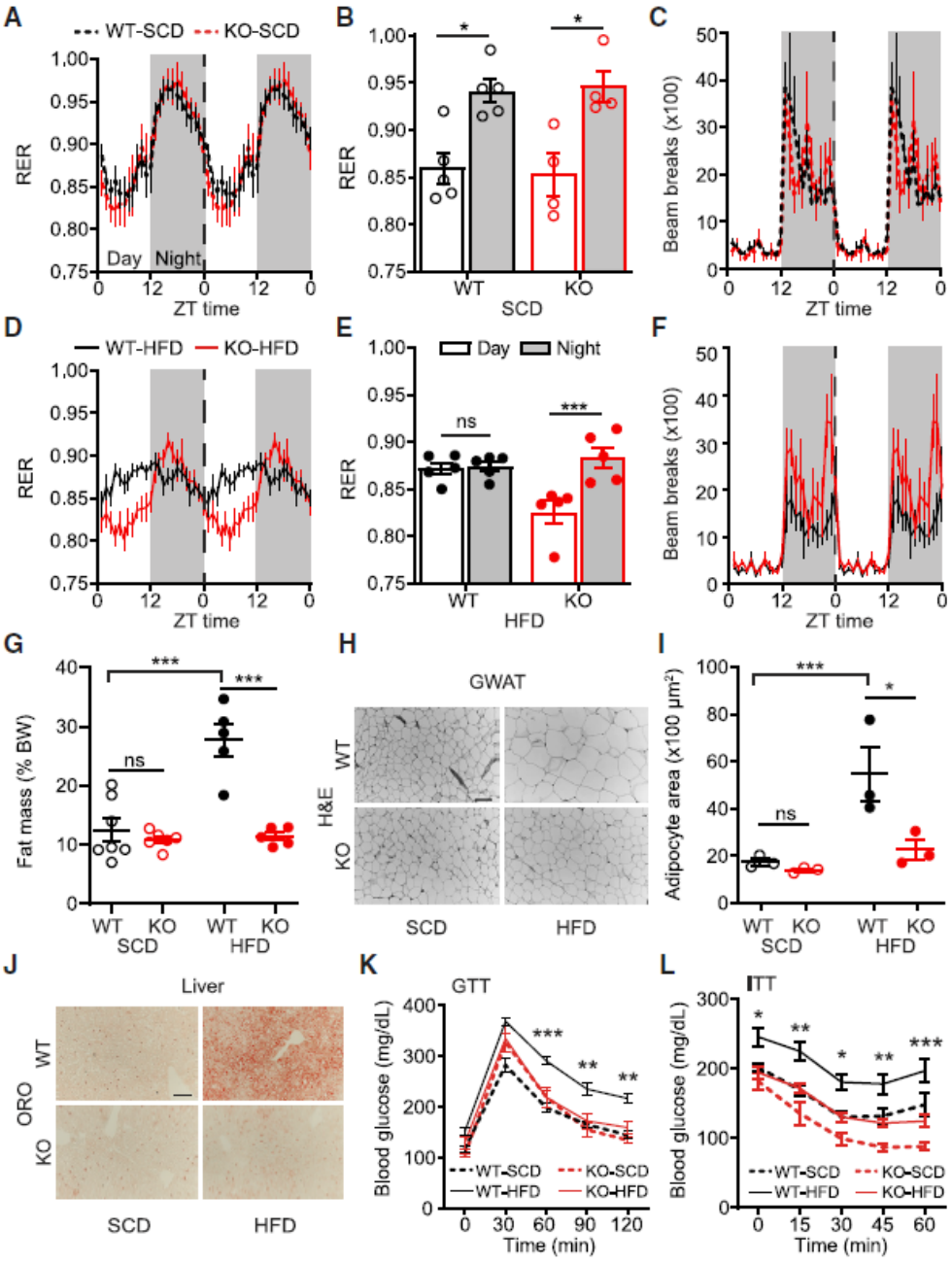

Figure 2. Drd1-KO Mice Are Resistant to HFD-Induced Metabolic Disease

A.(Ryan Grippo, Qijun Tang, Michael Scott) RER for WT-SCD and KO-SCD mice. Repeated measures two-way ANOVA; n = 4–5/group. Time is represented as zeitgeber time (ZT), where ZT0 indicates onset of day and ZT12 indicates onset of night (shaded gray). Data are plotted in 1-h intervals. Vertical dotted line indicates the point at which

24-h data are double plotted for clarity. The same representation applies to (C), (D), and (F).

B.(Ryan Grippo, Qijun Tang, Michael Scott) Average RER during the day or night from (A). Repeated-measures two-way ANOVA with Bonferroni post hoc comparison; n = 4–5/group; $F_{time}(1,7) = 57.5$; $p < 0.001$.

C.(Ryan Grippo, Qijun Tang, Michael Scott) Double-plotted ambulatory infrared beambreak activity for WT-SCD and KO-SCD mice. Repeated-measures two-way ANOVA with Bonferroni post hoc comparison; n = 4–5/group.

D.(Ryan Grippo, Qijun Tang, Michael Scott) Double-plotted RER for WT-HFD and KO-HFD mice. Repeated-measures two-way ANOVA with Bonferroni post hoc comparison; n = 5/group.

E.(Ryan Grippo, Qijun Tang, Michael Scott) Average RER during the day or night from (D). Repeated-measures two-way ANOVA with Bonferroni post hoc comparison; n = 5/group; $F_{time}(1,8) = 15.8$; $p = 0.004$.

F.(Ryan Grippo, Qijun Tang, Michael Scott) Double-plotted ambulatory infrared beambreak activity for WT-HFD and KO-HFD mice. Repeated-measures two-way ANOVA with Bonferroni post hoc comparison; n = 5/group; $F_{genotype}(1,8) = 5.4$; $p = 0.05$.

G.(Ryan Grippo, Qijun Tang, Qi Zhang) Fat mass as percentBWfor WT and KO mice on SCD or HFD. Two-way ANOVA with Bonferroni post hoc comparison; n = 5–7/group; $F_{diet}(1,19) = 20.3$, $p < 0.001$; $F_{genotype}(1,19) = 26.5$, $p < 0.001$.

H.(Ryan Grippo, Qijun Tang, Qi Zhang) Representative GWAT H&E stain for groups in (G). Scale bar represents 100 mm.

I.(Aarti Purohit) Quantification of GWAT adipocyte area. Two-way ANOVA with Bonferroni post hoc comparison; n = 3/group; $F_{diet}(1,8) = 13.5$, $p = 0.006$; $F_{genotype}(1,8) = 8.2$, $p = 0.02$.

J.(Ryan Grippo, Qijun Tang, Qi Zhang) Representative liver oil red O (ORO) histology for groups in (G), where hepatic lipid content stains as red. Scale bar represents 100 mm.

K-L.(Qi Zhang) Blood glucose levels during (K) glucose tolerance test (GTT) (repeated-measures three-way ANOVA with Bonferroni post hoc comparison; n = 8–12/group; $F_{genotype}(1,35) = 5.5$, $p = 0.03$; $F_{diet}(1,35) = 21.9$, $p < 0.001$) and (L) insulin tolerance test (ITT). Repeated-measures three-way ANOVAwith Bonferroni post hoc comparison; n = 9–12/group; $F_{genotype}(1,36) = 26.4$, $p < 0.001$; $F_{diet}(1,36) = 18.4$, $p < 0.001$. Statistical significance between WT-HFD and KO-HFD is depicted.

Data are represented as mean ± SEM. *p < 0.05; **p < 0.01; ***p < 0.001; ns, not significant. See also Figure S2.

c2.2.3 Re-expression of Drd1 Within the NAc Increases Daytime HFD Consumption without Inducing Obesity.

Energy homeostasis is controlled by a variety of neuronal circuits that influence food intake and energy expenditure suggesting that the obesity resistant phenotype of KO mice is due to a reduced central drive to over consume palatable foods [53,142,143]. Therefore, we limited Drd1 ablation to distinct populations of neurons by crossing floxed Drd1 ($Drd1^{fl/fl}$) mice with different Cre driver lines. Drd1 is mostly expressed in GABAergic populations except for a select group of CaMKII-positive cells in the hippocampus [77,144]. To distinguish the role of Drd1 between these populations during palatable food consumption, we genetically ablated Drd1 expression using either $CaMKII^{Cre/+}$ or $VGAT^{Cre/+}$ driver lines, respectively [144–146]. On HFD, $CaMKII^{Cre/+}$;$Drd1^{fl/fl}$ mice gained an equivalent amount of weight compared to $CaMKII^{Cre/+}$;$Drd1^{+/+}$ controls (Figure S3B). However, like germline Drd1-null animals (Figure S1D), select ablation of Drd1 expression in GABAergic neurons ($VGAT^{Cre/+}$;$Drd1^{fl/fl}$ mice) completely protected animals from diet-induced obesity (Figures 3A-B, and S3A).

Next, we restored Drd1 expression to the nucleus accumbens (NAc), a primary DA recipient region within the mesolimbic pathway, in Drd1-KO mice by bilaterally delivering an adeno-associated virus 1 (AAV1) containing a Cre recombinase dependent Drd1 transgene (Drd1-HA; NAc-Rescue). Because Cre is knocked-in to replace the endogenous *Drd1a* gene in these mice, Drd1-HA expression remains confined to the cells with active *Drd1a* promoter at the targeted site [130]. Successful targeting of Drd1-HA was determined by anti-HA immunohistochemistry (Figure 3C and

S3E), and functional expression was evaluated following intraperitoneal injections of the Drd1 agonist SKF-81297 (i.p.; 7.5 mg/kg) (Figure S3D) [130]. Drd1-KO mice injected with AAV1 encoding the light-activated, membrane-localized cation channel Channelrhodopsin-2 (ChR2-eYFP) to the NAc were used as controls (NAc-Control). Surprisingly, re-expression of Drd1 within the NAc resulted in no appreciable increase in BW on HFD (Figure 3D, S3F, and S3I). Additionally, we observed no difference in twenty-four-hour consumption compared to controls on either diet, however, NAc-Rescue mice increased the portion of Day consumption on HFD (NAc-Control: 19.8±1.2%; NAc-Rescue: 31.1±1.5%; Figures 3E-F, and S4G-H). This elevated rest phase consumption resulted in a marginal, but statistically significant increase in percentage fat mass, GWAT adipocyte area and hepatic steatosis (Figures 3G-H, and S3J-L). However, similar to germline KO mice, NAc-Rescue mice maintained glucose tolerance and insulin sensitivity (Figures 3I-J). Despite increasing the portion of rest-phase feeding, re-expression of Drd1 within the NAc is not sufficient to induce HFD overconsumption and obesity, indicating that another Drd1-expressing brain region governs this response.

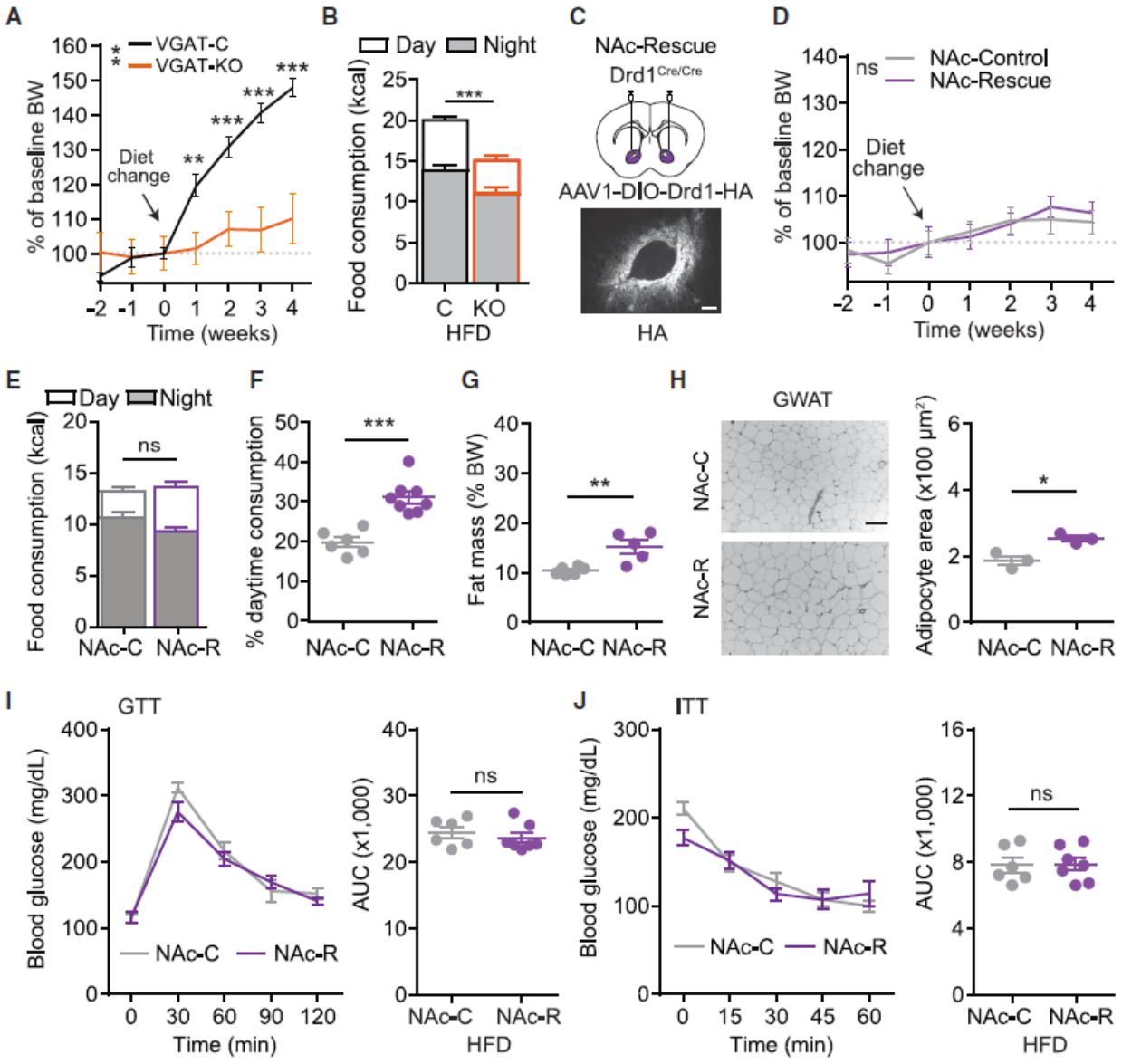

Figure 3. Selective Re-expression of Drd1 within the NAc of Drd1-KO Mice Partially Rescues HFD-Induced Phenotypes, Excluding Obesity

A.(Michael Sidikpramana, Andrew Steele) Percent BW change relative to week 0 for VGAT$^{+/+}$;Drd1$^{fl/fl}$ (VGAT-C) and VGAT$^{Cre/+}$;Drd1$^{fl/fl}$ (VGAT-KO) mice following access to high-fat/low-sugar diet. Repeated measures two-way ANOVA with Bonferroni post hoc comparison; n = 7–16/group; $F_{genotype}(1,21) = 10.4$; p = 0.004.

B.(Michael Sidikpramana, Andrew Steele) Daily total calorie consumption of VGAT-C and VGAT-KO mice on HFD. Day (white) and night (gray) consumption are segregated for clarity. Student's two-tailed t test; n = 7–16/group.

C.(Qijun Tang) Top: schematic diagram illustrating NAc bilateral injection of AAV1-DIO-Drd1-HA or AAV1-ChR2-YFP in KO ($Drd1^{cre/cre}$) mice. Bottom: anti-HA immunohistochemical labeling within the NAc is shown. Scale bar represents 100 mm.
D.(Qijun Tang) Percent BW change relative to week 0 for NAc-Control (NAc-C) and NAc-Rescue (NAc-R) mice on HFD. Repeated-measures two-way ANOVA with Bonferroni post hoc comparison; n = 6–8/group.
E.(Qijun Tang) Daily total calorie consumption of NAc-C and NAc-R mice on HFD. Student's two-tailed t test; n = 6–8/group.
F.(Qijun Tang) Portion of day consumption on HFD. Student's two-tailed t test; n = 6–8/group.
G.(Ryan Grippo, Michael Scott, Qijun Tang) Fat mass as percent BW on HFD. Student's two-tailed t test; n = 5–6/group.
H.(Qijun Tang, Aarti Purohit) Representative GWAT histology with H&E stain (left) and quantification of GWAT adipocyte area (right). Scale bar represents 100 mm. Student's two-tailed t test; n = 3/group.
I-J.(Qi Zhang, Qijun Tang) Blood glucose levels over time (left; repeated-measures two-way ANOVA with Bonferroni post hoc comparison; n = 6–7/group) and area under the curve (AUC) quantification (right; Student's two-tailed t test; n = 6–7/group) during GTT (I) or ITT (J).
Data are represented as mean ± SEM. *p < 0.05; **p < 0.01; ***p < 0.001; ns, not significant. See also Figure S3.

c2.2.4 HFD and Drd1-signaling Modulate Behavioral Circadian Period and SCN Neurophysiology

The observed temporal change of feeding pattern in WT-HFD suggests a disruption in circadian rhythmicity. In addition to alterations in peripheral circadian clock gene expression, access to HFD lengthens centrally regulated activity rhythms [62]. To determine whether HFD-induced disruption of circadian behavioral rhythms is dependent on Drd1 signaling, we monitored wheel running activity of WT and KO mice following four weeks of SCD or HFD access. As expected, WT-HFD mice exhibited a lengthened free-running period compared to WT-SCD animals that was reversible upon diet change. However, no difference between KO-HFD and SCD controls was observed

(Figures 4A-C, and S4A-B). Resistance to HFD-induced period lengthening in KO mice suggests a role for Drd1 signaling in the disruption of central circadian rhythms during dietary challenge.

Since the HFD-induced circadian period lengthening is Drd1-dependent, we sought to determine whether acute exposure to HFD changes DA tone in the SCN. To address this, we determined the DOPAC and DA content from hypothalamic tissue punches containing the SCN in WT animals following one-hour access to either SCD or HFD (Figure S4C). The DOPAC/DA ratio is an estimate of DA turnover reflecting active DA release and catabolism, which rapidly increases within the NAc in response to HFD [121,147]. WT mice given one hour access to HFD during their inactive phase (ZT6) consumed significantly more food than SCD controls (SCD: 0.3±0.08kcal; HFD: 5.4±0.5kcal; Student's two-tailed t-test, $p<0.001$). Accordingly, the hypothalamic DOPAC/DA ratio of animals fed HFD was elevated (SCD: 0.24±0.02; HFD: 0.35±0.02; Figure 4D). Previously, we have demonstrated that a fraction of the ventral tegmental area (VTA) DA neurons innervate the SCN [80], representing a potential source of DA to this region. By using a Cre-dependent rabies viral tracing strategy, we validated that the SCN-Drd1 neurons specifically receive VTA dopaminergic projections (Figure S4D). Thus, consumption of palatable foods increases DA turnover around the SCN region and therefore may modulate the function of the central circadian clock.

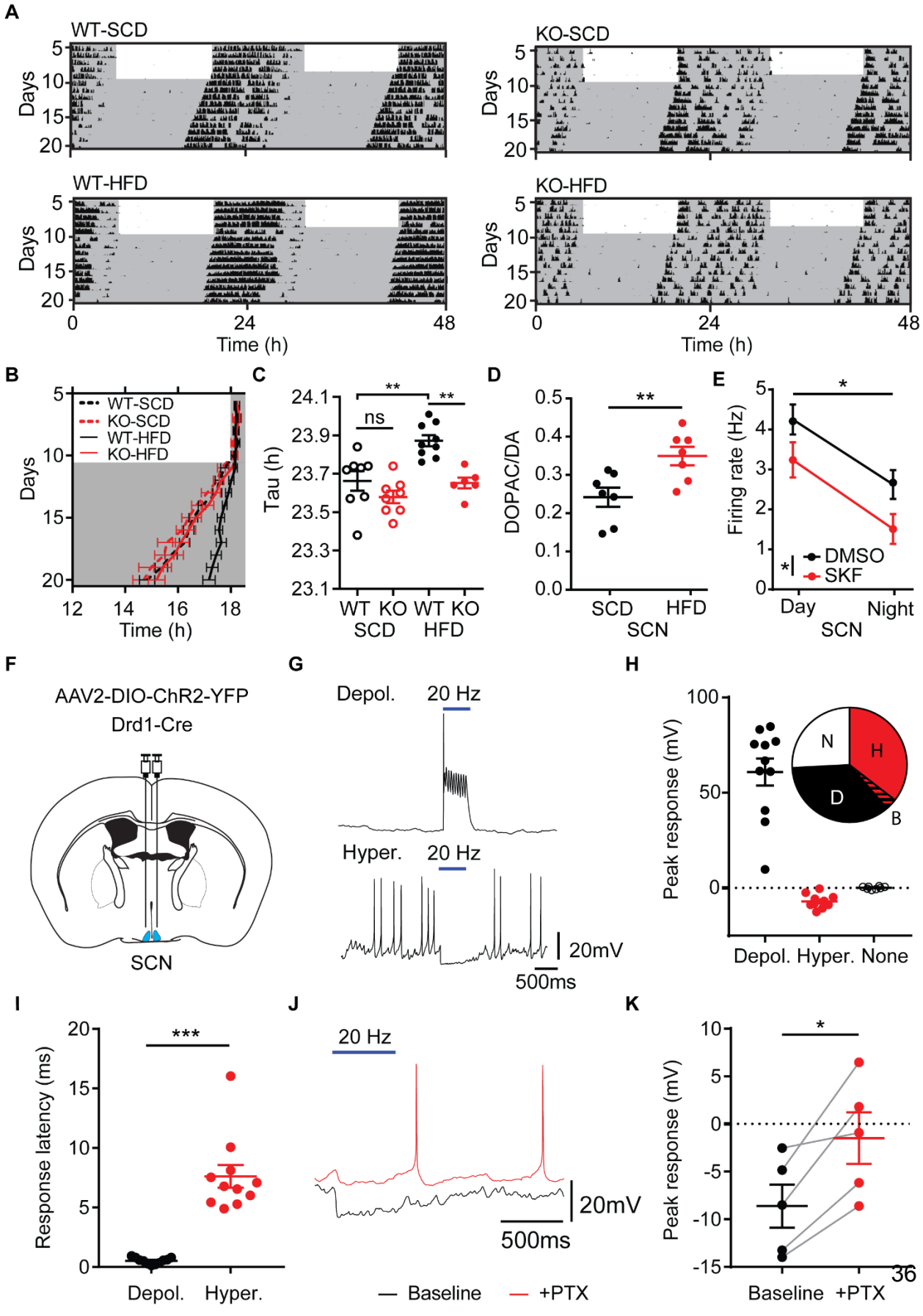
A
WT-SCD
KO-SCD
WT-HFD
KO-HFD
Days
Time (h)
B
WT-SCD
KO-SCD
WT-HFD
KO-HFD
Time (h)
C
Tau (h)
ns
WT KO WT KO
SCD HFD
D
DOPAC/DA
SCD HFD
SCN
E
Firing rate (Hz)
DMSO
SKF
Day Night
SCN
F
AAV2-DIO-ChR2-YFP
Drd1-Cre
SCN
G
Depol. 20 Hz
Hyper. 20 Hz
20mV
500ms
H
Peak response (mV)
N
H
D
B
Depol. Hyper. None
I
Response latency (ms)
Depol. Hyper.
J
20 Hz
20mV
500ms
Baseline +PTX
K
Peak response (mV)
Baseline +PTX

Figure 4. Elevated Drd1 Signaling Reduces Neuronal Firing Rate in the SCN

A.(Ryan Grippo) Representative double-plotted actogram of wheel-running activity in constant darkness (DD). White and gray background indicate the light and dark phase of the LD cycle, respectively.

B.(Ryan Grippo) Average daily activity onset time. Repeated measures three-way ANOVA with Bonferroni post hoc comparison; n = 7–10/group; $F_{genotype}(1,28) = 11.7$, $p = 0.002$; $F_{diet}(1,28) = 15.5$, $p < 0.001$.

C.(Ryan Grippo) Average DD free running period (Tau). Two-way ANOVA with Bonferroni post hoc comparison; n = 6–9/group; $F_{genotype}(1,27) = 16.2$, $p < 0.001$; $F_{diet}(1,27) = 14.01$, $p < 0.001$.

D.(Ryan Grippo, Nidhi Purohit, Jay Hirsh) Quantification of dopamine turnover (DOPAC/DA ratio) following 1-h SCD or HFD exposure in hypothalamic tissue punches containing the SCN. Student's two-tailed t test; n = 7/group.

E.(Sean Chadwick) Mean firing rate of cell-attached SCN neuron recordings following SKF-81297 (5 mM) incubation at ZT8–ZT11 (day) or ZT14–ZT17 (night). Two-way ANOVA; n = 13–26/group; $F_{time}(1,70) = 16.9$, $p < 0.001$; $F_{treatment}(1,70) = 6.8$, $p = 0.01$.

F.(Ryan Grippo) Schematic of bilateral AAV2-DIO-ChR2-YFP injection in the SCN of $Drd1^{cre/+}$ mice.

G.(Sean Chadwick) Representative traces from whole-cell current clamp recordings. SCN neurons exhibit both depolarizing (top) and hyperpolarizing (bottom) responses to 20-Hz stimulation.

H.(Sean Chadwick) ChR2 stimulation-induced average peak responses for depolarizing (depol.), hyperpolarizing (hyper.), and non-responsive (none) neurons. Distribution of recorded responses is depicted. B indicates one cell exhibiting both responses (see Figure S4H).

I.(Sean Chadwick) Response latency of each group in (H). Student's two-tailed t test; n = 11/group.

J.(Sean Chadwick) Representative traces from whole-cell current clamp recordings for ChR2 stimulation-induced postsynaptic responses before and after 5-min 100 mM PTX incubation.

K.(Sean Chadwick) ChR2 stimulation-induced average peak responses before and after PTX incubation. Student's two-tailed paired t test; n = 5/group.

Data are represented as mean ± SEM. *$p < 0.05$; **$p < 0.01$; ***$p < 0.001$; ns, not significant. See also Figure S5.

Rewarding foods have been shown to hasten a behavioral phase shift in response to photic stimulation and modulate circadian entrainment, as daily presentation of palatable food entrains circadian rhythms to the time of food availability [148–150]. Because KO mice fail to show HFD-induced circadian period lengthening, we evaluated the consequence of long-term HFD access on the central circadian clock by quantification of two rhythmic molecular markers within the SCN, c-Fos and Per2, at antiphasic time points (ZT1 and 13). We detected a significant time of day effect in both c-Fos and Per2 expression, however, we observed no diet or genotype effect (Figures S4E-F). These data suggest that while acute access to HFD elevates DA turnover within the SCN, prolonged access to HFD does not significantly disrupt the peak-to-trough expression pattern of circadian regulated proteins.

To reconcile the dichotomous observations that in response to HFD there is increased DA turnover in the SCN but no change in circadian gene expression patterns, we evaluated the impact of increased Drd1 signaling on neuronal activity within the SCN. To accomplish this, we incubated acute brain slices from WT mice with the selective Drd1 agonist (SKF-81279; 5μM) and performed loose cell-attached recordings at ZT8-11 (day) and ZT14-17 (night). Incubation with SKF-81297 significantly decreased the firing rate of neurons within the SCN during both phases (Day: DMSO 4.3±0.4Hz; Day: SKF 3.2±0.4Hz; Night: DMSO 2.6±0.4Hz; Night: SKF 1.5±0.4Hz; Figure 4E). Since Drd1 is a G_s-coupled GPCR, and the majority of SCN neurons are GABAergic [151,152] (Figure S4G), we hypothesized that stimulation of Drd1-expressing SCN neurons attenuates the overall firing rate of the local microcircuitry. Therefore, we performed

whole cell current clamp recordings from the SCN of Drd1$^{Cre/+}$ mice injected with an AAV2 that expresses ChR2 Cre-dependently (AAV2-DIO-ChR2-YFP; Figure 4F). Neurons were randomly selected during electrophysiological recordings independent of ChR2 expression within the anatomically defined region of the SCN. While 26% of recorded cells (8 cells) had no response to light stimulation, 35% of the cells depolarized within 1-2ms of the stimulation with time-locked optogenetic responses indicative of ChR2 expression in these cells (11 cells). Additionally, 35% of the SCN-neurons hyperpolarized following a minimum of 4 ms delay (11 cells; Figures 4G-I, and S4H), while one neuron displayed both light-induced action potentials and post-stimulation hyperpolarization (Figure S4I). Perfusion of a $GABA_A$ channel inhibitor, picrotoxin (PTX; 100 μM), diminished the amplitude of the inhibitory responses, confirming that they are ChR2-driven postsynaptic currents (Figures 4J-K, and S4J). These data identify a local inhibitory response to Drd1-SCN neuron activation, revealing that the HFD-induced elevated DA tone may directly modulate SCN firing rate.

c2.2.5 Re-expression of Drd1 Within the SCN Restores Diet-induced Obesity

Although HFD does not significantly dampen circadian gene expression within the SCN (Figure S4), the increased DA turnover within the SCN in response to HFD and the dampened electrical firing rate in response to Drd1 agonist treatment (Figure 4) suggests that DA-dependent SCN-Drd1 signaling may play a prominent role in the increased daytime food intake and obesity observed in WT-HFD mice (Figure 1 and 4). To demonstrate whether Drd1 expression in the SCN is sufficient to establish HFD-induced obesity, we virally re-introduced Drd1 within the central circadian

pacemaker by delivering Drd1-HA to the SCN of KO mice (SCN-Rescue) (Figure 5A) [80,153]. Mice injected with AAV1 expressing ChR2-eYFP were used as controls (SCN-Control). Remarkably, HFD-induced obesity and the subsequent metabolic consequences were completely restored in SCN-Rescue animals as we observed a significant increase in BW, food consumption, adipose mass, adipocyte hypertrophy, hepatic steatosis, glucose intolerance, and insulin resistance relative to SCN-Controls (Figures 5B-J, and S5A-G). SCN-Rescue mice maintained a predominantly nocturnal pattern of food consumption on SCD, while on HFD they significantly increased daytime consumption (SCD: 20.3±3.1%; HFD: 37.4±2.3%; Student's two-tailed t-test, $p<0.001$) (Figures 5D-E, and S5B-C). Most notably, nighttime consumption was not reduced on HFD, leading to an overall increase in food consumption and substantial weight gain (Figures 5B-E). Unlike restoration in the NAc, genetic reconstruction of Drd1 expression within the SCN of KO mice enabled out-of-phase overconsumption of HFD leading to all of the metabolic consequences observed in WT-HFD mice.

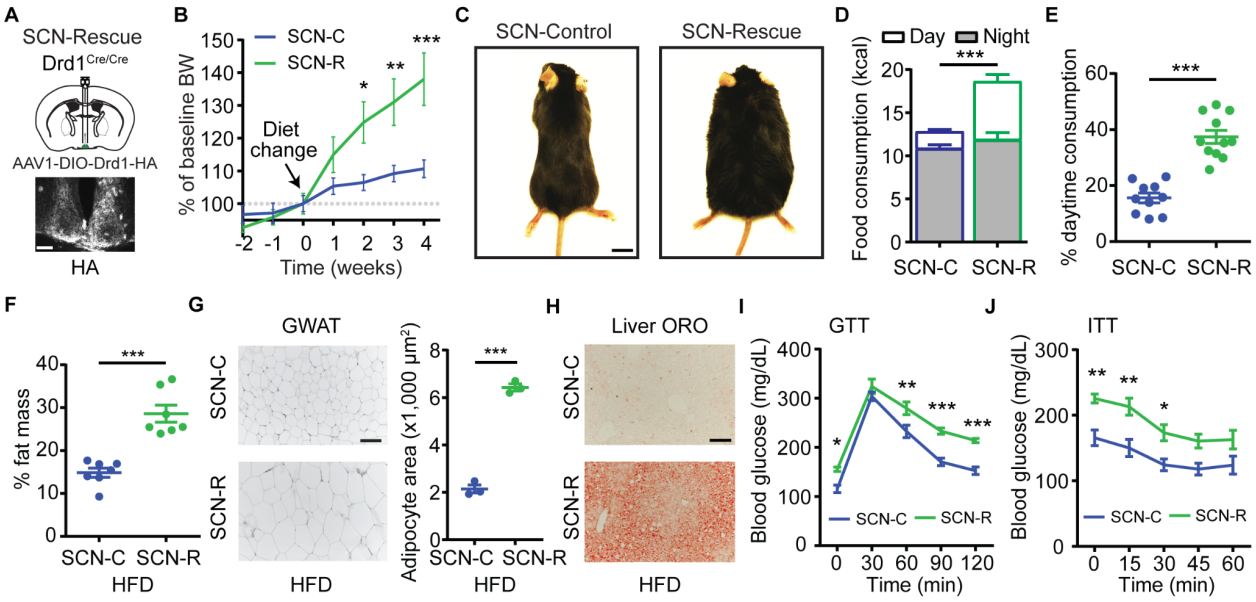

Figure 5. Re-expression of Drd1 within the SCN of Drd1-KO Mice Restores HFD-Induced Obesity

A.(Ryan Grippo) Top: schematic diagram illustrating AAV1-DIO-Drd1-HA SCN bilateral injection in the Drd1-KO ($Drd1^{cre/cre}$) mice. Bottom: anti-HA fluorescent immunohistochemistry
staining within the SCN of SCN-Rescue mice is shown. Scale bar represents 100 mm.
B.(Ryan Grippo) Percent BW change relative to week 0 for SCN-C and SCN-R mice on HFD. Repeated-measures two-way ANOVA with Bonferroni post hoc comparison; n = 10–12/group; $F_{genotype}(1,20) = 4.5$; $p = 0.05$.
C.(Ryan Grippo) Representative images of SCN-C and SCN-R mice (A and B). Scale bar represents 1 cm.
D.(Ryan Grippo) Daily total calorie intake on HFD. Day and night consumption is segregated for clarity. Student's two-tailed t test; n = 10–11/group.
E.(Ryan Grippo) Portion of food intake during the day on HFD. Student's two-tailed t test; n = 10–11/group.
F.(Ryan Grippo, Michael Scott) Fat mass as percent BW. Student's two-tailed t test; n = 7/group.
G.(Qijun Tang, Aarti Purohit) Left: representative GWAT H&E. Scale bar represents 100 mm. Right: quantification of GWAT adipocyte area is shown. Student's two-tailed t test; n = 3/group.
H.(Qijun Tang) ORO of liver. Scale bar represents 100 mm.
I.(Qi Zhang, Qijun Tang) GTT; repeated-measures two-way ANOVA with Bonferroni post hoc comparison; n = 8–9/group; $F_{genotype}(1,15) = 27.1$; $p < 0.001$.
J.(Qi Zhang, Qijun Tang) ITT; repeated-measures two-way ANOVA with Bonferroni post hoc comparison; n = 6–8/group; $F_{genotype}(1,12) = 11.2$; $p = 0.006$.
Data are represented as mean ± SEM. *$p < 0.05$; **$p < 0.01$; ***$p < 0.001$. See also Figure S5.

c.2.3 Discussion

Modern society places a significant burden on the primitive circadian machinery whereby the central pacemaker is under constant dysregulation by artificial lighting. Moreover, easy access to palatable foods contributes to maladaptive eating, obesity and metabolic disease in rodents and humans [103,104,154]. Diets rich in fat and sugar increase out-of-phase food consumption, however, the neuronal correlates of meal

timing have remained elusive. Here, we identify a novel mechanism by which energy-rich foods dysregulate properly timed consumption by interfering with neural activity of the central circadian pacemaker within the SCN. This modulation results in increased foraging between meals and overconsumption leading to obesity. We observe that Drd1 expression is necessary for HFD-induced rest-phase hyperphagia, amplitude reduction in circadian oscillations of metabolic rhythms, lengthening of wheel running circadian period, and obesity. We also demonstrate that DA turnover within the SCN increases in response to HFD, while stimulation of the Drd1 signaling in the SCN dampens the overall activity of this nucleus. Lastly, Drd1 expression only within the SCN is sufficient to promote HFD overconsumption and metabolic disease. Therefore, we hypothesize that elevated DA during access to HFD increases out-of-phase foraging and overconsumption by Drd1 mediated reduction in SCN activity. In this view, DA, beyond providing hedonistic signaling via the mesolimbic circuit, also hinders anorexic output from the central circadian pacemaker between mealtimes contributing to excessive calorie intake. Diet regimens that involve time restricted feeding are growing in popularity because they attenuate BW gain and significantly improve metabolic profiles in rodents and humans [97,98,102,155]. Our findings demonstrate that the lack of Drd1-signaling imposes self-restricted, energy-rich food consumption predominantly during the active-phase, and provides timely insight to how rewarding, energy dense foods interfere with meal timing and diet adherence.

Surprisingly, re-expression of Drd1 signaling within the NAc, a hub of reward processing, fails to increase daily HFD consumption and induce obesity in KO mice

(Figure 3). These results parallel another study in which NAc-Rescue mice fail to perform at control levels in a progressive ratio task although they exhibit marked improvements in instrumental responding for reward [130]. Of note, NAc-Rescue animals increase their daytime HFD consumption, but compensate for the increase by reducing nighttime consumption, which leads to the maintenance of twenty-four hour HFD intake similar to the KO mice levels (Figure 1 and 5). Although this pattern of feeding in NAc-Rescue mice does not induce weight gain or alteration in glucose and insulin responsiveness, it leads to a moderate increase in adiposity (Figure 3). This increase might be the result of the metabolic disorganization caused by out-of-phase food consumption similar to what has been observed in day time TRF experiments [98,101]. By contrast, re-expression of Drd1 within the SCN increases daytime foraging, without significantly disrupting feeding at night, resulting in daily overconsumption (Figure 6). We postulate that the Drd1-dependent DA signaling within the NAc supports foraging for palatable foods [156], but the increased out of phase energy intake is compensated for by a homeostatic response. Our observations reveal a critical role for the Drd1-SCN signaling in energy balance during HFD consumption and also suggests that increased daytime consumption without an increase in overall energy intake is insufficient for significant weight gain.

Activities that enhance dopaminergic signaling such as exercise, access to a running wheel or energy-dense diets are known to influence circadian regulated behaviors [62,78,157,158]. Most relevant to our studies, consumption of HFD increases the period length of general activity rhythms, which is driven by the period of the

Drd1-positive SCN cells (Figure 4) [62,78]. Accordingly, Drd1 agonist treatment lengthens the period of *Per2* expression in SCN slices [159]. In line with these reports, the wheel running activity period of WT but not Drd1-KO mice rapidly and reversibly changes in response to HFD (Figures 5 and S5) suggesting that the diet composition governs behavioral circadian periods in a Drd1-signaling dependent manner.

Drd1-DA neurotransmission outside the SCN has also been implicated in a variety of circadian behaviors [23,39,136,160–162]. For instance, while NAc Drd1-activity regulates the transitions from sleep to wakefulness, Drd1 in the dorsal striatum plays a critical role in food anticipatory activity (FAA) following calorie restriction [39]. Ablation of these striatal dopamine signaling pathways in Drd1-KO mice could formally contribute to the observed circadian feeding patterns on HFD. However, in our studies, WT and KO mice demonstrate similar levels of rest phase locomotor activity (Figure 2) and hourly putative sleep duration (Figure S2) suggesting minimal roles for these pathways in the resistance of diet-induced obesity in KO-HFD mice. Additionally, reinstatement of WT-like HFD-induced metabolic and behavioral responses in SCN-Rescue animals reiterates that the circadian structure of rewarding food consumption and the associated weight gain is facilitated primarily through Drd1 signaling within the SCN. A complement to our current approach is selective SCN ablation of the Drd1 expression, which would reveal whether Drd1-signaling in this nucleus is required for diet-induced obesity. However, our efforts towards this goal could only accomplish partial Drd1 knock-down (Figures S5H-K), which was not sufficient to

prevent diet-induced obesity. Therefore, future studies will focus on combinatorial transgenic ablation strategies to generate a complete SCN specific Drd1-KO line.

A vast majority of SCN neurons are GABAergic and exhibit synchronous neural activity that fluctuates across the day:night cycle [152]. Their activity is high during the day, producing an inhibitory tone within their projection sites throughout the hypothalamus (DMH and SPVZ), thalamus, and basal forebrain [163,164]. In mice, this diurnal activity suppresses behavioral responses usually observed during the nighttime such as feeding and foraging [165]. Here, we demonstrated that increased SCN-Drd1 signaling or optogenetic stimulation of Drd1-SCN neurons reduces neuronal activity within the SCN or inhibits postsynaptic SCN neurons, respectively. Therefore, we postulate that in response to rewarding foods, increased DA tone decreases the overall excitability within the SCN. This decrease in activity mimics the nighttime SCN neuronal activity, which is permissive for foraging, leading to overconsumption of available energy-rich foods. The precise downstream targets of the SCN-Drd1 circuit will be the focus of future investigations seeking to uncover how circadian rhythms integrate with the orexigenic signals at the neurocircuitry level.

c.2.4 Acknowledgements

We are especially thankful for technical assistance from Aundrea Rainwater, Elena Tenore, Tarun Vippa, Charles Brennan, Sydney P. Williams, Charles Sheehan, and Yağmur Halezeroğlu. Jacqueline Parker and Alexander Duval (HPLC), Wenfan Ke and Eyleen O'Rourke (Oil-Red-O), Maisie Crook, Elise L. Savier, and Jianhua Cang (Rabies

virus tracing). Additionally, we are grateful for assistance from the research histology core, UVA school of medicine (H & E histology), UVA department of biology genomics core facility (AnThu Ngyugen, 16s sequencing), and UT Southwestern metabolic core (fecal bomb calorimetry). Lastly, we are thanking Ignacio Provencio for manuscript revision, as well as Michael Menaker for experiment feedback. This work was supported by NIH National Institute of General Medicinal Sciences R01GM121937 (A.D.G.), University of Virginia (UVA) Faculty Start-up Funds (A.D.G.), UVA Brain Institute 2018 Seed Funding Award (A.D.G.), UVA Presidential Fellowship for Collaborative Neuroscience (Q.Z.), NIH5R01GM84128 (J.H.), NIH National Institute of General Medical Sciences unC3GM125570 (A.D.S), Whitehall Foundation Research Grant (A.D.S.), 1R01MH116694-01A1 (M.M.S.), American Diabetes Association, Pathway to Stop Diabetes Award 1-18-INI-14 (J.N.C.), and lastly we acknowledge the Keck Center for Cellular Imaging for the usage of the Leica confocal microscopy system (RR025616).

c2.5 Author Contributions

R.M.G., Q.T., and A.D.G. conceived and designed the experiments, with input from all co-authors. R.M.G., Q.T., Q.Z., E.B.A., K.J.C., A.M.P., N.M.P., M.D.S., and M.S. performed viral surgeries, generation of experimental cohorts, and contributed to food consumption and BW data collection and analysis. Specifically, M.S. and A.D.S. collected data for germline Drd1 null mice and VGAT conditional knockout mice, Q.Z. performed qPCR, GTT and ITT experiments and analysis, S.R.C. conducted slice electrophysiology experiments, E.B.A. and M.M.S. performed progressive ratio

experiments, Y.G. and M.W. performed microbiome analysis, L.S. and A.S. performed immunoblotting experiments, Q.T., R.M.G. and J.N.C. performed retrograde tracing experiments, and R.M.G., N.M.P. and J.H. performed HPLC experiments. M.M.S. and C.D.D. provided guidance in experimental design and data interpretation. R.M.G., Q.T. and A.D.G. wrote the manuscript with input from all co-authors.

c2.6 Materials and Methods

Lead contact and materials availability

This study did not generate new unique reagents or mouse lines. Further information and requests should be directed to and will be fulfilled by the Lead Contact, Ali D. Güler (aguler@virginia.edu).

Experimental model and subject details

All animal care experiments were conducted in concordance with University of Virginia Institutional Animal Care and Use Committee (IACUC). Animals were housed in a temperature and humidity controlled vivarium (22-24°C, ~40% humidity) until experimental use on a 12-hour:12-hour light:dark (LD) cycle and were provided with food and water ad libitum and cotton nesting material (Ancare, Bellmore, NY). All behavioral assays were conducted with male C57BL6/J mice which were 12-14 weeks old at the onset of food intake experiments. In addition to wild-type C57BL6/J mice, the following mouse lines were used: *Drd1a*$^{Cre/+}$ (Drd1-HET) [26], CamKIIa-cre$^{T29\text{-}1Stl/}$J [84], Drd1$^{tm2.1Stl}$/J (Floxed-Drd1 or Drd1$^{fl/fl}$) [55], Drd1^{tm1Jcd}/J (Drd1 -/-) [27], Slc32a1tm2(cre)Lowl/J (VGAT-Cre) [57], and C57BL/6-Tg(Nms-icre)20Ywa/J (NMS-Cre) [85]. *Drd1a*$^{Cre/Cre}$ (KO) mice and littermates were raised on Teklad 8664 (Envigo, United Kingdom) placed on the cage floor as Drd1-KO mice were more likely to consume food when it was readily accessible.

Mouse diets

Standard chow diet (SCD):Teklad 8664 (Envigo, United Kingdom: 3.1 kcal/gram; 19% fat, 31% protein, 50% carbohydrates), Teklad 7912 (Envigo, United Kingdom: 3.1 kcal/gram; 17% fat, 25% protein, 58% carbohydrates) or PicoLab Rodent Diet 20 5053 (3.07 kcal/gram; 13% fat, 24% protein, 62% carbohydrates; 3.2% sucrose). High-fat, high-sugar diet (HFD): Open Source D12451 (4.73 kcal/gram; 45% fat, 20% protein, 35% carbohydrates; 17% sucrose). For Figure 3 and Figure S3 floxed animals, Normal chow diet (NCD), Teklad 2018 (3.1 kcal/gram; 18% fat, 24% protein, 58% carbohydrates). High-fat, low-sugar diet: BioServ F3282 (Flemington, New Jersey: 5.49 kcal/gram; 60% fat, 15% protein, 26% carbohydrates). Ensure original vanilla (24.3% fat, 16.2% protein, 59.5% carbohydrates).

Food intake measurements

Adult mice were housed individually in standard home cages with *ad libitum* access to SCD food and water throughout all experiments. For longitudinal feeding experiments, 12-14 week old mice were then randomly assigned into two different feeding regimens, SCD or HFD. All mice were maintained on SCD for an additional two weeks to measure baseline food intake and weight change. SCD animals remained on SCD for an additional four weeks at the time of the “diet switch” while the HFD group was given *ad libitum* access to HFD. Pre-weighed food pellets were placed on the cage floor and refreshed weekly. Body mass was measured weekly. For the daily feeding studies, animals were maintained on SCD or habituated to HFD for at least three days prior to the start of intake measurements. Pre-weighed food pellets were given on the cage floor at the start of the experiment, and body mass and food intake was measured at intervals of 12 h (ZT 0 and ZT 12) over a 72 h period starting at ZT 12. Food intake measurements were obtained by subtracting the mass of the residual food pellets from the total food given. Total caloric intake was calculated by multiplying the calories per gram of food and the mass of food consumed.

Constant darkness food intake

Mice were individually housed in standard cages, entrained to a 12-hour:12-hour light:dark (LD) cycle, then released into constant darkness (DD) for at least seven days. Following release to DD, homecage general activity was monitored using infrared (IR) beam beaks with six minute internals. The initiation of the subjective night and circadian free-running period (DD night; CT 12) was predicted for each animal using ClockLab collection and analysis system (Actimetrics, Wilmette, IL). Initiation of subjective day (DD day; CT 0) was calculated by the addition of half the free-running period length to CT 12 for each individual animal. The final collection point was determined by adding the duration of the endogenous free running period to the CT 12.

Fecal bomb calorimetry

Fecal output data was collected over a period of 72 hours. TheGI feces within the bedding was collected, freeze dried (Labconco) and weighed. For analysis of fecal calorie content, samples were collected, 2 mice/ n sample (~1 gram/sample) for fecal bomb calorimetry (Par 6200 isoperibol calorimeter, UT southwestern).

Histological analysis and imaging

Animals were deeply anesthetized (ketamine:xylazine, 280:80 mg/kg, i.p.) and perfused intracardially with ice cold 0.01 M phosphate buffer solution (PBS) followed by fixative solution (4% paraformaldehyde (PFA) in PBS at a pH of 7.4). After perfusion, brains were dissected and post-fixed overnight at 4°C in PFA. Freshly collected brains, after cervical dislocation were incubated in cold 4% PFA for 48 hours. Fixed brains were then rinsed in PBS, transferred into 30% sucrose in PBS for 24 hours, and then frozen on dry ice. Coronal sections (30 µm) were collected with a cryostat (Microm HM 505 E). Sections were permeabilized with 0.3% Triton X-100 in PBS (PBS-T) and blocked with 3% normal donkey serum (Jackson ImmunoResearch) in PBS-T (PBS-T DS) for 30 min at room temperature. Sections were then incubated overnight in primary antibodies diluted in PBS-T DS. For visualization, sections were washed with PBS-T and incubated with appropriate secondary antibodies diluted in the blocking solution for 2 hours at room temperature. Sections were washed three times with PBS and mounted using

DAPI Fluoromount-G (Southern Biotech). Images were captured on a Zeiss Axioplan 2 Imaging microscope equipped with an AxioCam MRm camera using AxioVision 4.6 software (Zeiss). Confocal microscope imaging was performed in W.M. Keck Center for Cellular Imaging, University of Virginia, with Leica SP5 X imaging system. The following primary antibodies were used for fluorescent labelling: anti-Drd1 (rat, 1:500, Sigma D2944), anti-HA (rabbit, 1:500, Cell Signaling Technology C29F4), anti-c-Fos (rabbit, 1:1000, synaptic systems), anti-GAD65/67 (rabbit, 1:2,000, Abcam ab49832), anti-tyrosine hydroxylase (chicken, 1:500, Millipore AB9702), anti-GFP (rabbit, 1:1k, Invitrogen A-6455). The secondary antibodies (Jackson ImmunoResearch) used were Cy2- or Cy3-conjugated donkey anti-rat IgG (1:250), donkey anti-rabbit (1:250) and Alexa Fluor 488-conjugated goat anti-chicken IgY (1:250, Invitrogen A11039).

PER2-DAB

Brains sections were permeabilized and blocked via the process described above. anti-PER2 (rabbit; 1:1000 AlphaDiagnostic International, PER21-A) primary antibody was incubated at 4 °C for 20 hours. Secondary antibody and DAB staining was processed with a VECTASTAIN Elite ABC-HRP Kit following the company-recommended protocol.

Oil-Red-O

PFA fixed tissue was rinsed in 1% PBS, transferred to 30% sucrose overnight, then frozen in 2-Methylbutane chilled by dry ice. 8 µm thick sections were collected with a cryostat (Microm HM 505 E) and mounted onto gelatin coated slides. Slides were treated with Oil Red O (ORO) solution (3mg/ml in 60% isopropanol) for 18 hours. Sections were then imaged by Nikon ECLIPSE Ti microscope equipped with a Nikon DS-Ri2 color camera.

Hematoxylin & Eosin (H & E) staining

Bouin's solution fixed tissues were washed 2 x 5 min in PBS and 3 x 5 min in 70% EtOH. Tissues were then sent to UVa Research Histology Core for paraffin embedding,

sectioning (6µm) and H&E staining. Sections were imaged in the same way as ORO sections above.

Western blot p-HSL

Samples of GWAT were collected from *ad libitum* fed mice at ZT 6 and flash frozen in liquid nitrogen. Adipose samples were homogenized in lysis buffer and centrifuged at 18,000g at 4°C for 20 minutes. The resultant supernatant was collected into a fresh eppendorf tube and protein levels in extracts were determined using the BCA method (Peirce). Protein was loaded equally (30 µg/lane) into lanes of a 4-15% gradient gel (BioRad) and separated by SDS-PAGE, and blotted onto 0.2 micron PVDF membranes. Blots were blocked for 1 hour at room temperature in a half-strength mixture of LiCOR Blocker (LiCOR Blocker (TBS): 1X TBS buffer). Primary antibody against HSL (Cell Signalling Technology 4107), and pHSL 660 (Cell Signalling Technology 4126) rabbit polyclonal used at 1:2000. The blots were washed in 1X TBS containing 0.01% Tween-20, and secondary antibody goat-anti-rabbit LiCOR 800CW was applied in LiCOR Blocker (TBS): 1X TBS buffer, used at 1:10,000 dilution for one hour at room temperature. Signal was normalized against tubulin using hFAB rhodamine-labelled anti-tubulin antibody fragment (BioRad 12004166), used at 1:2,000, and incubated along with LiCor 800 CW secondary. Finally, the blot was washed 6 times for 5-10 minutes each in 1X TBS + 0.01% Tween-20 followed by 2 final rinses for 5-10 minutes in 1X TBS alone. The blot was dried and imaged by fluorescence on a LiCor BioRad ChemiDoc MP station and bands quantified using BioRad ImageLab software. Protein concentrations of pHSL were determined by quantitative blot immunolabeling by a trained experimenter, blind to genotype and dietary conditions

Viral expression and stereotaxic surgery

During surgery, animals were anesthetized with isoflurane (induction 5%, maintenance 2%–2.5%; Isothesia) and placed in a stereotaxic apparatus (Kopf). A heating pad was used for the duration of the surgery to maintain body temperature and ocular lubricant was applied to the eyes to prevent desiccation. A double-floxed inverted open reading

frame (DIO) cassette containing recombinant AAV was used to express specific transgenes in Cre-expressing neurons. AAV was delivered using a 10 µl syringe (Hamilton) and 26-gauge needle (Hamilton) at a flow rate of 100 nl/min driven by a microsyringe pump controller (World Precision Instruments, model Micro 4). The syringe needle was left in place for 10 min and was completely withdrawn 20 min after viral delivery. Following surgery, mice were administered ketoprofen (3 mg/kg) subcutaneously as an analgesic. Animals were tested at least two weeks following virus injection to ensure optimal transgene expression. All surgical procedures were performed in sterile conditions and in accordance with University of Virginia IACUC guidelines.

Viral constructs

AAV2-hSyn-DIO-ChR2-YFP, AAV1-hSyn-ChR2-eYFP, AAV1-CAG-DIO-Drd1-HA (500 nl; 1.1 x 10^13 viral genomes/ul) were injected into the NAc (ML: + 1.15 mm, AP: + 0.98 mm, DV: - 5.75 mm), SCN (ML:±0.29 mm, AP: - 0.30 mm, DV: -5.75 mm). All coordinates are relative to bregma (George Paxinos and Keith B. J. Franklin).

Retrograde tracing

Rabies virus tracing: 500nl AAV1-synP-FLEX-splitTVA-EGFP-B19G was injected to SCN of Drd1-HET mice using the method described above. Three weeks after AAV injection, 120nl EnvA-dG-Rabies-H2B-mCherry was delivered to the same coordinates. After one week, animals were deeply anesthetized (ketamine:xylazine, 280:80 mg/kg, i.p.) and perfused intracardially with ice cold 0.01 M phosphate buffer solution (PBS) followed by fixative solution (4% paraformaldehyde (PFA) in PBS at a pH of 7.4). Tissue was then processed for antibody labeling as described above.

Circadian behavioral analysis

To record the rhythm of locomotor activity, adult male mice were individually housed in activity wheel-equipped cages (Nalgene) in light-tight boxes under a 12h :12h LD cycle for at least 7 days. Fluorescent lights (100 mW/cm^2) were used for behavioral

experiments. Food and water were provided ad libitum. Wheel running rhythms were monitored and analyzed with ClockLab collection and analysis system (Actimetrics, Wilmette, IL). The free-running period was calculated according to the onset of activity across seven days in constant darkness. Activity onset was identified through ClockLab software as the first bin above a threshold of 5 counts preceded by at least 6 hours of inactivity and followed by at least 6 hours of activity. When necessary, onset and offset points were edited by eye. All data was analyzed by a trained scorer blind to genotype.

Putative sleep analysis by infrared chamber

WT-HFD and KO-HFD mice were individually housed in standard cages with *ad libitum* access to water and food. Assessment of activity/inactivity was recorded by Animal Activity Meter: Opto-M4 (Columbus Instruments, Columbus, OH). This system provides horizontal infrad-red beams that are 0.5 inches apart. The accompanying software provides counts of total and ambulatory activity of animals, in 10 second intervals. We examined total activity counts in the X-plane. Zero total beam-break activity for more than 40 consecutive seconds was determined to be putative sleep as described in [86].

SKF-81297 to NAc-rescue locomotor assay

Mice were habituated to experimental housing conditions for 30 minutes. Following 20 minutes of baseline activity recordings, 7.5 mg/kg SKF-81297 (in saline) was administered by i.p. Injection. An additional 90 minutes of animal activity was recorded for analysis. Movement was tracked by EthoVision XT 11 (Noldus) and analyzed by EthoVision XT 11 (Noldus) and a custom Matlab script.

Glucose tolerance

Five weeks after the time of diet change, mice were fasted for 16 hours (ZT 10 - ZT 2), and fasted glucose was recorded using a Glucometer (One Touch Ultra) by tail bleeds [10]. Subsequently, mice received an i.p injection of glucose (1g/kg BW in saline), and blood glucose was measured in intervals of 30 minutes for 2 hours.

Insulin tolerance

Five weeks after the time of diet change, mice were fasted for 4 hours (ZT 1 - ZT 5), and fasted glucose was recorded using a Glucometer (One Touch Ultra) by tail bleeds. Subsequently, mice received an i.p injection of insulin (0.75units/kg of BW in saline), and blood glucose was measured in intervals of 15 minutes for 1 hour [87]. The time of collection (ZT 2 for GTT and ZT 5 for ITT) was chosen during peak response to the glucose challenge which falls between ZT 2 and ZT 8 [88].

Body composition

Six weeks after the time of diet change SCAT, GWAT, and liver were harvested, weighed, placed into a chilled 4% PFA solution or Bouin's solution (fisher scientific) for fixation. Whole tissue was imaged (Canon EOS Rebel Xsi) before fixation. A ruler was used to scale each tissue.

Echo MRI

Body fat and lean mass four weeks after diet change were assessed using an Echo MRI (The EchoMRI™-100H) following the manufacturer's protocol.

Comprehensive Lab Animal Monitoring System (CLAMS)

Indirect calorimetry in a CLAMS system (Columbus Instruments) was used to evaluate whole-body states and ambulatory locomotor activity during *ad libitum* access to SCD or HFD. Four weeks after diet change, mice were acclimated to metabolic cages for 48 hours and then monitored for 72 hours following the manufacturer's instructions. Energy expenditure (EE) in watts per kilogram of lean mass [W/kg] was calculated with the following formula described in [89].

EE [W/kg]=1/60*((0.2716 [W*min/ml]*VO2 [ml/kg/hour])+(0.07616 [W*min/ml]*VCO2 [ml/kg/hour])

The unit Watts was converted to kcal/hour by multiplying factor of 0.86 to report EE as kcal/hour/kg of lean mass. The resting metabolic rate (RMR) was quantified and defined as the average of the lowest 5 consecutive energy expenditure values (18 minute intervals) across a twenty-four hour day.

QPCR

Six weeks after the time of diet change, WT-SCD, KO-SCD, WT-HFD, and KO-HFD mice were sacrificed by cervical dislocation every four hours along the LD cycle (3 mice/timepoint: ZT 1,5,9,13,17,21). Tissue collected from mice during the Night phase were sacrificed in the dark under IR light with night-vision goggles. Dissected liver and GWAT tissue was flash frozen in liquid nitrogen. RNA was extracted with the RNeasy Lipid Tissue Mini Kit (QIAGEN). For liver and GWAT, 1100 ng of RNA was reverse-transcribed using a SuperScript™ IV First-Strand Synthesis System kit (Thermo Fisher). Quantitative PCR was performed using the iQ™ SYBR® Green Supermix system (BIO-RAD). Beta-actin was used as a housekeeping gene for the analysis of *Bmal1*, *Per2*, and *Rev-erbα*. The relative mRNA levels were calculated using the $2^{-\Delta Ct}$ method. The ΔCt values were obtained by calculating the differences: Ct(gene of interest) – Ct(housekeeping gene) in each sample. All groups were normalized relative to WT-SCD median of 1.

FITC-Dextran

For the intestinal permeability assay, tracer fluorescein isothiocyanate (FITC) labeled dextran (4kDa; Sigma-Aldrich) was used to assess in vivo intestinal permeability. At ZT 2 mice were deprived of food 4 hours prior to and 4 hours following an oral gavage (ZT 6) using 150 µl of 80 mg/ml FITC-dextran. Blood (50µl) was collected from tail bleeds, and fluorescence intensity was measured on fluorescence plates using an excitation wavelength of 485 nm and an emission wavelength of 530 nm [90].

Foraging assay

Animals were habituated to experimental conditions for 4 days prior to testing. On the 1st and 2nd day 1 pellet of HFD was placed on the homecage floor for diet habituation. On the 3rd day mice were moved to a larger testing cage (144 in^2; 18 (L) x 8 (W) x 8 (H)) with ad libitum access to SCD and 1 pellet of HFD on cage floor. 4th day: ad libitum access to SCD in home cage. After this habituation, the foraging assay was performed at either ZT 8 (Day) or ZT 15 (Night). Mice were place into the testing cage with 1~1.5cm deep bedding for 30 minutes. A pellet of HFD diet was buried beneath the bedding at one end of the testing cage. Mice were then placed onto the opposite end of the testing cage, video recorded, and tracked by EthoVision XT 11 (Noldus) (Day) or a night-vision sports camera (Night) for 3 minutes. The latency of the animals' first intentional foraging of the food area scored by an investigator blind to genotype. The mice (1/15 WT and 2/10 KO) that failed to perform a foraging behavior within 2 minutes were counted as 120 seconds.

Progressive ratio test

Operant conditioning occurred in noise-controlled chambers under red lighting (Med-Associates, St. Alban, VT, USA). Prior to progressive ratio (PR) test, mice underwent fixed ratio (FR) training sessions for a minimum of three days. During training, a single nosepoke (FR1) in the center hole (of three possible entries) resulted in the delivery of a food reward (chocolate pellet) from an automatic dispenser. After earning 50 reinforcers, training advanced to a FR3 schedule of reinforcement, whereby three nosepokes in the center hole were required for the delivery of the food reward. After earning 50 reinforcers on this schedule, training advanced to FR5. For progressive ratio test, one reward pellet was delivered per completed trial in which the nosepoke requirement increased on the following schedule: 1, 3, 5, 10, 20, 30, 50, 70, 100, 130, 170, 210, 260, 310, and 370. Animals were allowed 30 minutes to complete each level of trial following the initial nosepoke. Mice were trained and tested during both the light and dark phase and the order of testing was counterbalanced. In between tests, animals were placed in a reversed light cycle for 7 days for entrainment. Training and testing began at ZT 0 (Day) or ZT 12 (Night).

Open field testing

Animals participating in the progressive ratio experiments underwent open field testing to measure locomotor behavior. Testing occurred in a closed, translucent plexiglass open field chamber (42x42 cm) at ZT 1 (Day) and ZT 13 (Night). Mice were placed on the edge of the open field and given five minutes to explore the area while distance travelled (cm) was recorded with EthoVision XT tracking software (Noldus, Leesburg, VA, USA).

HPLC

WT mice were habituated to HFD or SCD on the cage floor on the day prior to tissue collection. Animals were given 1 hour access to either HFD or SCD and sacrificed by cervical dislocation. Fresh brains were dissected from adult wild-type male animals and 1 mm coronal slices were collected using a mouse brain matrix (Zivic Instruments). Hypothalamic samples containing the SCN were collected with a 1.5 mm in diameter tissue biopsy punch (Miltex), frozen in liquid nitrogen, and stored at 80°C until further processing. Tissue punches were homogenized by sonication in 50 µL of 0.04N perchloric acid solution. The homogenate was centrifuged at 13,200 rmp for 12 min at 4°C, followed by spin filtration (Sigma Aldrich) at 11,000 rpm for 4 min at 4°C. 15 µL of the resulting supernatant was loaded into an autosampler connected to a high-performance liquid chromatography instrument with an electrochemical detector (Decade, Antec Leyden B.V., Zoeterwoude, the Netherlands) to measure the levels DA and 3,4-Dihydroxyphenylacetic acid (DOPAC) and serotonin. Retention time for was determined through comparison with standards diluted in 0.04N perchloric acid. DOPAC tR range 4.56±0.015 min, DA: tR range 10.01±0.24 min, Serotonin: tR range: 22.165± 0.035 min. Mobile phase: pH 3, 10% acetonitrile, 0.50mmol DSA. 0.8V 0.125 ml/min, 26 °C 24 minutes 0.5µM of DSA. Identification of serotonin within the chromatogram was used to confirm the SCN in collected tissue punch [91].

Temperature recordings

Body temperature was measured using a rectal probe attached to a digital thermometer (Physitemp Instruments, Clifton, NJ). Temperatures were collected at ZT 6 (Day) and ZT 18 (Night).

Slice electrophysiology

Slice visualization and data collection: SCN cells were visualized with infrared DIC in an upright Slicescope 6000 microscope. The SCN was identified by the shape of the both 3rd ventricle and most inferior middle region of the slice, as well as the presence of the optic chiasm. Images of patched brain regions were taken using Scientifica SciPro camera and Ocular imaging software. A Multiclamp 700B amplifier and Digidata 1550B digitizer (Molecular Devices; San Jose, California) were used to perform all patch clamp experiments. All experiments were conducted using 2.5-6MΩ microelectrodes pulled with a Sutter P97 puller. All brain slice solutions were saturated with 95% O2 and 5% CO2 gas. SKF-81297 was used at 5μM concentration in all incubation experiments.

Cell attached recordings: Male and female WT mice were individually housed in light-tight boxes under a 12 hr:12 hr LD cycle for at least 7 days. Mice between P31 and P55 were deeply anesthetized with isoflurane and brains were rapidly dissected and mounted for slicing in the compresstome slicer. Slices were taken with in ice cold HEPES based holding ACSF solution containing (in mM): 92 NaCl, 2.5 KCl, 1.25 NaH2PO4, 30 NaHCO3, 20 HEPES, 25 glucose, 2 thiourea, 5 Na-ascorbate, 3 Na-pyruvate, 2 CaCl2·4H2O and 2 MgSO4·7H2O with pH ranging from 7.3 to 7.4 and osmolarity ranging from 300 to 310 mOsm [94]. Slices were allowed to recover for ≤12 min at 34°C in the same HEPES based holding ACSF solution, and then allowed to come to room temperature. ‘Day’ collections condition (sacrificed at ZT 5-6) were incubated for a minimum of 90 minutes, and data was collected between ZT 8 and 11. ‘Night’ collections condition (sacrificed at ZT 11-12) were incubated and data was collected at ZT 14 to 17. After a minimum of 90 minutes of incubation slices were transferred to the microscope recording bath and superfused with a continuous flow (1.5 - 2 ml/min) recording ACSF which consisted of (in mM): 124 NaCl, 2.5 KCl, 1.2 NaH2PO4, 24 NaHCO3, 5 HEPES, 10 glucose, 2 CaCl2·4H2O and 2 MgSO4·7H2O

with pH ranging from 7.3 to 7.4 and osmolarity ranging from 300 to 310 mOsm, and included the vehicle or agonist. The resulting DMSO concentration in these buffers ranged from 0.01% to 0.12%. Vehicle control solutions contained the same amount of DMSO as the treatment conditions. Drug solutions were added directly to the bath after the recovery incubation. Cell attached recordings were made at 32 °C. For cell attached recordings the pipette was filled with ACSF, slight positive pressure applied when approaching the cell was released and the seal was allowed. Seal magnitude ranged from 5 to 50MΩ. In all experiments the pipette offset was <15mV, typically ranging from 1 to 11mV. Pipette offset was set just before initiating a recording, and the seal resistance was monitored closely. Recordings measuring spontaneous spiking lasted approximately one minute. Recordings were filtered offline at 1kHz and baseline was manually adjusted using ClampFit (Molecular devices) software. Action potential events were then extracted using ClampFit and analyzed using custom scripts in Matlab (Mathworks).

Optogenetic stimulation: Heterozygous Drd1-HET mice minimum of 8 weeks of age received bilateral injections of AAV2-DIO-ChR2-YFP to the SCN as previously described. After a minimum of 5 weeks recovery animals were deeply anesthetized (ketamine:xylazine, 280:80 mg/kg, i.p.) and transcardially perfused with an NMDG recovery ACSF solution containing (in mM): 92 NMDG, 2.5 KCl, 1.25 NaH_2PO_4, 30 $NaHCO_3$, 20 HEPES, 25 glucose, 2 thiourea, 5 Na-ascorbate, 3 Na-pyruvate, 0.5 $CaCl_2 \cdot 4H_2O$ and 10 $MgSO_4 \cdot 7H_2O$, pH adjusted to 7.3 to 7.4, osmolarity 300 to 310 mOsm [94]. Slices were held in the NMDG recovery ACSF for ≤ 12 min at 34°C, and then transferred to recording ACSF (described above) and allowed to rest at room temperature for 45 minutes before being transferred to microscope bath for data collection. All recordings were made at room temperature and the same K-Glu intracellular solution was used as described above. SCN cells were randomly patched without regard for YFP expression. After formation of gigaohm seal (>2GΩ), cell membrane was ruptured and current clamp recordings acquired. A minimal current injection hold of 0 to -15pA was used to compensate for minor current leakage. Whole cell voltage measurements made as described for whole cell incubation recordings.

Optogenetic stimulation consisted a 500ms 20 Hz square pulses of 488 nm light (10 pulses total, each pulse 10ms). Light was delivered at the beginning of each 10 second trace. For a subset of cells (5) which showed a hyperpolarized response to blue light stimulation, recording ACSF with 100μM Picrotoxin (PTX) was perfused for 6 minutes and cell responses to the optogenetic stimulation protocol were recorded. No further recordings were made on slices which were exposed to PTX. Response magnitudes and latencies were manually extracted in ClampFit, and consisted of an average of 5-6 traces.

Adipose area quantification

Samples of GWAT were collected and fixed for H & E staining as described above. Three digital images (20x) from non-overlapping fields were captured for each sample (Nikon ECLIPSE Ti microscope equipped with Nikon DS-Ri2 color camera). Quantitative analyses of adipocyte area were made using ImageJ (National Institutes of Health, Bethesda, MD). Results are expressed as mean±SE μm^2 per cell. Exclusions: any cut off adipocytes on the image edge, cells that were artificially divided into multiple cells due to artifact, cells that were combined due to faintness of borders in the original image, and cells <350μm^2 [95].

Statistical analysis

When comparing two groups of normally distributed data, a Student's two tailed t-test was used. To compare the effects of genotype and diet within 4 groups, two-way ANOVA test was used. When data was collected from the same animals across time, a three-way ANOVA test was performed to analyze time, genotype and diet effect. In experiments with single variable and more than two groups, a one-way ANOVA was performed. Following a significant effect in the ANOVA test, Bonferroni's post hoc comparison was used to determine differences between individual data points. Permutational multivariate analysis of variance (PERMANOVA) was used to evaluate

microbiome OTUs and conducted in R. Analyses were conducted using the GraphPad Prism 8 statistical software for Windows, or Prism 8 for Mac OS. All data are presented as means±standard error of the mean with $p<0.05$ considered statistically significant.

c2.7 Data and Software Availability

The metagenomic sequence data were deposited at NCBI under Bioproject: PRJNA580025, available from: https://www.ncbi.nlm.nih.gov/bioproject/PRJNA580025

c2.8 Supplemental Figures

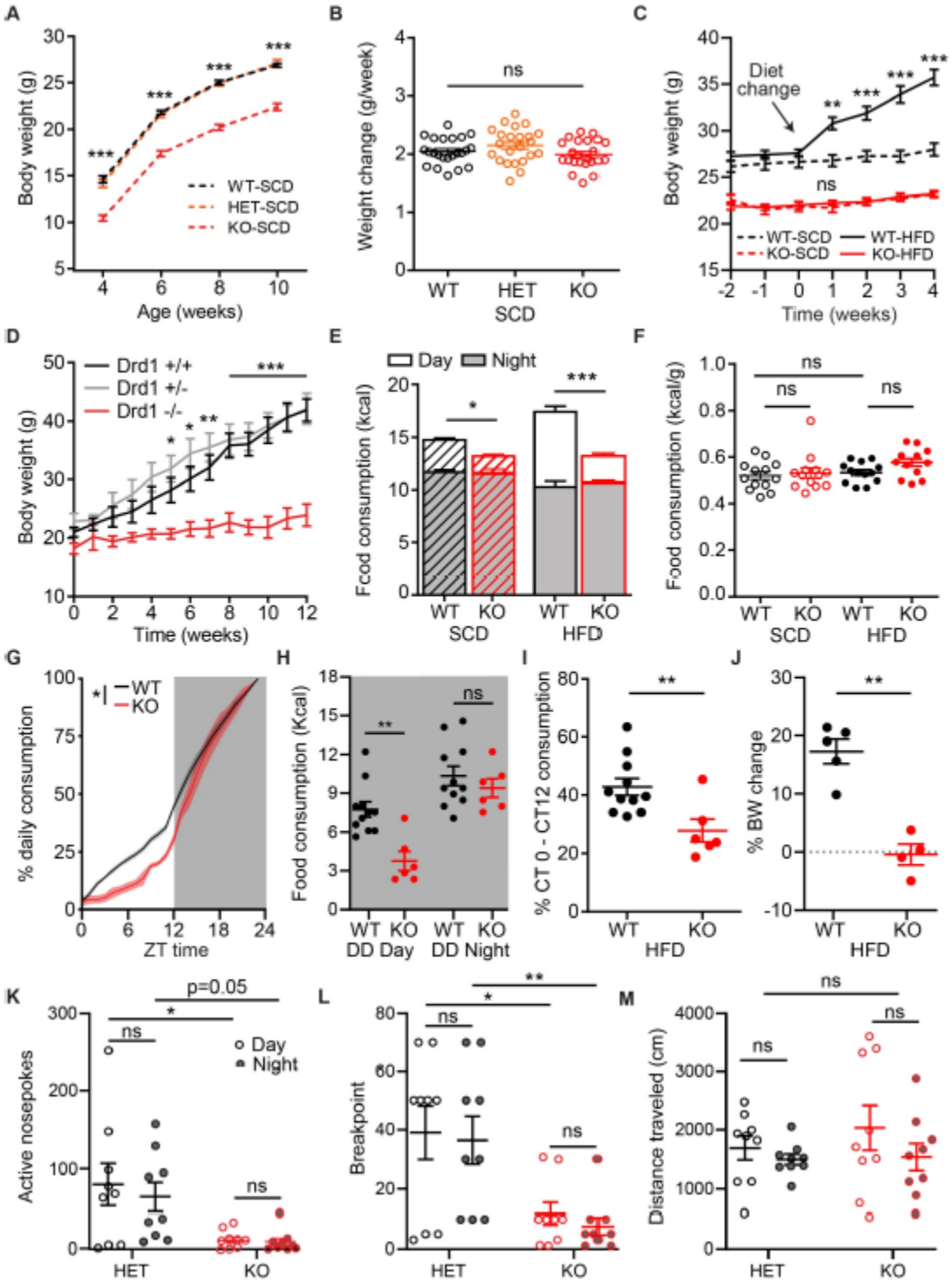

Figure S1. D1 Dopamine Receptor Expression is Required for HFD-induced Obesity. Related to Figure 1.

A.(Meghana Sunkara, Aarti Purohit, Ryan Grippo) KO mice raised on SCD are lean throughout development (4-10 weeks old). Post weaning BW change of $Drd1^{cre/cre}$ (KO), $Drd1^{cre/+}$ (HET) and $Drd1^{+/+}$ (WT) on SCD. Repeated-measures two-way ANOVA with Bonferroni post hoc comparison, n=23/group; $F_{genotype}(2,66)=77.1$, $p<0.001$. Statistical significance between WT and KO is depicted in the figure.

B.(Meghana Sunkara, Aarti Purohit, Ryan Grippo) Weekly rate of BW change for WT and KO animals from 4 to 10 weeks of age on SCD. One-way ANOVA, n=23/group. KO BW increased at a similar rate to WT and heterozygous (HET) littermates, suggesting that the growth retardation prior to weaning accounts for the majority of their reduced BW.

C.(Ryan Grippo, Qijun Tang) Raw value of BW change for WT and KO mice on SCD or HFD for data shown in Figure 1. Repeated-measures three-way ANOVA with Bonferroni post hoc comparison, n=7-13/group; $F_{genotype}(1,37)=155.7$, $p<0.001$; $F_{diet}(1,37)=13.3$, $p<0.001$. Statistical significance between diets within each genotype is depicted.

D.(Michael Sidikpramana, Andrew Steele) Weekly BW measurements of Drd1 null ($Drd1^{-/-}$), heterozygous ($Drd1^{+/-}$) and WT ($Drd1^{+/+}$) mice on a high-fat/low-sugar diet. Repeated-measures two-way ANOVA with Bonferroni post hoc comparison, n=4-8/group; $F_{genotype}(2,16)=15.2$, $p<0.001$. Statistical significance between $Drd1^{+/+}$ and $Drd1^{-/-}$ is depicted.

E.(Ryan Grippo, Qijun Tang) Daily total calorie consumption of WT and KO mice on SCD or HFD. Day (white) and Night (gray) consumption are segregated for clarity. Two-way ANOVA with Bonferroni post hoc comparison, n=13/group; $F_{genotype}(1,48)=54.5$, $p<0.001$; Fdiet(1,48)=12.1, p=0.001.

F.(Ryan Grippo, Qijun Tang) Daily food consumption normalized to BW. Two-way ANOVA with Bonferroni post hoc comparison, n=13/group. Normalized intake may not be different between genotypes due to the higher BW of WT-HFD mice which can underrepresent food intake in the overweight mice [166].

G.(Ryan Grippo, Meghana Sunkara) Cumulative liquid diet (ensure) consumption represented as percentage of whole-day consumption for KO and WT mice. Zeitgeber time (ZT), where ZT0 indicates onset of light-phase and ZT12 indicates onset of dark phase (shaded gray). Repeated measures two-way ANOVA, n=4/group; $F_{genotype}(1,6)=6.5$, $p=0.04$.

H.(Ryan Grippo, Qijun Tang) Calorie intake during the 12-hour subjective day (DD-Day) or subjective night (DD-Night) for WT-HFD and KO-HFD mice.

Repeated-measures two-way ANOVA with Bonferroni post hoc comparison, n=6-11/group; $F_{time}(1,15)=22.7$, $p<0.001$; $F_{genotype}(1,15)=15.7$, $p=0.001$.

I.(Ryan Grippo, Qijun Tang) Percent of total daily food intake consumed during the subjective day (DD-Day; CT 0 - 12) for WT and KO mice on HFD. Students two-tailed t-test, n=6-11/group.

J.(Ryan Grippo, Qijun Tang) Percent BW change following ten days in constant darkness (DD) on HFD. Student's two-tailed t test, n=4-5/group.

K.(Everett B. Altherr, Michael M. Scott) Active nosepoke counts for Drd1-HET (HET) and Drd1-KO (KO) mice during progressive ratio (PR) test during Day or Night. Repeated-measures two-way ANOVA with Bonferroni post hoc comparison, n=9/group; $F_{genotype}(1,16)=8.9$, $p=0.009$.

L.(Everett B. Altherr, Michael M. Scott) Breakpoint analysis for Drd1-HET and Drd1-KO mice during PR test during Day or Night. Repeated-measures two-way ANOVA with Bonferroni post hoc comparison, n=9/group; $F_{genotype}(1,16)=11.8$, $p=0.003$.

M.(Everett B. Altherr, Michael M. Scott) Distance traveled for Drd1-HET and Drd1-KO mice during an open field test at day or night. Repeated-measures two-way ANOVA with Bonferroni post hoc comparison, n=9/group. Since Drd1-KO mice traveled similar distance to controls in an open field test, this deficiency could not be attributed to significant motor impairment, but likely reflects operant learning deficiencies that have been previously reported [130]. Data are represented as mean±SEM.

*p<0.05,**p<0.01,***p<0.001, ns=not significant.

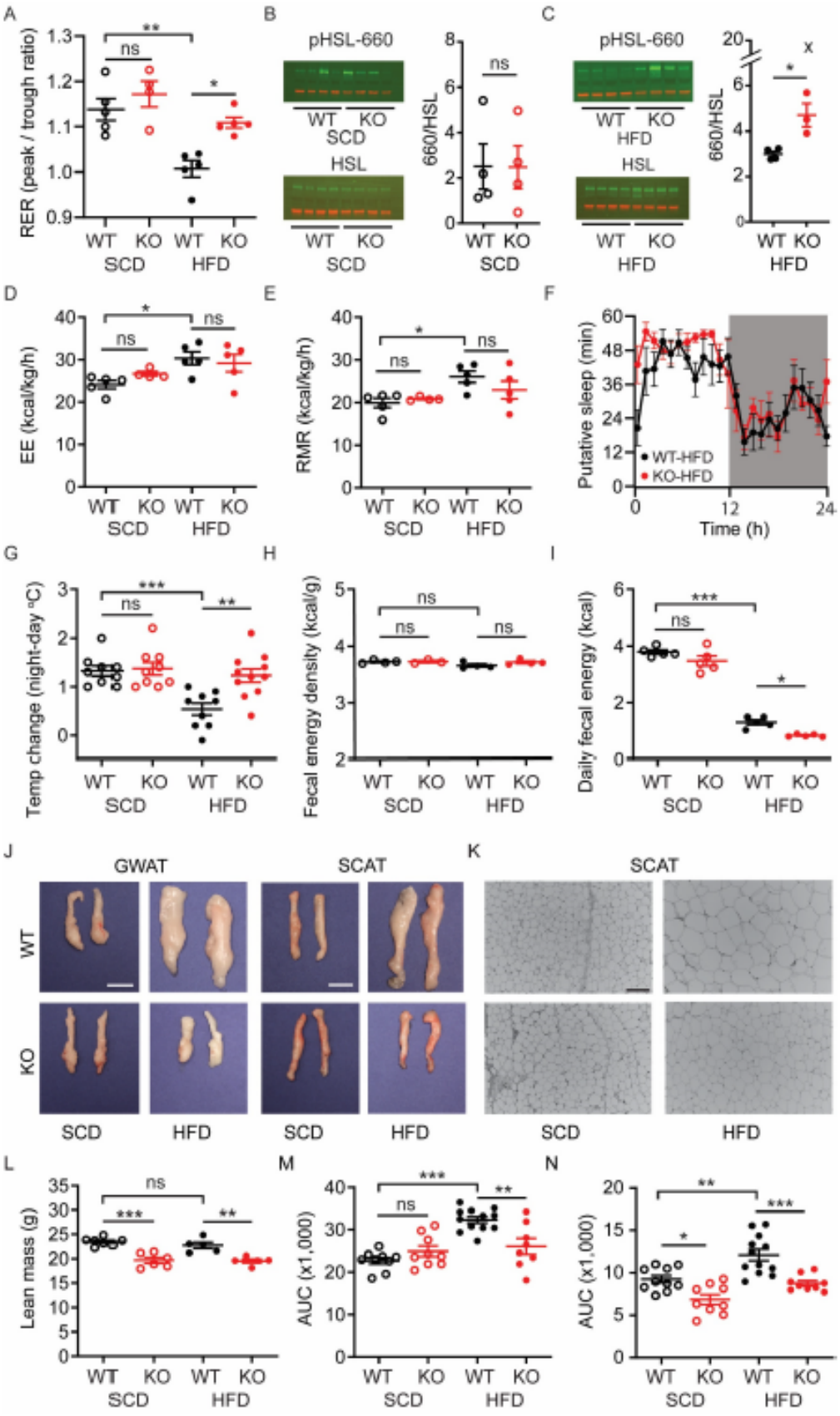
A
RER (peak / trough ratio)
1.3
1.2
1.1
1.0
0.9
**
ns
*
WT KO WT KO
SCD HFD
B
pHSL-660
WT KO
SCD
HSL
WT KO
SCD
660/HSL
8
6
4
2
0
ns
WT KO
SCD
C
pHSL-660
WT KO
HFD
HSL
WT KO
HFD
660/HSL
20
6
4
2
0
x
*
WT KO
HFD
D
EE (kcal/kg/h)
40
30
20
10
0
*
ns
ns
WT KO WT KO
SCD HFD
E
RMR (kcal/kg/h)
40
30
20
10
0
*
ns
ns
WT KO WT KO
SCD HFD
F
Putative sleep (min)
60
48
36
24
12
0
WT-HFD
KO-HFD
0
12
24
Time (h)
G
Temp change (night-day °C)
3
2
1
0
***
ns
**
WT KO WT KO
SCD HFD
H
Fecal energy density (kcal/g)
5
4
3
2
ns
ns
ns
WT KO WT KO
SCD HFD
I
Daily fecal energy (kcal)
6
4
2
0
***
ns
*
WT KO WT KO
SCD HFD
J
GWAT
SCAT
WT
KO
SCD
HFD
SCD
HFD
K
SCAT
SCD
HFD
L
Lean mass (g)
35
30
25
20
15
10
5
0
ns
***
**
WT KO WT KO
SCD HFD
M
AUC (x1,000)
40
30
20
10
0
***
ns
**
WT KO WT KO
SCD HFD
N
AUC (x1,000)
20
15
10
5
0
**
*
***
WT KO WT KO
SCD HFD

Figure S2. Supportive Metabolic Tests Illustrating the Resistance to High-Fat Diet-Induced Metabolic Syndromes of Drd1-KO Mice. Related to Figure 2.

A.(Ryan Grippo, Qijun Tang, Michael Scott) Group analysis of Night (ZT14-16)-Day (ZT3-5) RER ratio. Two-way ANOVA with Bonferroni post hoc comparison, n=4-5/group; $F_{diet}(1,15)=21.4$, $p<0.001$; $F_{genotype}(1,15)=10.4$, $p=0.006$.

B.(Anthony Spano, Laura Sipe) Left: Immunoblots visualized in green channel for pHSL 660 (top), and HSL (bottom) collected at ZT 6 from GWAT of WT and KO mice on SCD. Signal is normalized to tubulin levels (red channel). Right: pHSL 660/HSL ratio from left. Student's two tailed t-test, n=4/group.

C.(Anthony Spano) Left: Immunoblots visualized in green channel for pHSL 660 (top), and HSL (bottom) collected at ZT 6 from GWAT of WT and KO mice on HFD. Signal is normalized to tubulin levels (red channel). Student's two tailed t-test, n=4/group. One outlier in Drd1-KO group was detected by ROUT outlier test (Q=5%) and indicated as an x.

D.(Ryan Grippo, Qijun Tang, Michael Scott) Energy expenditure (EE; kcal/kg/hour) for WT and KO mice on SCD or HFD. Two-way ANOVA with Bonferroni post hoc comparison, n=4-5/group.

E.(Ryan Grippo, Qijun Tang, Michael Scott) Resting metabolic rate (RMR; kcal/kg/hour) for groups in (D). Two-way ANOVA with Bonferroni post hoc comparison, n=4-5/group.

F.(Ryan Grippo, Qijun Tang) Hourly putative sleep defined as total infrared beam breaks for more than 40 seconds in WT and KO mice on HFD. Repeated-measures two-way ANOVA, n=4-6/group. Although KO mice trend towards increased putative sleep during the light transition periods, they do not consume less HFD within this period.

G.(Ryan Grippo) Change in body temperature between ZT18 (Night) and ZT6 (Day) for groups in (D). Two way ANOVA with Bonferroni post hoc comparison, n=9-11/group; $F_{diet}(1,34)=13.5$, $p<0.001$; $F_{genotype}(1,34)=8.5$, $p=0.006$. Similar to WT-SCD animals, KO-HFD mice maintained lower body temperatures (Tb) during the midday (ZT6) compared to WT-HFD mice (WT-SCD: 36.5±0.1°C; KO-SCD: 36.4±0.1°C; WT-HFD: 37.2±0.1°C; KO-HFD: 36.5±0.1°C). Two-way ANOVA with Bonferroni post-hoc comparison, $p<0.001$. All groups had similar Tb at midnight (ZT 18; WT-SCD: 37.8 ± 0.1°C; KO-SCD: 37.7 ± 0.1°C; WT-HFD: 37.7 ± 0.1°C; KO-HFD: 37.8 ± 0.1°C) resulting in a significant Night:Day amplitude difference between WT-HFD and KO-HFD mice.

H.(Ryan Grippo) Fecal energy density measured by fecal bomb calorimetry for groups in (D). Two-way ANOVA with Bonferroni post hoc comparison, n=3-4/group.

I.(Ryan Grippo) Estimated energy lost to fecal waste in twenty-four hours for groups in (D). Two-way ANOVA with Bonferroni post hoc comparison, n=5/group; $F_{diet}(1,16)=567.3$, $p<0.001$; $F_{genotype}(1,16)=13.4$, $p=0.002$.

J.(Ryan Grippo, Qi Zhang, Qijun Tang) Representative dissected GWAT (left) and SCAT (right) images for groups in (D). Scale bar=1 cm.

K.(Ryan Grippo, Qi Zhang, Qijun Tang) Representative SCAT histology with Hematoxylin and Eosin (H&E) stain for groups in (D). Scale bar=100 um.

L.(Ryan Grippo, Michael Scott) Lean mass measured by Echo MRI four weeks after SCD or HFD diet in WT and KO mice. Two-way ANOVA with Bonferroni post hoc comparison, n=5-7/group; $F_{genotype}(1,19)=49.7$, $p<0.001$.

M.(Qi Zhang) Area under the curve (AUC) for GTT (from Figure 2). Two-way ANOVA with Bonferroni post hoc comparison, n=8-12/group, $F_{diet}(1,35)=21.1$, $p<0.001$; $F_{genotype}(1,35)=3.9$, $p=0.06$.

N.(Qi Zhang) AUC for ITT (from Figure 2L). Two-way ANOVA with Bonferroni post hoc comparison, n=9-12/group, $F_{diet}(1,36)=18.8$, $p<0.001$; $F_{genotype}(1,36)=27.3$, $p<0.001$. Data in all panels are represented as mean±SEM. *p<0.05,**p<0.01,***p<0.001.

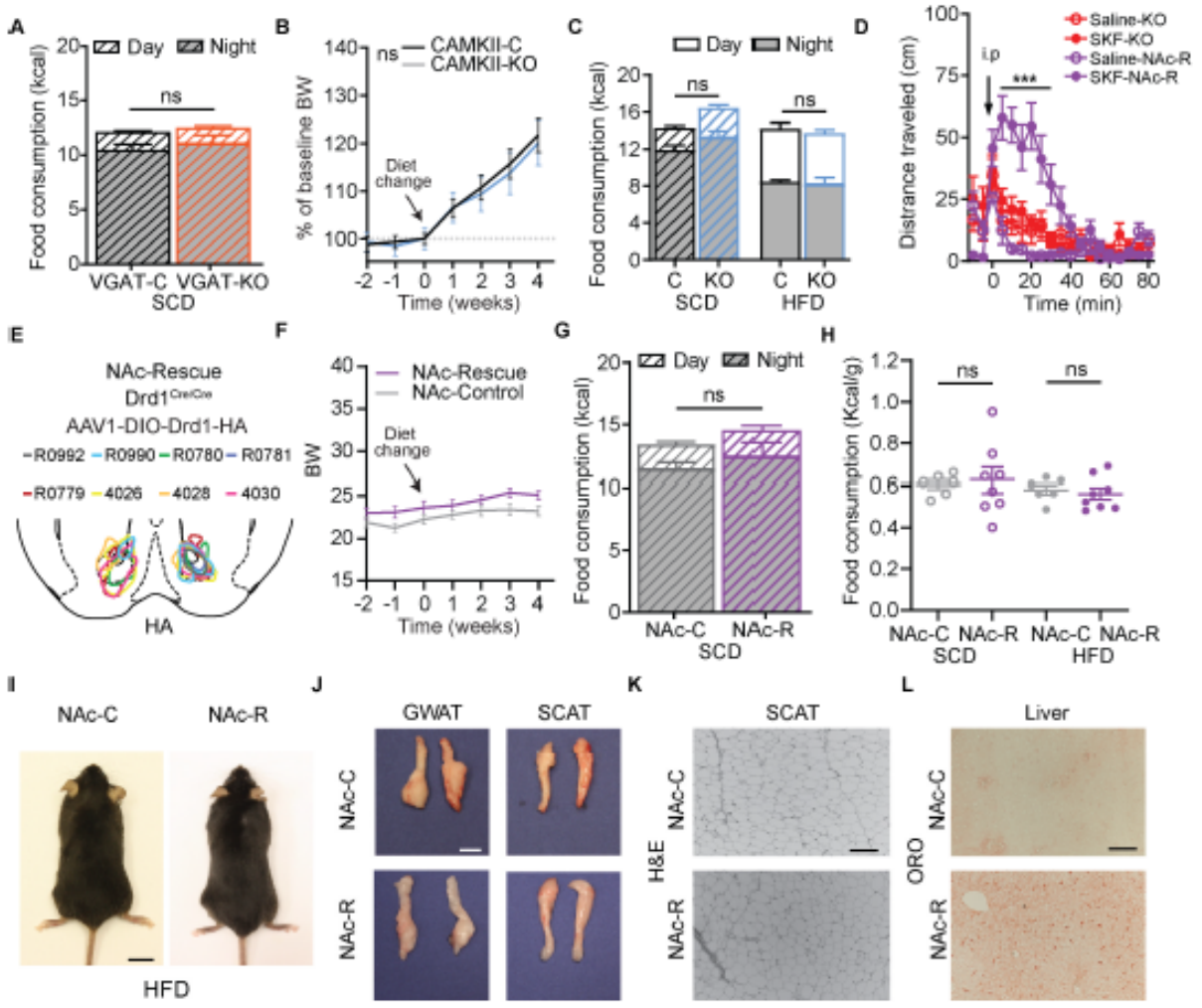

Figure S3. Additional Results Illustrating the Resistance of NAc-Rescue Mice to HFD Induced Obesity. Related to Figure 3.

A.(Michael Sidikpramana, Andrew Steele) Daily total calorie consumption of VGAT-C and VGAT-KO mice on SCD. Day- (white) and Night (gray) consumption are segregated for clarity. Student's two tailed t-test, n=7-16/group.

B.(Michael Sidikpramana, Andrew Steele) Percent BW change relative to week 0 for CAMKII$^{+/+}$;Drd1$^{fl/fl}$ (CAMKII-C) and CAMKII$^{Cre/+}$;Drd1$^{fl/fl}$ (CAMKII-KO) mice on HFD. Repeated-measures two-way ANOVA with Bonferroni post hoc comparison, n=10-11/group.

C.(Michael Sidikpramana, Andrew Steele) Daily total calorie consumption of CAMKII-C and CAMKII-KO mice on SCD or HFD. Day- (white) and Night (gray) consumption are segregated for clarity. Two-way ANOVA with Bonferroni post hoc comparison, n=9-11/group.

D.(Qijun Tang) Distance traveled by NAc-Rescue (NAc-R) or KO control mice following vehicle (saline) or Drd1 agonist SKF-81297 administration (i.p.). Repeated measures three-way ANOVA with Bonferroni post hoc comparison, n=7-8/group; $F_{treatment}(1,13)=16.8$, p=0.001. Statistical significance between SKF-NAc-R and Saline-NAc-R is depicted in the figure.

E.(Qijun Tang) Diagram showing traces of Drd1-HA expression pattern in NAc-Rescue mice.

F.(Qijun Tang) Raw value of BW change for NAc-C and NAc-R for data shown in Figure 3. Repeated-measures two-way ANOVA n=6-8/group. The arrow indicates the time of diet switch from SCD to HFD.

G.(Qijun Tang) Daily total calorie consumption of NAc-Control (NAc-C) and NAc-Rescue (NAc-R) mice on SCD. Student's two tailed unpaired t-test, n=6-8/group.

H.(Qijun Tang) Daily food consumption for NAc-C and NAc-R on SCD and HFD normalized to BW. Two-way ANOVA n=6-8/group.

I.(Ryan Grippo, Qi Zhang, Qijun Tang) Representative mouse images of NAc-Control (NAc-C) or NAc-Rescue (NAc-R) following the HFD feeding paradigm in Figure 1A. Scale bar=1 cm.

J.(Ryan Grippo, Qi Zhang, Qijun Tang) Representative images of dissected GWAT (left) and SCAT (right) for groups in (I). Scale bar=1 cm.

K.(Ryan Grippo, Qi Zhang, Qijun Tang) Representative SCAT histology (H&E) for groups in (I), scale bar=100 μm.

L.(Qijun Tang) Representative liver histology using Oil-red-O for groups in (I) where hepatic lipid content stains as red. Scale bar=100 μm. Data in all panels are represented as mean±SEM. *p<0.05,**p<0.01,***p<0.001.

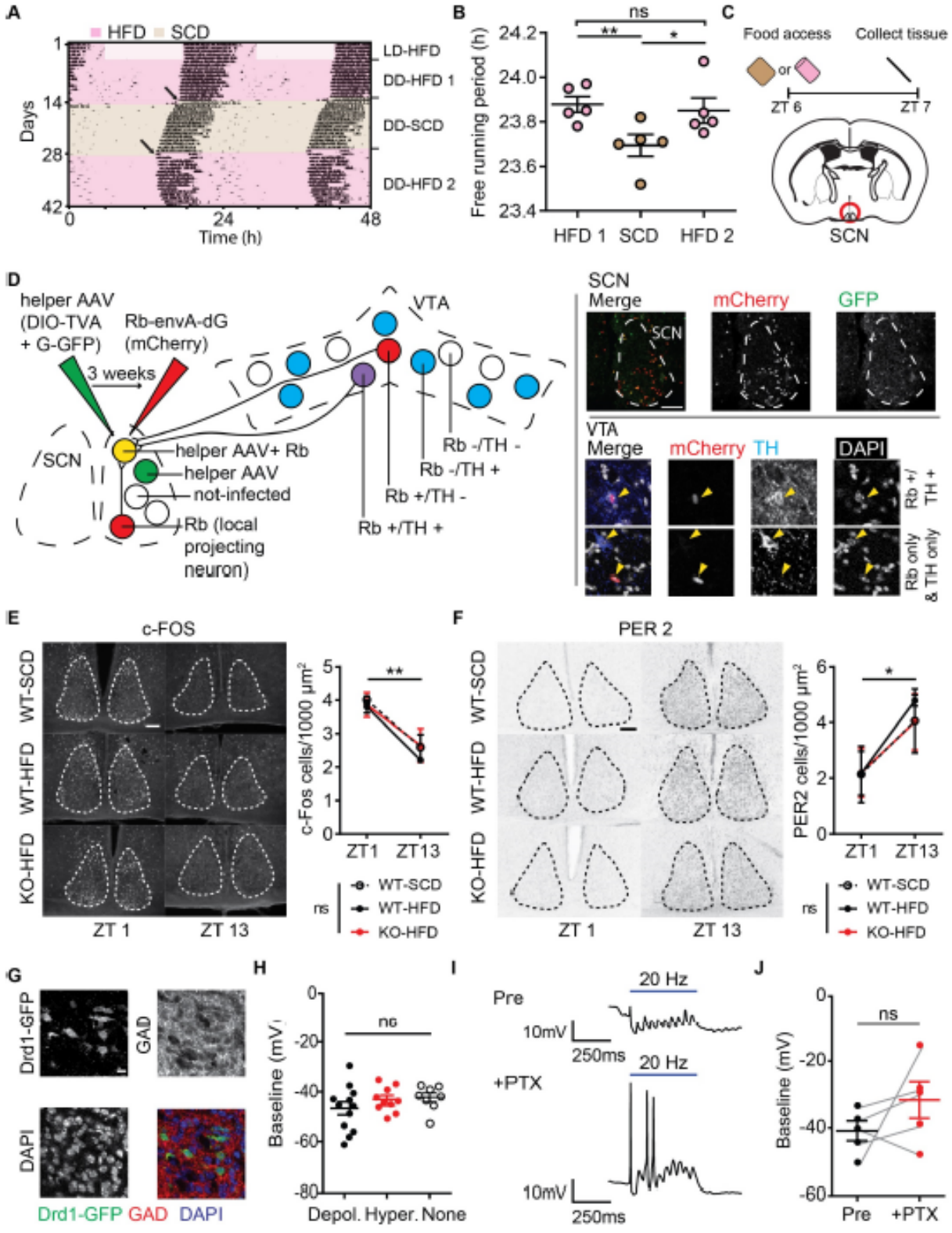
A
HFD SCD
LD-HFD
DD-HFD 1
DD-SCD
DD-HFD 2
Days
Time (h)
B
ns
**
*
Free running period (h)
HFD 1 SCD HFD 2
C
Food access
Collect tissue
or
ZT 6
ZT 7
SCN
D
helper AAV
(DIO-TVA
+ G-GFP)
Rb-envA-dG
(mCherry)
3 weeks
SCN
VTA
helper AAV+ Rb
helper AAV
not-infected
Rb (local
projecting
neuron)
Rb +/TH +
Rb +/TH -
Rb -/TH +
Rb -/TH -
SCN
Merge
mCherry
GFP
VTA
Merge
mCherry TH
DAPI
Rb +/
TH +
Rb only
& TH only
E
c-FOS
WT-SCD
WT-HFD
KO-HFD
ZT 1
ZT 13
c-Fos cells/1000 µm²
ZT1 ZT13
ns
WT-SCD
WT-HFD
KO-HFD
F
PER 2
PER2 cells/1000 µm²
G
Drd1-GFP
GAD
DAPI
Drd1-GFP GAD DAPI
H
Baseline (mV)
Depol. Hyper. None
I
Pre
20 Hz
10mV
250ms
+PTX
J
Baseline (mV)
Pre +PTX

Figure S4. HFD Lengthens the Free Running Period but Does Not Dampen the Molecular Oscillation Amplitude. Related to Figure 4.

A.(Ryan Grippo) Representative double plotted actogram of wheel running activity for WT-HFD mice exposed to dietary change in DD following 6 weeks HFD access. The first two weeks on running wheels following LD entrainment are labeled as DD-HFD 1. Diet change to SCD (DD-SCD) for two weeks preceded the reintroduction of HFD (DD-HFD-2) for an additional two weeks. Tan shading represents SCD and pink shading represents HFD access in DD. Arrows indicate time of diet and cage change.

B.(Ryan Grippo) Average free running period in DD during periods described in (A). Repeated-measures one-way ANOVA with Bonferroni post hoc comparison, n=5; $F(2,8)=12.9$, $p=0.003$.

C.(Ryan Grippo, Nidhi Purohit, Jay Hirsh) Schematic of food access paradigm (top) and location of tissue punch collection (bottom) for HPLC analysis of DA turnover for experiments conducted in Figure 4D.

D.(Qijun Tang) Left: Schematic illustration of rabies virus retrograde tracing. Right: Representative confocal images of SCN (scale bar=100 μm) and VTA (scale bar=10 μm). Cells of interest are indicated by triangles. Rb: Rabies virus.

E.(Krystyna Cios, Qijun Tang) Left: representative images for SCN c-Fos staining at indicated time points. Region of quantification is depicted by dotted lines. Scale bar=100μm. Right: Quantification of c-FOS-positive cell density in SCN at day (ZT1) or night (ZT13). Two-way ANOVA, n=3/group; $F_{time}(1,6)=20.7$, $p=0.004$.

F.(Krystyna Cios, Qijun Tang) Left: representative images for SCN Per2 staining at indicated time points. Region of quantification is depicted by dotted lines. Scale bar=100 um. Right: Quantification of PER2-positive cell density in SCN at day (ZT1) or night (ZT13). Two-way ANOVA, n=3/group; $F_{time}(1,6)=10.1$, $p=0.02$. The immediate early gene c-FOS has a peak expression during the day and a trough at night, while PER2 displays the reverse expression pattern [167,168].

G.(Qijun Tang) Representative confocal image of the colocalization for DAPI, GAD65/67 and Drd1 promoter driven Cre-GFP in the SCN. Scale bar=10μm.

H.(Sean Chadwick) Baseline membrane potential of three types of neurons described in (Figure 4H) before light stimulation. One-way ANOVA, n=8-12/group.

I.(Sean Chadwick) Example trace for one SCN neuron that has both hyperpolarizing and depolarizing response to light stimulation from Figure 4H. Top: Before picrotoxin incubation (Pre), the light stimulation induces hyperpolarization with re-occurring depolarization events timelocked to each light pulse without exhibiting action potentials. Bottom: Following incubation of picrotoxin (+PTX), action potential light stimulation evokes action potentials.

J.(Sean Chadwick) Baseline membrane potential of neurons that hyperpolarize in response to ChR2 stimulation, before (Pre) or after picrotoxin incubation (+PTX). Student's two tailed paired t-test, n=5/group.
Data are represented as mean±SEM, *p<0.05,**p<0.01,***p<0.001.

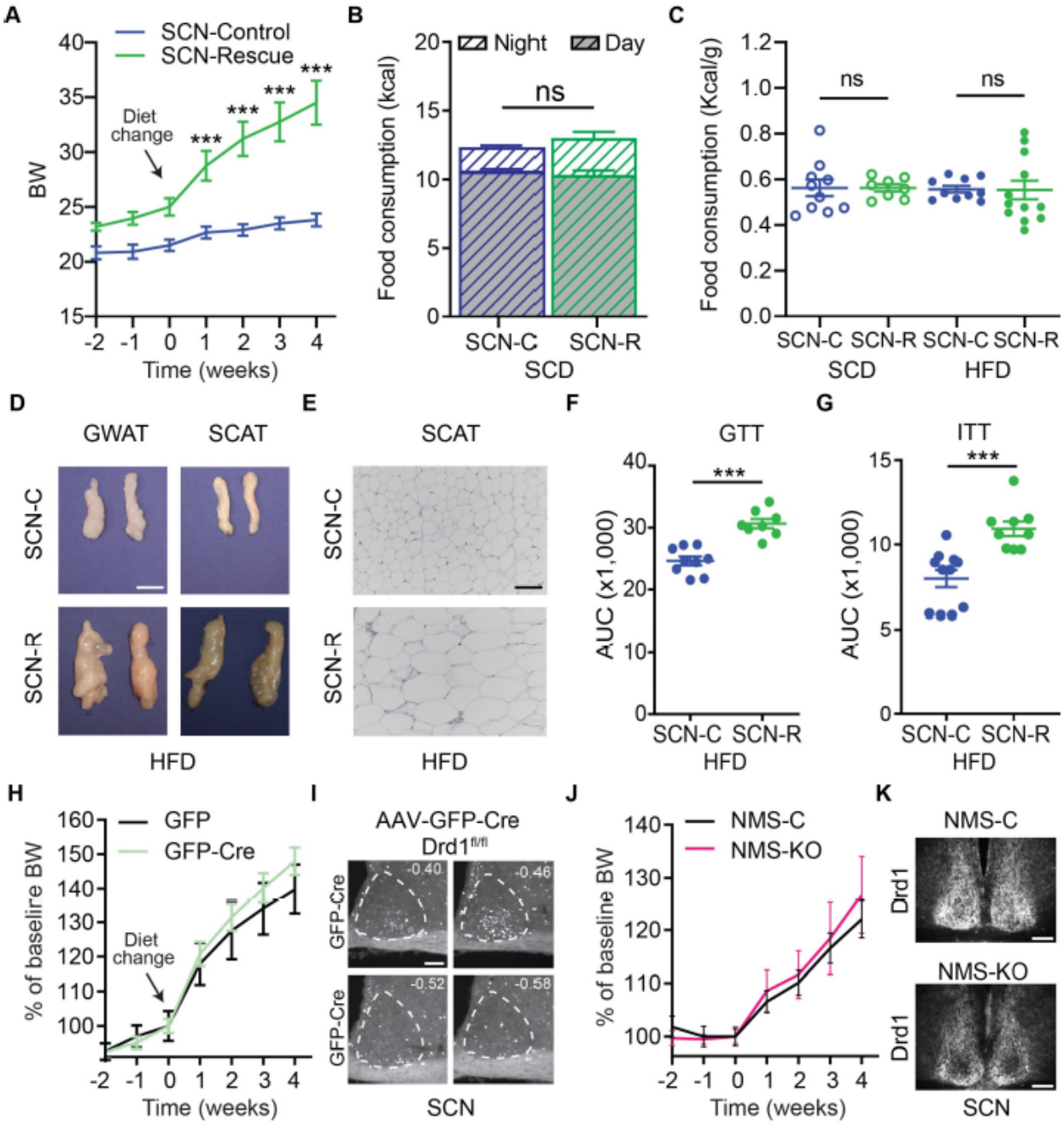

Figure S5. Additional Results Illustrating HFD-Induced Obesity in SCN-Rescue Mice. Related to Figure 5.

A.(Ryan Grippo) Raw value of BW change for SCN-C and SCN-R for data shown in Figure 5. Repeated-measures two-way ANOVA n=6-8/group; $F_{diet(1,20)}=28.2$, $p<0.001$. The arrow indicates the time of diet switch from SCD to HFD.

B.(Ryan Grippo) Daily total calorie consumption of SCN-Control (SCN-C) and SCN-Rescue (SCN-R) mice on SCD. Day- (white) and Night (gray) consumption are segregated for clarity. Student's two tailed t-test, n=8-10/group.
C.(Ryan Grippo) Daily food consumption normalized to BW. Two-way ANOVA, n=6-8/group
D.(Ryan Grippo, Qi Zhang, Qijun Tang) Representative images of dissected GWAT (left) and SCAT (right) following the HFD feeding paradigm in Figure 1A. Scale bar=1 cm.
E.(Ryan Grippo, Qi Zhang, Qijun Tang) Representative SCAT H&E histology for groups in (B). Scale bar=100 μm.
F.(Qi Zhang, Qijun Tang) AUC for GTT in figure 5I. Student's two tailed t-test, n=8-9/group.
G.(Qi Zhang, Qijun Tang) AUC for ITT in figure 5J. Student's two tailed t-test, n=6-8/group.
H-K.(Ryan Grippo) Attempted generation of SCN specific Drd1-KO mice.
H-I.(Ryan Grippo) Strategy 1: The $Drd1^{fl/fl}$ mice SCN were targeted with AAV-Cre-GFP injections. (H) Percent BW change relative to week 0 for AAV8-GFP (GFP) or AAV8-GFP-Cre (GFP-Cre) injected $Drd1^{fl/fl}$ mice. Repeated-measures two-way ANOVA, n=4/group. (I) Representative images showing expression of GFP-Cre in the SCN of AAV8-GFP-Cre injected mice, only 10.9%±3.1% DAPI+ cells are GFP-Cre+ in the SCN (1453±308 cells/mouse, n=4 mice) providing insufficient level of tissue penetration. Scale bar=50μm, images represent the mouse with the most amount of viral expression. Approximate distance relative to bregma is noted in each SCN section.
J-K.(Ryan Grippo) Strategy 2: $Drd1^{fl/fl}$ mice were crossed to NMS-Cre line ($NMS^{Cre/+}$;$Drd1^{fl/fl}$). (J) Percent BW change relative to week 0 for $NMS^{+/+}$;$Drd1^{fl/fl}$ (NMSControl) and $NMS^{Cre/+}$;$Drd1^{fl/fl}$ (NMS-KO) mice on HFD. Repeated-measures two-way ANOVA, n=5-7/group. (K) Anti-Drd1 fluorescent immunohistochemistry staining within the SCN of Control (top) and $NMS^{Cre/+}$;$Drd1^{fl/fl}$ mice (bottom). SCN-Drd1 ablation was limited in the NMS-Cre;$Drd1^{fl/fl}$ line (the number of SCN-Drd1 cells that express NMS is calculated to be at most ~65% [169,170]. Therefore, both of these approaches left animals prone to diet-induced obesity. Scale bar=100 μm. Data are represented as mean±SEM.
*p<0.05,**p<0.01,***p<0.001.

Chapter 3 A leptin responsive hypothalamic circadian circuit underlying development of food entrainment

Qijun Tang[1†], Brandon Podyma[1,2†*], Elizabeth Godschall[1], Charles D. Brennan[1], Qi Zhang[1], Sydney P. Williams[1], Roberta Onoharigho[1], Ricardo Salinas[1], Joey Olivieri[1], Christopher D. Deppmann[1*], Ali D. Güler[1*]

[1]University of Virginia, Department of Biology
[2]University of Virginia, Medical Scientist Training Program
[†]Co-first authors

Correspondence

*To whom correspondence should be sent:
Ali D. Güler
Departments of Biology and Neuroscience
University of Virginia
Charlottesville, VA 22904-4328
Email: aguler@virginia.edu

Christopher D. Deppmann
Departments of Biology, Cell Biology, Neuroscience and Biomedical Engineering
University of Virginia
Charlottesville, VA 22904-4328
Email: deppmann@virginia.edu

Brandon Podyma
Department of Biology, Medical Scientist Training Program
University of Virginia
Charlottesville, VA 22904-4328
Email: brandonpodyma@gmail.com

This work was in close collaboration with Brandon Podyma *et. al.*, many results presented here may also be included in the Ph.D. dissertation of Dr Brandon Podyman, and graduation thesis of other co-authors. Major contributors to each work are indicated in the figure legends.

c3.1 Abstract

In contrast to light-dependent entrainment of the central circadian pacemaker, the molecular and neural underpinnings of entrainment via non-photic Zeitgebers (*German*; “time giver”), such as food, remain unclear. We show that the meal-associated timing of leptin, and its subsequent actions in the dorsomedial nucleus of the hypothalamus (DMH), delays the development of food entrainment. We also delineate a hypothalamic circuit from DMH to SCN which orchestrates circadian behavioral output. This work suggests DMH as an important integrating hub of non-photic and photic entrainment, and positions leptin as a critical mediator of this circadian network.

c3.2 Main

Biological clocks synchronize to salient non-photic cues beyond light, such as timed availability of food, receptive mates, or exercise [24–26]. Food timing has been recognized as a non-photic cue for the past century, since it was first observed that once daily scheduled feeding led to the development of circadian activity prior to mealtime (food anticipatory activity, FAA) [25]. More recently, evidence is growing that food timing matters in humans, with evidence that humans also exhibit non-photic entrainment to food [171–174]. Despite this, identification of anatomic or molecular substrates of food entrainment has eluded the field due to the possibility that food entrainment is regulated by a coordinated multi-core network, because single brain area lesions or gene mutations are not sufficient to fully hijack food entrainment [29,43].

Thus, we aimed to delineate the anatomical connections and modulators linking this non-photic entrainment network.

c3.2.1 Mis-timed leptin suppresses development of food entrainment

We began by hypothesizing that a food-associated satiety signal released at or just after mealtime could mediate an effect on the food-timing responsive circadian system. Leptin levels are strongly under the control of both meal timing and the circadian clock via the SCN, though it is unknown whether leptin itself can alter circadian behavior [175–177]. In vitro application of leptin was reported to phase shift the circadian oscillation of SCN neuron activity in rats [178]. We further proved that systemic administration of leptin is able to shift the central but not peripheral molecular circadian rhythm in mice, without affecting the circadian locomotor activity (Fig 1A, Extended data Fig 1L). To study the effect of leptin on circadian behavior, we then developed a cross-over study design to test whether desynchronizing of the timing of leptin from food consumption is able to disrupt the FAA, by injecting leptin or placebo saline to wildtype mice in advance of scheduled delivery of a set amount of food (scheduled feeding, SF). We observed robust FAA development by day 2 in the saline group, and this progression was largely suppressed by leptin (Fig 1B-D, Extended data Fig 1A-C). The defect in FAA development in leptin injected mice paralleled a slower rate of food consumption (Fig 1E-H, Extended data Fig 1F). Limiting the rate of food consumption in non-injected wildtype mice still allowed for robust FAA development, suggesting that a slowed rate of consumption was not the confounding factor of FAA development (Extended data Fig 1G). Given this, we propose that FAA and rate of food consumption,

both of which are altered by leptin, provide orthogonal means to measure the output strength of the food entrained clock.

In the cross-over experiment, treatment groups were switched on day 6. Notably FAA and rapid food consumption deficits extend to day 6 in those mice that were injected with saline on day 6 but had received leptin on days 1-5 (Fig 1 B-H, Extended data Fig 1F). This provides evidence that disruption of the progression of food entrainment was the dominating reason that led to the behavior defects, despite the previously reported acute suppression effect of leptin on locomotor activity and food intake [179]. Further, those mice that began receiving leptin on day 6 did not have a significant change in their FAA on subsequent days, but did exhibit slightly decreased food consumption rates (Fig 1E). This delayed suppression effect on food consumption rate at not the day of treatment switch but subsequent days further suggests that leptin's effects on food timing mechanisms extend beyond acute effects, and alter underlying food entrainment circuitry.

There were no differences in locomotor activity or energy expenditure outside of the FAA window between saline or leptin treated groups. However, reduced energy expenditure was observed during the pre-meal time window in leptin treated group, likely secondary to decreased FAA (Extended data Fig 1D, H-K). We further characterized metabolic outputs and found no differences in body weight between treatment groups throughout the scheduled feeding paradigm (Extended data Fig 1E). Interestingly, respiratory exchange ratios (RER) showed an anticipatory rise paralleling FAA development, with no differences observed between treatment groups (Fig 1I-K).

RER therefore appears to be an additional output of the peripheral food entrainment system, though one which is leptin-independent.

All together, these results suggest that mistimed leptin flux prevents the centrally mediated behavioral priming (FAA, rapid food consumption) necessary to adapt to scheduled feeding, without disrupting appropriate metabolic peripheral responses to scheduled feeding or the maintaining of acquired food entrainment, potentially by hijacking the necessary coordination between peripheral and central clocks.

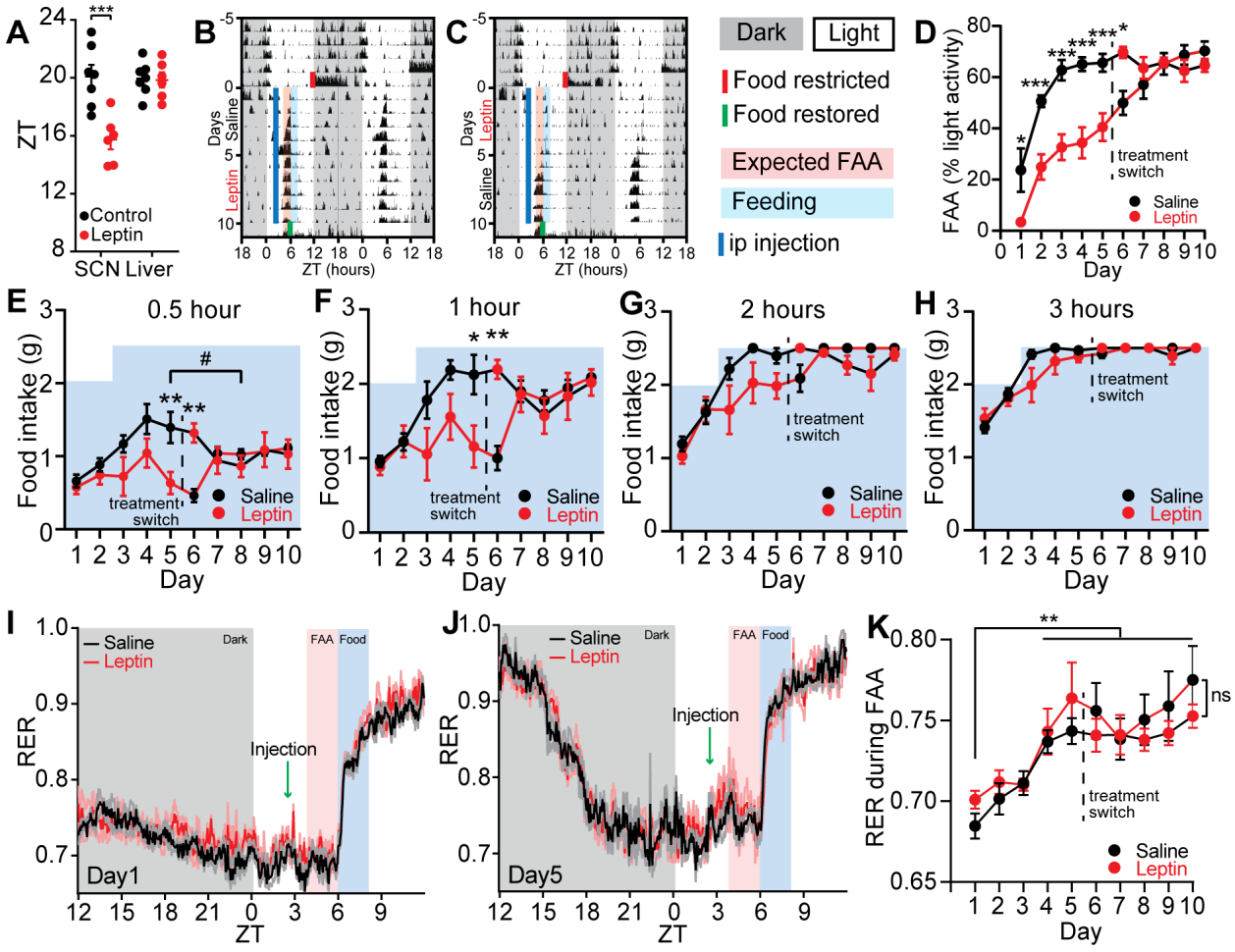

Figure 1. Mistimed leptin alters the circadian behavioral responses to scheduled feeding

A.(Elizabeth Godschall, Qijun Tang) The ZT phase of the first bioluminescence peak of SCN and Liver from PER2::luciferase mice, injected with saline (control) or leptin at ZT6. Two-way ANOVA with Bonferroni post hoc comparison; n = 6-7 / group; $F_{treatment}$ (1, 22) = 12.45, p=0.0019.

B-C.(Brandon Podyma) Representative actograms of single mice on a 12:12 L:D cycle under *ad libitum* conditions that are then subjected to scheduled feeding (SF) beginning at lights off on SF day 0 and receiving either (A) saline (SF days 1-5) then leptin (SF days 6-10) or (B) leptin (days 6-10) then saline (days 11-15). Mice are housed in 12:12 LD, fasted at lights off on day 5 (solid red line), injected with saline or leptin at 2.5 hours after lights on (ZT2.5, solid blue line), and fed at ZT6 (2 g on days 1&2, 2.5 g on remaining days). Red shaded area is the FAA time window 2 hours pre-meal time (ZT4-6), and blue shaded area is the first 2 hours after food delivery (ZT6-8). Food is restored at ZT6 on day 16.

D.(Brandon Podyma) Quantification of FAA. FAA is defined as the locomotor activity in the two-hour window prior to food delivery as a percentage of light-phase activity, excluding the activity 1 hour post-injection. Note that red dots indicate same day leptin treatment, and red line indicates those mice that were in the leptin then saline treatment group. Repeated measures
two-way ANOVA with Bonferroni post hoc comparison; n = 8-9 / group; $F_{treatment}$ (1, 15) = 22.96, p<0.001.

E-H.(Roberta Onoharigho, Qijun Tang) Food intake of mice during SF, at (D) 0.5 hour, (E) 1 hour, (F) 2 hours, and (G) 3 hours after food delivery. Blue shading indicates the total amount of food that was available for mice to consume on each day. Repeated measures two-way ANOVA with Bonferroni post hoc comparison; n = 6 / group. # in (D): day 5 vs day 8, p = 0.0284.

I-J.(Roberta Onoharigho, Qijun Tang) 24-hour respiratory exchange ratio (RER) at (H) day 1 and (I) day 5 of SF.

K.(Roberta Onoharigho, Qijun Tang) Average RER within the FAA window over 10 days of SF. Repeated measures two-way ANOVA with Bonferroni post hoc comparison; n = 4 / group; $F_{treatment}$ (1, 6) = 0.5830, p=0.4741; F_{time} (9, 54) = 23.10, p<0.001. Days 4-10 for both treatment groups are all statistically significantly increased compared to day 1 within treatment groups.

Data are represented as mean ± SEM. *p < 0.05; **p < 0.01; ***p < 0.001; ns, not significant.

c3.2.2 Proper timing of DMH LepR neuronal activity is crucial for the development of food entrainment revealed by calcium imaging

Although leptin is capable of shifting the SCN PER2 rhythm (Fig 1K-L) [178], because of the low level of leptin receptor (LepR) expression in the SCN [180,181], leptin's effect on the SCN and the behavioral food entrainment is likely indirect. Dorsomedial hypothalamus (DMH) is a LepR rich area that has been strongly implicated in circadian behaviors and physiological processes, including feeding, locomotor activity, sleep-wake, and hormone rhythms [35,180,182–184]. We generated mice that express the calcium indicator GCaMP7s in the LepR-expressing DMH neurons (DMH LepR), allowing us to record calcium activity (as a proxy of neural activity) while simultaneously recording locomotor activity in home cages (Fig 2A-B, Extended data Fig 2A) [185]. We confirmed that this set-up allowed for robust measurement of FAA, and recapitulated our previous finding that leptin impairs the development of FAA (Fig 2C-D). We also observed strong acute elevation of DMH LepR calcium signal in response to food delivery, reproducing previous findings and confirming functionality of our system (Extended data Fig 2C) [186].

In response to scheduled feeding we found a significant anticipatory rise in DMH LepR intracellular calcium activity of saline-treated, but not leptin-treated mice during the pre-meal FAA window by day 5 (Fig 2E-I, Extended data Fig 2D-F). On day 6 of scheduled feeding, we withheld saline/leptin injections and delayed food delivery for 3.5 hours (scheduled feeding-late food, SF-LF). We observed that previously saline-treated mice had the anticipatory rise in DMH LepR intracellular calcium activity during the FAA

window, and extended to mealtime window, but that this peak was absent in previously leptin-treated mice (Fig 2E-H, Extended data Fig 2D-F). These data demonstrate the leptin sensitive entrainability of DMH LepR neurons to scheduled food availability.

We next tested whether perturbing the circadian timing of DMH LepR neural activity disrupts FAA development by chemogenetically activating DMH LepR neurons prematurely using hM3Dq (Fig 2J, Extended data Fig 3A). Similar to leptin treatment, we observe that premature activation of DMH LepR neurons with CNO injection impairs the development of FAA over the first 5 days of scheduled feeding, but does not significantly impair the expression or maintenance of FAA when CNO is removed, or when CNO is administered after establishment of FAA (Fig 2K-M, Extended data Fig 3B-E, 4). Taken together, these data highlight that proper circadian regulation of DMH LepR neural activity correlates with and is required for the development of food entrainment in response to scheduled feeding.

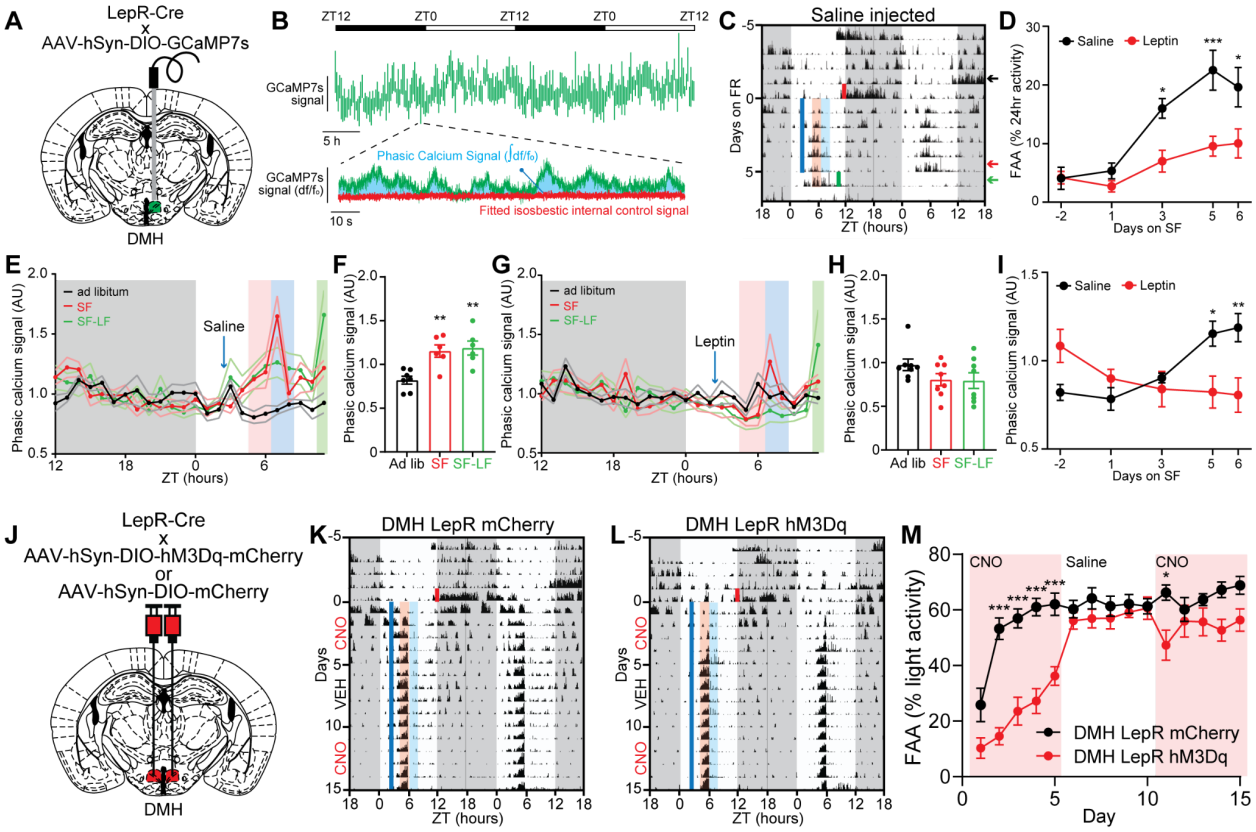

Figure 2. The dorsomedial hypothalamus mediates the effect of leptin on food entrainment

A.(Qijun Tang) Schematic diagram illustrating unilateral injection of AAV-hSyn-DIO-GCaMP7s and fiber optic cannula implant to the DMH of LepR Cre mice.

B.(Qijun Tang) Example data trace illustrating the analysis process to calculate "phasic calcium signal" as a readout for intracellular calcium activity in long-term fiber photometry calcium imaging.

C.(Qijun Tang) Representative locomotor actogram of a single animal recording GCaMP7s signal in DMH LepR neurons during SF. Color coded arrows indicate three days that are selected for quantification in panels E-H.

D.(Qijun Tang) Quantification of FAA during long-term DMH LepR GCaMP7s recording. Mixed-effects (REML) analysis with Bonferroni post hoc comparison; n = 5-8 / group; $F_{treatment}$ (1, 52) = 27.78, p<0.001.

E.(Qijun Tang) Average phasic GCaMP7s signal of DMH LepR neurons at 2 days before SF (black, *ad libitum*), 5th day of saline treated SF (red, SF), or 6th day of SF

where we withheld saline injection and food delivery was delayed for 3.5 hours (green, SF-LF).

F.(Qijun Tang) Quantification of the saline treated phasic calcium signal in the FAA window from (E). Mixed-effects (REML) analysis with Bonferroni post hoc comparison; n = 6-7 / group; F (2, 10) = 15.01, p=0.0010.

G.(Qijun Tang) Average phasic GCaMP7s signal of DMH LepR neurons at 2 days before SF (black, *ad libitum*), 5th day of leptin treated SF (red, SF), or 6th day of SF where we withheld leptin injection and food delivery was delayed for 3.5 hours (green, SF-LF).

H.(Qijun Tang) Quantification of the leptin treated phasic calcium signal in the FAA window from (G). Repeated measures one-way ANOVA with Bonferroni post hoc comparison; n = 8 / group; F (2, 14) = 2.508, p=0.1172.

I.(Qijun Tang) Quantification of the development of the phasic calcium signal during FAA. Mixed-effects (REML) analysis with Bonferroni post hoc comparison; n = 6-8 / group; $F_{treatment * time}$ (4, 50) = 6.985, p<0.001.

J.(Brandon Podyma) Schematic diagram illustrating bilateral injection of AAV-hSyn-DIO-hM3Dq-mCherry or AAV-hSyn-DIO-mCherry to the DMH of LepR Cre mice.

K-L.(Brandon Podyma) Representative actograms of (K) DMH LepR mCherry and (L) DMH LepR hM3Dq mice on SF that received CNO (SF days 1-5), saline (SF days 6-10), and CNO (SF days 11-15) injection at ZT2.5 during SF.

M.(Brandon Podyma) Quantification of FAA. Pink shading indicates days with CNO injection. No shading indicates saline injection. Repeated measures two-way ANOVA with Bonferroni post hoc comparison; n = 8-10 / group; F_{virus} (1, 16) = 15.98, p=0.0010.

Data are represented as mean ± SEM. *p < 0.05; **p < 0.01; ***p < 0.001; ns, not significant.

c3.2.23 DMH LepR neuron activation alters circadian behavior in an SCN dependent manner

Given the high correlation between increased DMH LepR neural activity and locomotor activity in anticipation to scheduled food access, it is surprising that shifted activation of DMH LepR neurons via hM3Dq did not shift locomotor activity (Fig 2K-M, Extended data Fig 3B-E, 4), potentially due to the decoupling of neuronal activity from food intake.

Therefore, we sought to remove the potential effect of food and assess the functionality of DMH LepR neurons on circadian behavior. Strikingly, in the constant darkness with ad libitum access to food, DMH LepR chemogenetic stimulation partitions circadian locomotor activity without changing the free-running period (Fig 3A-G). Activation early in the active phase (~CT14) advances the offset of locomotor activity to approximately 3 hours after CNO injection, with a concomitant reduction in 24 hour activity (Fig 3A-C, Extended data Fig 5A). Activation late in the active phase (~CT22) delays the offset of locomotor activity to approximately 2 hours following CNO injection, with no change in total locomotor activity compared to controls (Fig 3D-G, Extended data Fig 5B). To our surprise, this delayed running wheel activity in DMH LepR hM3Dq mice persisted after cessation of CNO injections in phase with the previous day's injection time (Fig 3E, G). These data demonstrate that activation of DMH LepR neurons can resculpt and entrain circadian locomotor activity in a time-dependent manner.

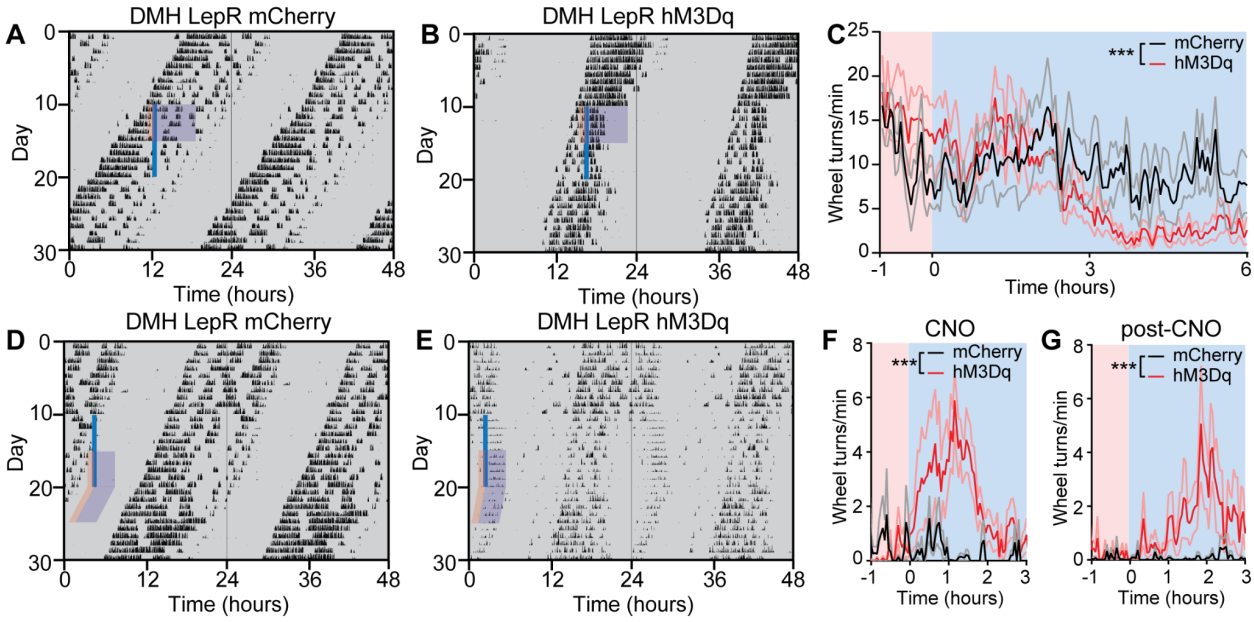

Figure 3. Activation of the DMH LepR neurons partitions circadian locomotor activity
(Brandon Podyma, Qijun Tang)
A-B. Representative actograms of LepR Cre animals bilaterally injected with (A) AAV-hSyn-DIO-mCherry or (B) AAV-hSyn-DIO-hM3Dq-mCherry and injected with CNO at ~CT14 (solid blue line), in *ad libitum*, constant dark conditions with access to a running wheel. Pink shading represents one hour prior to injection, and blue shading 6 hours after injection.
C. Average wheel running activity induced by chemogenetic activation of DMH LepR neurons at ~CT14. Color coded time window is indicated in (A-B). Repeated measures two-way ANOVA; n = 9-12 / group; $F_{time * virus}(140, 2660) = 2.114$, $p<0.001$.
D-E. Representative actograms of LepR Cre animals bilaterally injected with (D) AAV-hSyn-DIO-mCherry or (E) AAV-hSyn-DIO-hM3Dq-mCherry and injected with CNO at ~CT22 (solid blue line), in *ad libitum*, constant dark conditions with access to a running wheel. Pink shading represents one hour prior to injection, and blue shading 3 hours after injection.
F. Average wheel running activity induced by chemogenetic activation of DMH LepR neurons at ~CT22. Color coded time window is indicated in (D-E). Repeated measures two-way ANOVA; n = 9-12 / group; $F_{time * virus}(80, 1440) = 2.029$, $p<0.001$.
G. Quantification of sustained activity for 5 days after cessation of CNO injections. Color coded time window is indicated in (D-E). Repeated measures two-way ANOVA; n = 8-12 / group; $F_{time * virus}(80, 1440) = 1.745$, $p<0.001$.
Data are represented as mean ± SEM. *p < 0.05; **p < 0.01; ***p < 0.001; ns, not significant.

We then asked the SCN dependency of this DMH LepR neuron activation entrained behavior. We first identified that DMH LepR neurons innervate SCN neuromedin S (NMS) neurons via Cre-dependent monosynaptic retrograde viral rabies tracing (Fig 4A-B). Next, we electrolytically lesioned the SCN (SCNxx) in mice expressing DMH LepR hM3Dq or mCherry control, and then activated DMH LepR neurons at the same time of day for 10 consecutive days (Fig 4C-F). We observe an acute bout of wheel running activity in SCNxx DMH hM3Dq, but not control, mice after CNO injection, consistent with previous findings of DMH LepR induced locomotor activity (Fig 4E-F, Extended data Fig 5G-H) [187]. In contrast to the SCN-intact experiment, we did not

observe persistence of this activity following cessation of CNO injection on subsequent days (Fig 3L-M, Extended data Fig 5G-H). We then selectively activated SCN projecting DMH LepR neurons using red light responsive optogenetic actuator, Chrimson [188] (Figure 4G). Repetitive optogenetics activation of the SCN projecting DMH LepR neurons induced the same circadian behavior alteration as chemogenetics activation of all DMH LepR neurons (Figure 4H). These data suggest that DMH LepR makes a direct functional connection with the SCN, and activation of this circuit is able to promote locomotor activity in an SCN independent manner, but that the SCN is required for sustenance of this activity.

Similar to the effect of leptin (Figure 1A), repetitive chemogenetical activation of DMH LepR neurons shifted the central but not peripheral molecular circadian phase (Figure 4I). This provided further evidence that DMH^{LepR}-SCN circuit is a leptin responsive link between circadian system and metabolism.

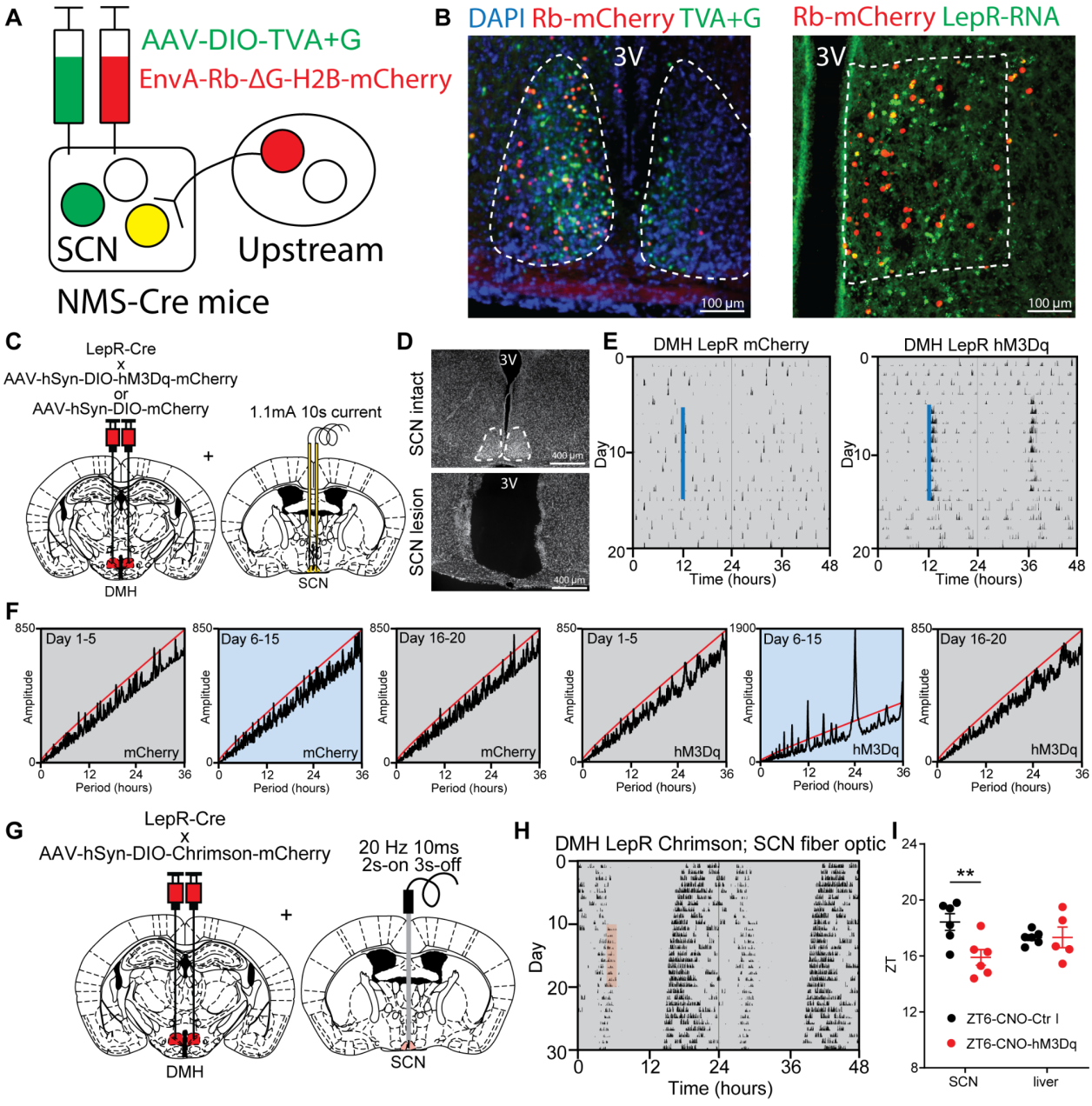

Figure 4. The DMH LepR neurons alter circadian behavior via the SCN

A.(Qijun Tang) Schematic illustration of NMS Cre dependent rabies virus retrograde tracing.

B.(Elizabeth Godschall, Qijun Tang) Representative images of SCN and DMH from retrograde tracing strategy in H.

C.(Qijun Tang) Schematic diagram illustrating bilateral injection of AAV-hSyn-DIO-hM3Dq-mCherry or AAV-hSyn-DIO-mCherry to the DMH of LepR Cre mice coupled with electrolytic lesioning of the SCN in the same mice.
D.(Qijun Tang) Representative images of intact and electrolytic lesioned SCN.
E.(Qijun Tang) Representative actogram of an SCN lesioned (left) DMH LepR mCherry, and (right) DMH LepR hM3Dq animal injected with CNO every 24 hours for 10 days in constant darkness. Solid blue line indicates CNO injection.
F.(Qijun Tang) Chi-square periodogram analyses of the wheel running activity in (L) for the days before (left, 1-5), during (middle, 6-10), and after (right, 11-15) CNO injection. Solid red line indicates p=0.001 significance.
G.(Qijun Tang) Schematic diagram illustrating bilateral injection of AAV-hSyn-DIO-Chrimson-mCherry to the DMH of LepR Cre mice coupled with fiber optic cannula implantation to the SCN.
H.(Qijun Tang) Representative actogram of an animal received optogenetics activation of SCN projecting DMH-LepR neurons 2 hours every day for 10 days in constant darkness. Pink shading indicates time of optogenetics activation.
I.(Qijun Tang) The ZT phase of the first bioluminescence peak of SCN and Liver from PER2::luciferase mice injected with CNO at ZT6 (ZT6-CNO-Ctrl), or PER2::luciferase;LepR-Cre mice with hM3Dq expressed in DMH LepR neurons and injected with CNO at ZT6 (ZT6-CNO-hM3). Two-way ANOVA with Bonferroni post hoc comparison; n = 5-6 / group; $F_{virust*tissue}(1, 19) = 5.495$, p=0.0301.

c3.3 Discussion

In this work we add to the growing recognition of non-photic cues in regulating the function of biological clocks, and identify leptin as a molecular signal capable of linking food intake with hypothalamic-mediated circadian behavior. We demonstrate a new neural input to the SCN from leptin responsive neurons of the DMH, a circuit which likely functions to indicate meal timing and energy status to the SCN. In the process we also identified an intriguing property whereby circadian locomotor activity may be divisible into at least two subunit clocks differentiable by the activity of DMH LepR neurons. We believe the methodological paradigms presented here offer a new platform to test the involvement of other molecular signals and anatomic regions in the

development and maintenance of food entrainment, and the relative function of inputs to the circadian system.

While this work implicates an important circadian role for leptin, previous findings have been mixed with regards to its role in circadian behavior, including scheduled feeding and food entrainment. Whereas leptin has been shown to advance the SCN when administered directly to brain slice of rats [178] or systemically to mice (Fig 1K-L) , leptin does not appear to alter circadian behavior in mice (Extended data Fig 1L) [189]. Previous work has also characterized FAA in the setting of genetic deletion of leptin or continuous leptin infusion, finding that leptin, while not necessary to produce FAA, can suppress FAA when administered continuously to obese, leptin-deficient mice, though not lean wildtype mice [33,190]. The data presented here lend further credence to the importance of the timing of leptin in particular, and position it as a putative circadian zeitgeber. This suggests the need for future work to investigate whether mistimed elevations in leptin, as might happen during shift work, may underlie some of the known adverse metabolic outcomes of mistimed eating.

Leptin appears to exert at least some of its effects via the DMH, a hypothalamic region that serves as an anatomic integration hub to control food intake, thermogenesis, locomotor activity, and, as we and others have demonstrated, circadian behavior [183,186,187,191,192]. Interestingly, at least one known projection target of DMH LepR neurons, AgRP neurons, have also been implicated in the development of FAA [193]. We therefore speculate that the DMH, via projections to the SCN, AgRP neurons, and perhaps other regions, could serve as a critical node for food entrainment, coordinating

circadian and appetitive behaviors via its projections. This type of arrangement could also allow for the previously demonstrated redundancy in the food entrainable network, as it has been convincingly shown that none of these individual regions are essential for food entrainment [41,193–197].

Finally, we demonstrate a novel mechanism for entrainment of a portion of circadian locomotor activity via SCN projecting DMH LepR neurons. Interestingly, this DMH LepR neuron activation induced entrainment does not alter the onset or period of locomotor activity, but rather is most notable for altering the timing of late bouts of activity (Fig. 3C-I). We believe this could suggest the existence of at least two divisible coupled clocks within the SCN defined by their innervation pattern, perhaps akin to the genetic separation of “morning” and “evening” oscillators proposed in drosophila [198]. Whether other circadian behaviors, including feeding, are also altered by this separation remains to be determined. An alternative hypothesis that these data do not exclude is that DMH LepR neurons could independently function as a circadian pacemaker in the face of scheduled feeding. This is supported by the endogenous cycling of DMH LepR neural activity observed in saline treated scheduled fed mice (Fig. 2E-I), suggesting that DMH LepR neurons can not solely be an input to another circadian pacemaker [29]. Further, we suggest that the DMH cannot solely be considered an output pathway as it does not inhibit FAA once it has already developed (Fig. 2K-M). It is possible these findings can be reconciled by a reciprocal connection from the SCN to the DMH, which would allow DMH LepR neurons to be both an input and an output.[199]. Together, our results demonstrate that this leptin-sensitive DMH-SCN circuit is an important part of the

biological clock entrainment network, one which may not be limited solely to food timing. Further investigation of the molecular and circuit logic of this connection, including its inputs and outputs, would provide rich foundational knowledge about the interplay between photic- and nonphotic-entrainment.

c3.4 Acknowledgement

We thank the members of the Güler, Deppmann, and Provencio labs (University of Virginia), and Steele lab (California State Polytechnic University, Pomona) for comments and suggestions on the preparation of the manuscript. We are thankful for technical assistance from Austin Byler Keeler, Jianhua Cang and Chad Daniel Meliza (electrolytic lesion, University of Virginia), and Pantong Yao (*in vivo* calcium imaging data interpretation, University of California San Diego). Additionally, we are grateful for the access to the confocal microscope generously provided by Cang and Liu lab (University of Virginia). This work was supported by NIH R01GM121937 and R35GM140854 (A.D.G.), NIH T32-GM7267-39, NIH T32-GM7055-45 (C.D.D.), and a UVA Wagner Fellowship (B.P.).

c3.5 Author Contribution

Q.T., B.P., A.D.G., and C.D.D conceived and designed the experiments, and wrote the manuscript with input from all co-authors. Q.T., and B.P. performed the generation of experimental cohorts, data collection, analysis and interpretation. Specifically, Q.T. performed all calcium imaging, CLAMS data acquisition and analysis, custom locomotor activity monitoring, and retrograde tracing. B.P. made the initial observations of leptin's

and DMH LepR's effects on FAA, and DMH LepR's effect on circadian behavior requiring the SCN. E.G. performed RNA scope staining. C.D.B. contributed to intracranial surgery. R.O. contributed to body weight and food intake measurements during SF. Q.Z. and S.P.W. contributed to DMH LepR neuron chemogenetic activation in constant darkness. E.G., C.D.B., Q.Z., S.P.W, R.O., R.S., and J.O. contributed to daily animal husbandry during long-term circadian behavior experiments.

c3.6 Declaration of Interests

The authors declare no competing interests.

c3.7 Materials and Methods

Mice.

All experiments were carried out in compliance with the Association for Assessment of Laboratory Animal Care policies and approved by the University of Virginia Animal Care and Use Committee. Animals were housed on a 12-h light/dark cycle with food (PicoLab Rodent Diet 5053) and water *ad libitum* unless otherwise indicated. All experiments were performed on male mice 12 weeks or older unless otherwise indicated. In addition to wild-type C57BL6/J mice, the following mouse lines were used: LepR-Cre (B6.129-Lepr$^{tm3(cre)Mgmj}$/J, The Jackson Laboratory #032457, RRID:IMSR_JAX:032457) [200], NMS-Cre (C57BL/6-Tg(Nms-icre)20Ywa/J, The Jackson Laboratory #027205, RRID:IMSR_JAX:027205) [169], PER2LUC (B6.129S6-Per2^{tm1Jt}/J, The Jackson Laboratory #006852, RRID:IMSR_JAX:006852) [21].

Scheduled feeding (SF).

For scheduled feeding, mice were first acclimated to single housing for 7 days, followed by acclimation to IR beam interruption chambers (Columbus Instruments, or custom built) for a minimum of 72 hours. For daytime scheduled feeding, mice were fasted at lights off (ZT12) on day 0. Mice were weighed, and injected with either vehicle (saline), 5mg/kg leptin, or 0.3mg/kg CNO at ZT2.5. Mice were then refed 3.5 hours later at ZT6 (ZT6.5 for fiber photometry experiment). On the first 2 days mice were fed 2g, and on all remaining days were fed 2.5g. For the small-pallet food delivery experiment, food (2g on first 2 days, and 2.5g on day 3-5) was evenly splitted to 4 pallets and delivered at ZT6, ZT7, ZT8, ZT9, and whole pallet of 2.5 food was given at ZT6 on day 6-10. In the leptin treatment experiment, after 5 days treatment groups are switched, so those mice previously given a placebo received a satiety signal and vice versa for the remaining 5 days. In DREADD groups, 5 days of CNO is switched to 5 days saline before switching back to 5 days CNO. We quantify FAA as the amount of locomotor activity expressed in the two-hour window prior to feeding (ZT4-6) as a function of 24 hour locomotor activity, subtracting out the 1 hour of activity post-injection to account for any handling induced locomotion. WT groups injected with saline or leptin were age and weight-matched. Surgery operated groups were age matched.

Stereotactic surgery.

Briefly, animals were anesthetized with isoflurane (induction 5%, maintenance 2%–2.5%; Isothesia) and placed in a stereotaxic apparatus (KOPF for all other surgeries, RWD life science for retrograde tracing and optogenetics). A heating pad was

used for the duration of the surgery to maintain body temperature and ocular lubricant was applied to the eyes to prevent desiccation. 500 nl of AAV (AAV8-hSyn-DIO-mCherry, plasmid from Addgene #44361, virus packed at UNC Vector Core [56]; AAV8-hSyn-DIO-hM3Dq-mCherry plasmid from Addgene #50459, virus packed at UNC Vector Core; AAV1-hSyn-DIO-GCaMP7s virus from Addgene #104491-AAV1 [201]) was delivered using a 10 µL syringe (Hamilton) and 26-gauge needle (Hamilton) at a flow rate of 100 nl/min driven by a microsyringe pump controller (World Precision Instruments, model Micro 4). The syringe needle was left in place for 10 min and was completely withdrawn 17 min after viral delivery. For *in vivo* calcium imaging, an optic fiber guide cannula was implanted unilaterally following viral delivery, at 0.2mm dorsal to the viral injection coordinates, and stabilized on the skull with dental cement (C&B METABOND, Parkell). For electrolytic lesions, a parylene insulated, tip exposed 2 Mohm tungsten electrode was placed bilaterally into the SCN, and current of 1.1 mA was applied for 11 seconds. Two weeks minimum were allowed for recovery and transgene expression after surgery. Stereotaxic coordinates relative to Bregma (George Paxinos and Keith B. J. Franklin): SCN: ML: ± 0.3 mm, AP: − 0.35 mm, DV: − 5.75 mm; DMH: ML: ± 0.3 mm, AP: − 1.8 mm, DV: − 5.45 mm. After the surgery, the animals were housed individually. All surgical procedures were performed in sterile conditions and in accordance with University of Virginia IACUC guidelines.

Retrograde tracing

Rabies virus tracing: 200nl AAV1-synP-FLEX-splitTVA-EGFP-B19G (Addgene #52473-AAV1) was injected to SCN of NMS-Cre mice using the stereotactic surgery

method described above. Three weeks after AAV injection, 120nl EnvA-dG-Rabies-H2B-mCherry (Salk Viral Vector Core) was delivered to the same coordinates. After one more week, fresh brains were harvested and processed for antibody labeling or RNAscope probing as described above.

Histological analysis and imaging.

In the case of fixed tissue collection, animals were deeply anesthetized (ketamine:xylazine, 280:80 mg/kg, i.p.) and perfused intracardially with ice cold 0.01 M phosphate buffer solution (PBS) followed by fixative solution (4% paraformaldehyde (PFA) in PBS at a pH of 7.4). After perfusion, brains were harvested and post-fixed overnight at 4°C in PFA. In the case of fresh tissue collection, brains were harvested after cervical dislocation and decapitation, then incubated in 4% PFA at 4°C for 48 h. Fixed brains were then transferred into 30% sucrose in PBS for 24 h, and then frozen on dry ice. Frozen brains were sectioned immediately or stored in -80°C for future processing. Coronal sections (30 µm) were collected with a cryostat (Microm HM 505 E). Sections were permeabilized with 0.3% Triton X-100 in PBS (PBS-T) and blocked with 3% normal donkey serum (Jackson ImmunoResearch) in PBS-T (PBS-T DS) for 30 min at room temperature. Sections were then incubated overnight at 4°C (or otherwise indicated) in primary antibodies diluted in PBS-T DS. For visualization, sections were washed with PBS-T and incubated with appropriate secondary antibodies diluted in the blocking solution for 2 h at room temperature. Sections were washed three times with PBS and mounted using DAPI Fluoromount-G (Southern Biotech). Images were captured on a Zeiss Axioplan 2 Imaging microscope equipped with an AxioCam MRm

camera using AxioVision 4.6 software (Zeiss). The following primary antibodies were used for fluorescent labeling: anti-c-Fos (rabbit, 1:1k, synaptic systems #226003), anti-GFP (rabbit, 1:1k, Invitrogen A-6455), anti-dsRed (1:1k, Clontech/Takara #632496). The secondary antibodies (Jackson ImmunoResearch) used were Cy2- or Cy3-conjugated donkey anti-rabbit (1:250).

RNAscope probing for RNA

RNAscope in situ hybridization was performed on fixed brain slices with a probe to detect LepR RNA (LepR probe info, RNAscope® Multiplex Fluorescent Reagent Kit v2 Assay, ACD). All procedures were carried out in accordance with the manufacturer's instructions. Sections were immersed with RNAscope® hydrogen peroxide to block the activity of endogenous peroxidases. After a wash in distilled water, sections were permeabilized with RNAscope® protease IV for 30 min at 40°C. Sections were hybridized with the LepR probe at 40°C for 2 h, followed by amplification incubation steps: Amp 1, 30 min at 40°C; Amp 2, 30 min at 40°C; Amp 3, 15 min at 40°C. HRP signals were developed with RNAscope® Multiplex FL v2 HRP and TSA® Plus fluorophores (HRP-C1 and 1:750 TSA® Plus Cy5). Sections were washed with the provided washing buffer 2 × 2 min in between each step. anti-dsRed IHC was then perferfored to enhance the mCherry signal. Sections were then coverslipped with DAPI Fluoromount-G (Southern Biotech). Confocal microscope imaging was performed in Cang and Liu labs, University of Virginia, on a Zeiss LSM 800 microscope (Carl Zeiss).

Bioluminescence

To observe the effect of leptin on the phase of molecular circadian rhythm of liver or SCN, 5mg/kg leptin solution was ip. injected at ZT6 for 4 days to the PER2LUC mice housed under 12:12 LD cycle. On the 5th day, mice were sacrificed around ZT 5. Brains were immediately extracted and dropped into ice cold Hanks' Balanced Salt Solution (HBSS). After 2 minutes, brains were embedded in low melting point agarose (Precisionary Instruments, Natick, MA) and sectioned at 300 μm on a Compresstome VF-200 Vibrating Microtome (Precisionary Instruments, Natick, MA, USA). SCN area on the brain slices and fresh liver tissue were further dissected out for bioluminescence recording using a method adapted from previous work [202]. SCN slices and liver tissues were cultured in 35 mm culture dishes with 1.2 ml of DMEM (D5030, Sigma) supplemented with 3.5 g/L D-glucose, 2 mM Glutamax (Gibco), 10 mM HEPES, 25 U/ml penicillin/streptomycin, 2% B-27 Plus (Gibco), and 0.1 mM D-Luciferin sodium salt (Tocris). The culture dishes were covered with 40 mm diameter glass cover slides and sealed by high-vacuum grace (Dow Corning), and maintained in a non-humidified incubator at 36.8 °C. Bioluminescence from firefly luciferase in each of SCN slices or liver sections was recorded in 6 min intervals by a 32-channel/4-photomultiplier tube luminometer LumiCycle (Actimetrics) in the incubator. The bioluminescence data were collected and analyzed in LumiCycle Analysis software (Actimetrics). The first peak of the recordings were manually recorded by a trained scorer, blinded for treatment conditions.

In vivo fiber photometry recording

The viral vector and fiber optic implant were delivered to the target brain area within one surgical procedure as described above. Experiments were started after at least 2 weeks post surgery for recovery and transgene expression. For long-term recordings, mice were individually housed in their regular home cages and transferred to the recording room 3 days before experiment to acclimate to the environment. Implanted fiber-optic cannula (Thorlabs, 0.39 NA, Ø200 µm Core) was connected to fiber-optic cable (Doric Lenses, 0.37 NA, Ø200 µm Core) with the use of a zirconia mating sleeve (Doric Lenses). The fiber-optic cables were wrapped with metal sheath (Doric Lenses) to prevent breakage and connected to rotary joints (Doric Lenses) to allow free-movement. The fiber photometry system used in this work records the fluorescent signal from both calcium-dependent (465nm) and calcium-independent isosbestic (405nm) excitation light wavelengths, in which the isosbestic wavelength excitation signal can be used to control for the artifacts from animal movement, fluorescent reporter expression and photobleaching. The signal was collected at 120Hz sampling rate. To limit the photobleaching of the fluorescent reporter during the long-term recording, the signal was only collected for 2 minutes per 12 minutes (3/7 saline treated and 1/8 leptin treated mice in the SF experiment, the data were collected for 10 minutes per hour. These datasets were included in analysis when possible. See below for details). Animals that did not exhibit Ca2+ signal increase in response to food presentation were considered mis-targeted and were excluded from the analysis (Extended data Fig 2C-F).

Fiber photometry data analysis.

Data was processed in Matlab with custom scripts using a method modified from work described previously 50. To eliminate the artifact from motion or protein expression, the calcium-independent isosbestic (405nm induced) signal was fitted to the calcium-dependent (465nm induced) signal with a linear least-squares fit. The fluorescence change over baseline fluorescence (ΔF/F0) was calculated as (465nm induced signal - fitted 405nm induced signal) / (median of 465nm induced signal). Notably, in the long-term experiments where multiple short-term sessions were recorded, F0 was the median for the entire experiment for consistency. The fitted 405nm induced signal was defined as the estimated baseline, so that the values on ΔF/F0 curves below 0 were cutoff. For each recording session, phasic calcium signal is the integral of ΔF/F0 adjusted curve (Fig 2B) and represents the intracellular calcium activity during that session. The calculated phasic calcium signal was further averaged by hour and normalized to the average of the 12-hour dark phase signal in each given day. For food response during the scheduled feeding experiment, the food was delivered 1 minute after the initiation of the 2-minute recording session. The variability caused by signal strength was normalized by calculating z-score ((signal-average of baseline signal) / standard deviation of baseline signal) for food response experiments where the first 15 seconds of the 2-minute sessions were used as baseline.

Optogenetics-aided neural circuit mapping

200nl AAV5-Syn-FLEX-rc[ChrimsonR-tdTomato] virus from Addgene #62723-AAV5 [188] was injected to DMH (ML: ± 0.3 mm, AP: − 1.8 mm, DV: − 5.45 mm) of LepR-Cre mice, followed by implantation of fiber-optic cannula (Thorlabs, 0.39 NA, Ø200 μm

Core) to the SCN (ML: 0 mm, AP: − 0.5 mm, DV: − 5.55 mm), using the stereotactic surgery method described above. After at least two weeks of recovery, animals were individually housed in the running-wheel equipped cages. Implanted fiber-optic cannula was tethered to metal sheath wrapped fiber-optic cable (Doric Lenses, 0.37 NA, Ø200 μm Core) with the use of a zirconia mating sleeve (Doric Lenses). Arduino mega 2560 with custom script was used to trigger the red light (625 nm) LED (Thorlabs, M625F2) for optogenetics activation. The power of the red light exiting from the fiber optic cable was controlled to be 1.5~2.5 mW. The pattern of the LED light was programmed to be 10ms square-waves, 20Hz, 2s-on followed by 3s-off.

Circadian Behavioral Analysis.

Locomotor activity data were collected by wheel-equipped cages (Nalgene), or IR beam interruption chambers (Columbus Instruments, or custom built 91) in light-tight compartments under a 12h:12h LD cycle. Fluorescent lights (100 mW/cm2) were used for behavioral experiments. Food and water were provided ad libitum unless otherwise indicated. Wheel running activity was monitored and analyzed with the ClockLab collection and analysis system (Actimetrics, Wilmette, IL). IR beam interruption activity data were analyzed in Excel for quantification or converted to a ClockLab supported file format for circadian analysis.

Comprehensive Lab Animal Monitoring System (CLAMS)

Indirect calorimetry in a home cage CLAMS-HC system (Columbus Instruments) was used to evaluate metabolism during SF. Mice were acclimated to metabolic cages for at

least 3 days and then subjected to SF experiment as described above. RER (VCO2/VO2) and Energy expenditure (EE; 3.815*VO2+1.232*VCO2) were reported by the CLAMS-HC software.

Statistical Analysis

To compare the effects of treatment over time, repeated-measures two-way ANOVA test was used. In experiments with a single variable and more than two groups, repeated-measures one-way ANOVA was performed. In case data points were missing because of technical failure (i.e. power outage during fiber photometry recording), where repeated-measures ANOVA was not possible to perform, mixed-effects (REML) analysis was used instead. Following a significant effect in the ANOVA test, Bonferroni's post hoc comparison was used to determine differences between individual data points. Analyses were conducted using GraphPad Prism 8 statistical software for Windows. All data were presented as means ± standard error of the mean with $p < 0.05$ considered statistically significant.

c3.8 Extended Data Figures

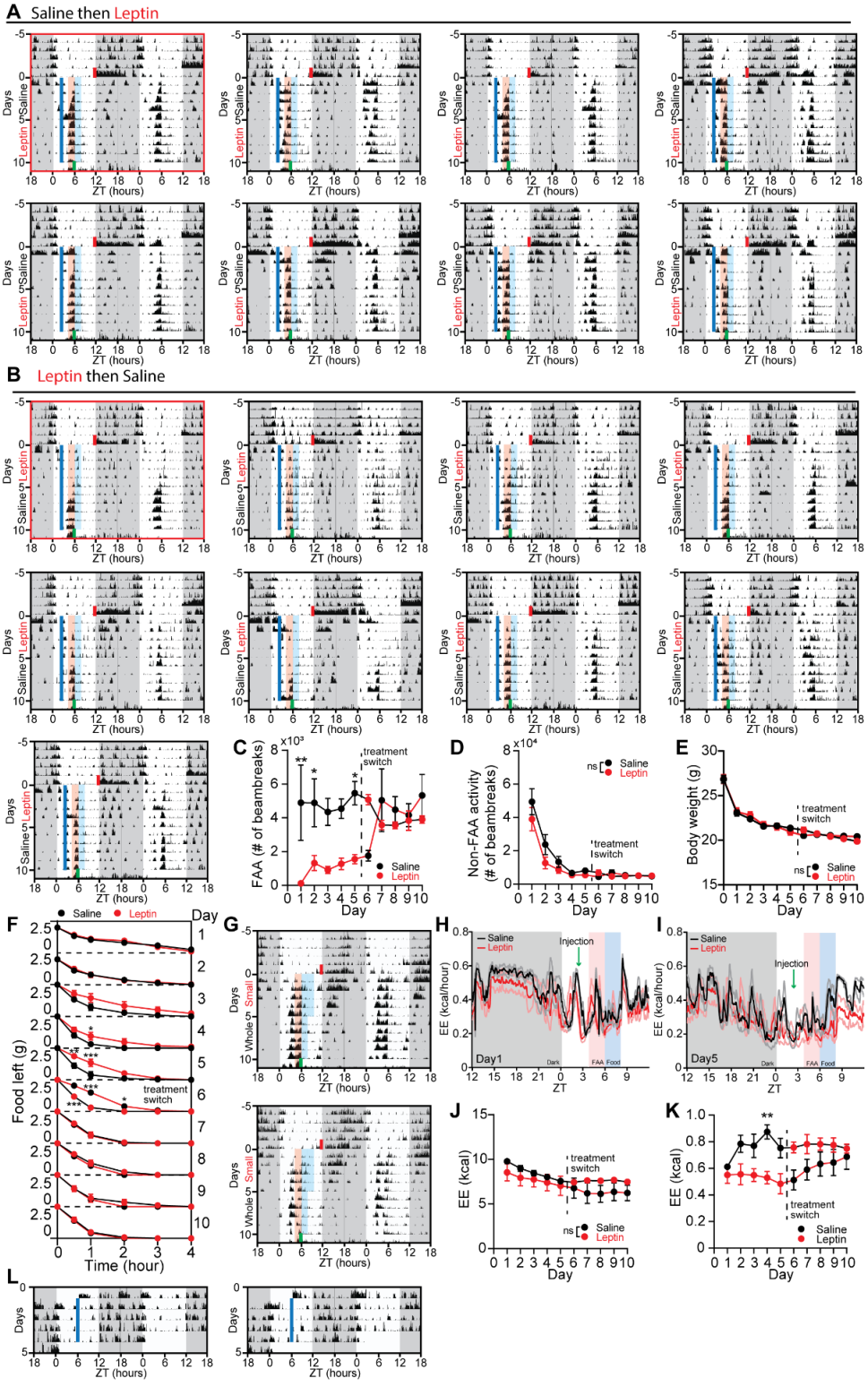

Extended data figure 1. Mistimed leptin alters the circadian behavioral responses to scheduled feeding

A-B.(Brandon Podyma) Actograms of all animals that received (A) saline then leptin or (B) leptin then saline, during scheduled feeding (SF). The actograms used as representative figures in Fig 1 are depicted with red boxes.

C.(Brandon Podyma) Absolute locomotor activity during the FAA window, 2 hours prior to food delivery time. Repeated measures two-way ANOVA with Bonferroni post hoc comparison; n = 8-9 / group; $F_{treatment}$ (1, 15) = 22.3, p<0.001.

D.(Brandon Podyma) Absolute locomotor activity for the 22 hours per day other than FAA. Repeated measures two-way ANOVA; n = 8-9 / group; $F_{treatment}$ (1, 15) = 1.639, p=0.2198.

E.(Brandon Podyma) Body weight of animals during SF. Repeated measures two-way ANOVA; n = 8-9 / group; $F_{treatment}$ (1, 15) = 0.007550, p=0.9319.

F.(Roberta Onoharigho, Qijun Tang) Rate of food intake of animals during SF. Data represented as food left in the cage at each time point up to 4 hours after food delivery. Mice received 2g of food on days 1 and 2, and 2.5g on the rest of the days. Repeated measures two-way ANOVA with Bonferroni post hoc comparison was performed for each day; n = 6 / group.

G.(Roberta Onoharigho, Qijun Tang) Actograms of two mice which received small pellets of food (see methods for details) for 4 hours for the first 5 days of SF, and a whole large pellet (2.5g) at ZT6 the next 5 days of SF.

H-I.(Roberta Onoharigho, Qijun Tang) 24-hour energy expenditure (EE) at (H) day 1 and (I) day 5 of SF.

J-K.(Roberta Onoharigho, Qijun Tang) Total energy expenditure (EE) (J) outside (ZT12-ZT4 and ZT6-ZT12), or (K) within FAA window (ZT4-ZT6) over 10 days of SF. Repeated measures two-way ANOVA with Bonferroni post hoc comparison; n = 4 / group.

L.(Elizabeth Godschall, Qijun Tang) Actograms of two mice which received 5 mg/kg leptin injection at ZT6, with ad libitum access to food.

Data are represented as mean ± SEM. *p < 0.05; **p < 0.01; ***p < 0.001; ns, not significant.

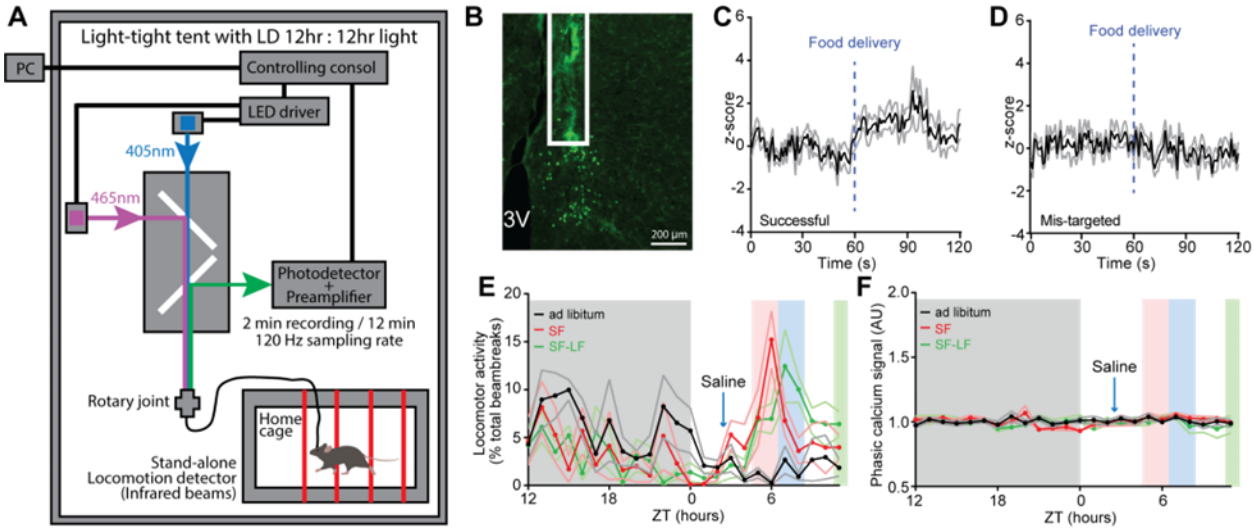

Extended data figure 2. Long term fiber photometry recording of DMH LepR GCaMP7s

A.(Qijun Tang) Schematic diagram illustrating long-term fiber photometry recording coupled with locomotor activity monitoring.

B.(Qijun Tang) Representative image showing the expression of GCaMP7s in DMH LepR neurons and fiber optic cannula implant (white box).

C-D.(Qijun Tang) Acute calcium signal response to food delivery on the 5th day of SF, in successful (C) and mis-targeted (D) mice. The mis-targeted animals in (D) were excluded for the analysis in Fig. 2E-I. n=6 mice/group.

E.(Qijun Tang) Locomotor activity of mis-targeted mice during SF. These mice developed strong FAA. n=5.

F.(Qijun Tang) Average phasic GCaMP7s signal of DMH LepR neurons in the mis-targeted mice at 2 days before SF (black, ad libitum), 5th day of saline treated SF (red, SF), or 6th day of SF where saline injection was withheld and food delivery was delayed for 3.5 hours (green, SF-LF). n=6. The unaltered phasic calcium signal of these mis-targeted mice during SF suggests that the pre-meal elevation of phasic calcium signal is not due to artifact of increased locomotor activity.

Data are represented as mean ± SEM. ns, not significant.

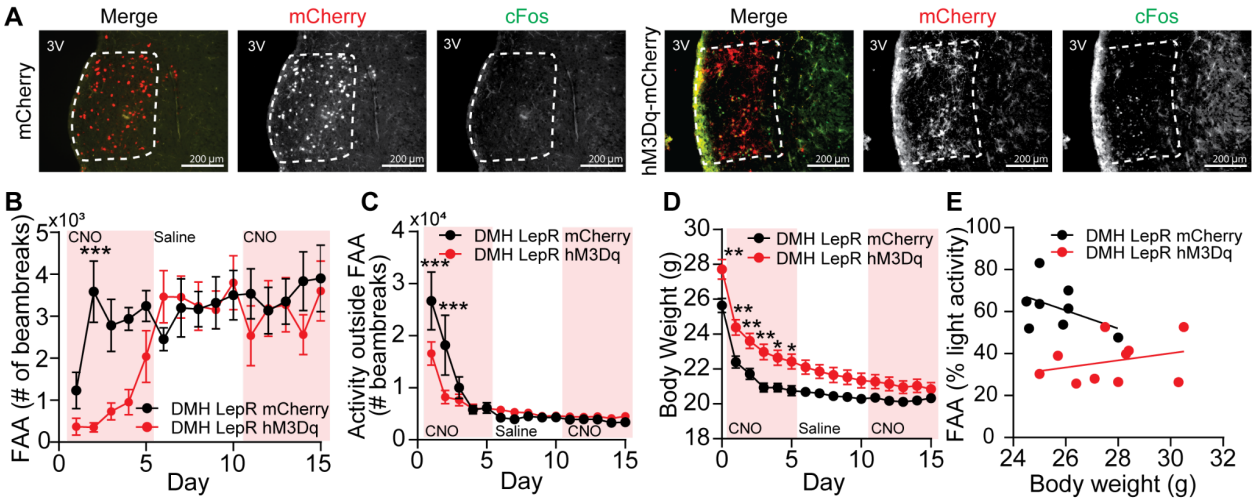

Extended data figure 3. Mistimed activation of DMH LepR neurons suppresses development of FAA

A.(Qijun Tang) Representative images showing the expression of mCherry or hM3Dq-mCherry in DMH LepR neurons and c-Fos response 2 hours after CNO injection.

B.(Brandon Podyma) Absolute locomotor activity during the FAA window on SF. Repeated measures two-way ANOVA with Bonferroni post hoc comparison; n = 8-10 / group; $F_{time*virus}$ (14, 224) = 4.647, p<0.001.

C.(Brandon Podyma) Absolute locomotor activity for the 22 hours per day other than FAA. Repeated measures two-way ANOVA with Bonferroni post hoc comparison; n = 8-10 / group; $F_{time*virus}$ (14, 224) = 4.082, p<0.001.

D.(Brandon Podyma) Body weight during SF. Repeated measures two-way ANOVA with Bonferroni post hoc comparison; n = 8-10 / group; F_{virus} (1, 16) = 7.342, p=0.0155.

E.(Brandon Podyma) Correlation between initial body weight (day before SF) with FAA level on 5th day of SF.

Data are represented as mean ± SEM. *p < 0.05; **p < 0.01; ***p < 0.001; ns, not significant.

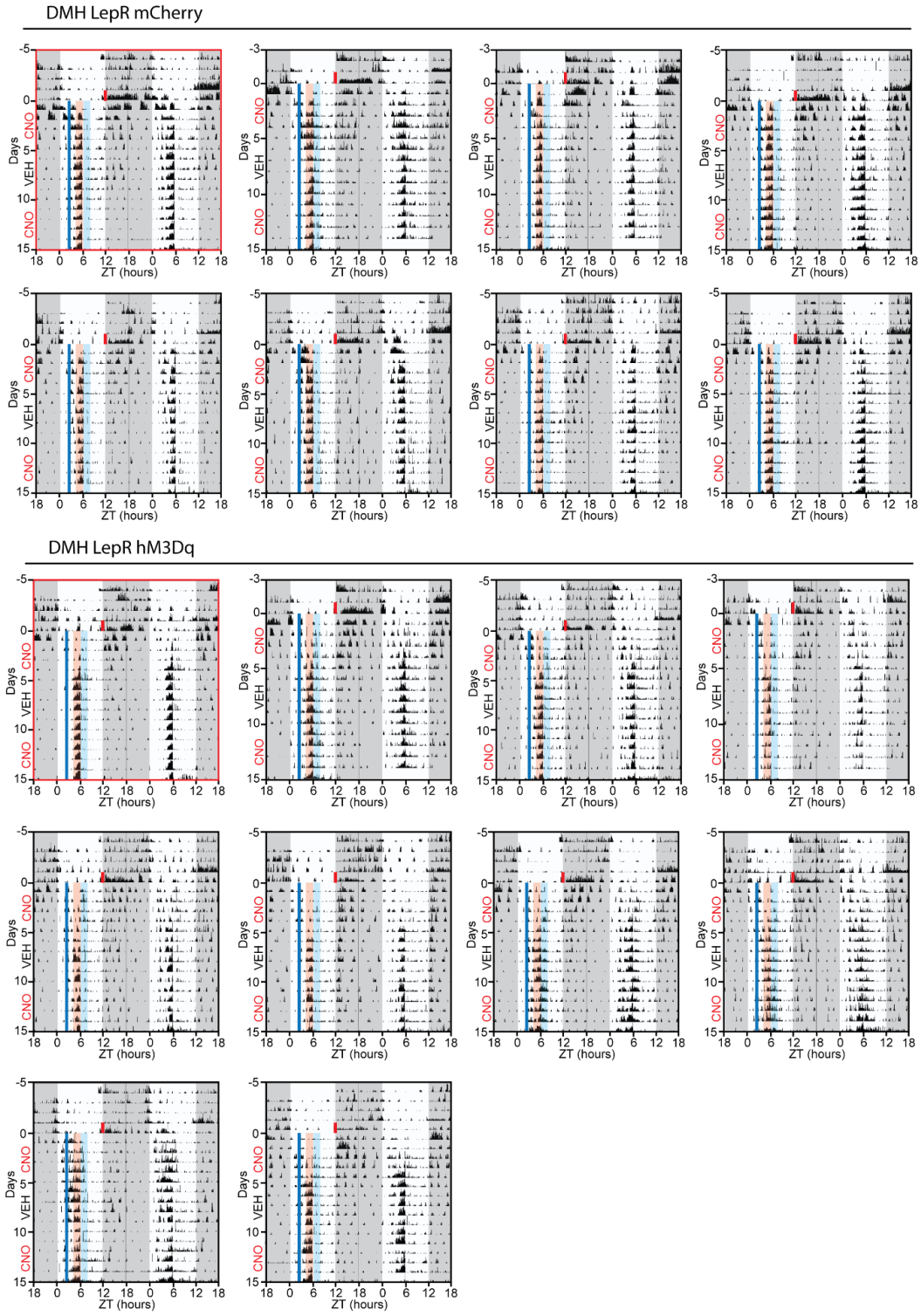

Extended data figure 4. Actograms of all DMH LepR mCherry and DMH LepR hM3Dq mice on SF.

(Brandon Podyma) The actograms used as representative figures in Fig 2 are depicted with red boxes.

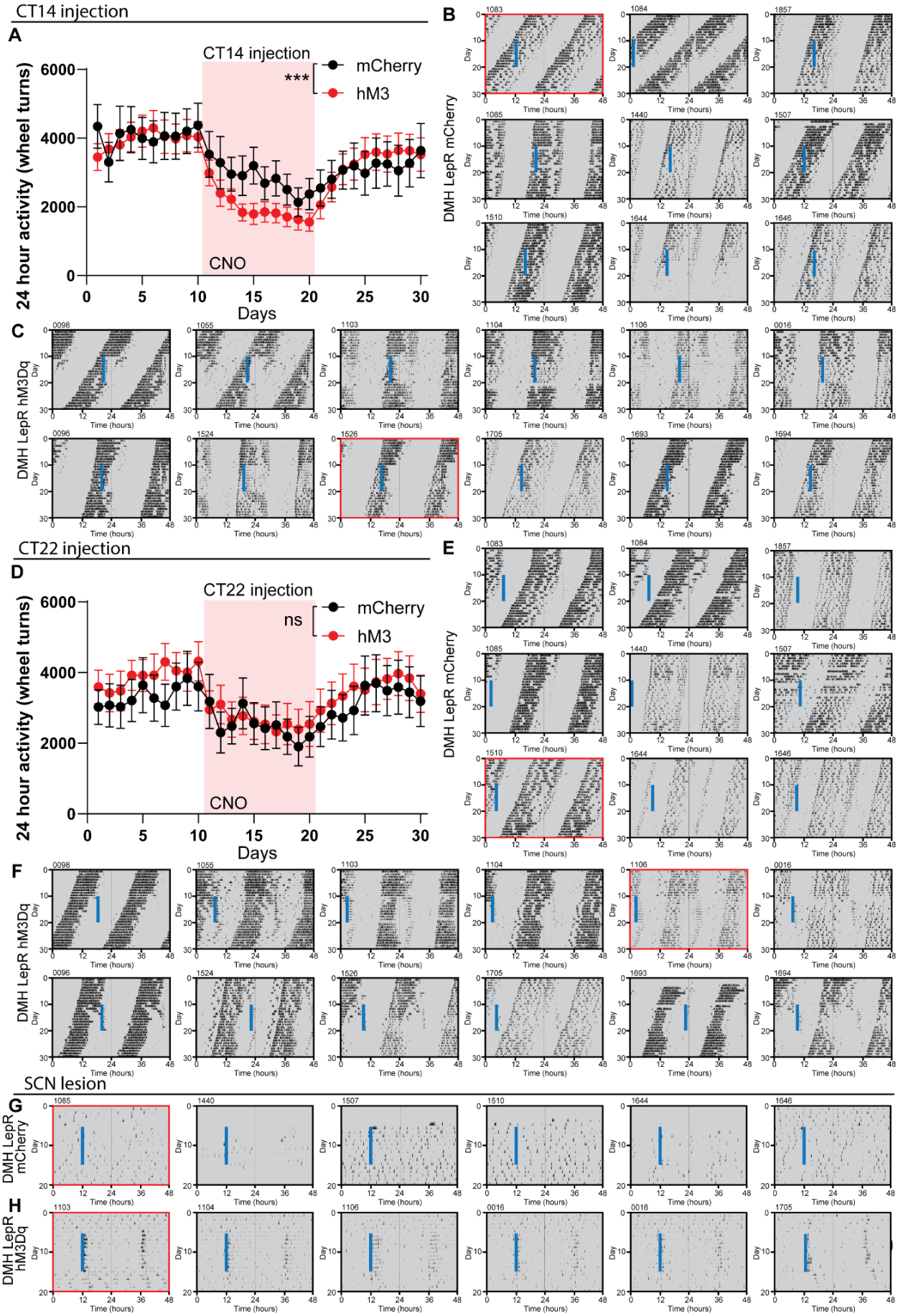
CT14 injection
A
CT14 injection
mCherry
hM3
***
CNO
24 hour activity (wheel turns)
Days
B
DMH LepR mCherry
C
DMH LepR hM3Dq
CT22 injection
D
CT22 injection
mCherry
hM3
ns
CNO
24 hour activity (wheel turns)
Days
E
DMH LepR mCherry
F
DMH LepR hM3Dq
SCN lesion
G
DMH LepR mCherry
H
DMH LepR hM3Dq
Time (hours)
Day

Extended data figure 5. Effect of chemogenetic activation of DMH LepR neurons on circadian locomotor activity pattern

(Brandon Podyma, Qijun Tang)

A. 24-hour total wheel revolutions of DMH LepR mCherry and DMH LepR hM3Dq animals before, during, and after CNO injections at ~CT14. Animals were housed under *ad libitum*, constant dark conditions. Pink shading represents days with CNO injection. Repeated measures two-way ANOVA; n = 9-12 / group; $F_{treatment * time}$ (29, 551) = 2.468, p<0.001.

B-C. Actograms of all LepR Cre animals bilaterally injected with (B) AAV-hSyn-DIO-mCherry or (C) AAV-hSyn-DIO-hM3Dq-mCherry and injected with CNO at ~CT14 (solid blue line). The actograms used as representative figures in Fig 3 are depicted with red boxes.

D. 24-hour total wheel revolutions of DMH LepR mCherry and DMH LepR hM3Dq animals before, during, and after CNO injections at ~CT22. Animals were housed under *ad libitum*, constant dark conditions. Pink shading represents days with CNO injection. Repeated measures two-way ANOVA; n = 9-12 / group; $F_{treatment}$ (1, 19) = 0.2061, p=0.6550.

E-F. Actograms of all LepR Cre animals bilaterally injected with (E) AAV-hSyn-DIO-mCherry or (F) AAV-hSyn-DIO-hM3Dq-mCherry and injected with CNO at ~CT22 (solid blue line). The actograms used as representative figures in Fig 3 are depicted with red boxes. Notablally, animal #1084 in E was excluded from quantification in Fig. 3I, because the injection time on the 10th day was near the locomotor activity onset (<3 hours) of the following day, due to the short free-running period.

G-H. Actograms of all LepR Cre animals with electrolytic lesions of the SCN and bilaterally injected with (G) AAV-hSyn-DIO-mCherry or (H) AAV-hSyn-DIO-hM3Dq-mCherry and injected with CNO every 24 hours for 10 days (solid blue line). The actograms used as representative figures in Fig 3 are depicted with red boxes.

Data are represented as mean ± SEM. *p < 0.05; **p < 0.01; ***p < 0.001; ns, not significant.

Chapter 4 Discussion and Perspective

In line with previously reported results, we observed direct projection of DMH LepR neurons to the SCN using viral rabies retrograde tracing [199](Chapter 3 Figure 4). Single-cell analysis of the hypothalamic LepR neurons revealed that a considerable number of DMH LepR neurons express TH, therefore potentially dopaminergic [203]. Together with the strong effect of Drd1 signaling on the organization of SCN circadian rhythmicity (Addendum Figure 1), DA signaling is a highly potential mechanism for the DMH^{LepR}-SCN circuit to serve as a link between metabolic stages and circadian system regulation. The experiments below would provide great insight for further understanding the role of this circuit in regulating the interplay between biological clock and metabolism.

- The new tools to examine neuromodulator levels *in vivo*, such as GRAB-DA and dLight [204,205], provide us great assets in visualizing DA release at target sites. Characterizing the dopamine level in the SCN during different energy states, including fed, fasted, TRF, HFD, will provide a well-rounded knowledge about the DA dynamics in the SCN.
- The functionality of the DMH^{LepR}-SCN circuit in circadian behavior regulation has been demonstrated (Chapter 3 Figure 4). However, to further validate the role of DA as the key neurotransmitter, characterizing the behavioral phenotype of the mice with selective knockout of TH in the DMH-LepR neurons is necessary.
- The VTA^{DA}-SCN circuit has been studied for its role in circadian and metabolism regulation [80,206]. It is important to characterize the level of innervation of VTA^{DA} and $DMH^{LepR/TH}$ neurons. Using fluorescent DA reporter in the SCN to

monitor the acute DA release by optogenetically activating VTA^{DA} or $DMH^{LepR/TH}$ neurons is a potential strategy.

- The effect of leptin and DMH-LepR neuron activation on food entrainment is not identical (Chapter 3 Figure 1 & 2). One potential interpretation is the wide distribution of LepR, including VTA [180]. Notebally, leptin has been shown to convey its food suppressive effect through VTA [207]. The role of VTA^{DA}-SCN circuit in food entrainment is therefore an insightful topic that remains to be investigated.

In the field of food clock study, FAA is the most widely used behavioral readout of food entrainment. Body temperature, blood cortisol level, anticipatory operant behaviors are also widely used. In our work, we studied three other behaviors that showed entrainment to scheduled food access, rate of food intake, RER, and energy expenditure. Among them, the rate of food intake implies the drive to eat and how prepared the animals are for the upcoming food. It is an attractive topic to me to test the motivational drive for food in food entrained animals across circadian time. I expect higher motivation at a certain entrained period than the rest of the day. It has been shown that animals can entrain to multiple scheduled food access [47]. If the animals are given access to food and water at different times, it remains to be answered if the animals will develop entrainment to these two stimuli at different time, and if the motivational behavior to each stimulus will only be elevated at associated time (ie. lever pressing for water and nose poke for food). Further, if a learning task coupled with scheduled reward is posted, the speed of learning might be elevated at certain circadian

time. These questions will provide great insights for the scenarios in our life where rewards determine the efficiency of learning or drive. Correct reward at the correct time of the day might prove to be a more efficient method in driving behavior.

As shown in this thesis, metabolism closely interacts with the biological clock system. While metabolic processes and behaviors are under control of the circadian system and show daily rhythmicity, feeding behaviors alter circadian rhythms in turn. Personalized meal plans have been used as treatments to various metabolic diseases. The nutrient compensation of the food is the focus for them. However, there may be great value to also consider the timing. It has been shown in the mouse model that chocolate, potentially a highly rewarding food, at breakfast time speeds up entrainment to a shifted light cycle [81]. I can imagine that for people constantly traveling across time zones, a more rewarding meal at breakfast can assist faster adjustment of the body to the new light cycle, whereas limiting the value of breakfast but have a highly rewarding dinner may be essential for the ones who encounters occasionally shifted work schedule but hope to keep original internal clock for the following days.

In summary, proper circadian coordination plays an essential role in health and potentially learning and work efficiency. Understanding of the behavior readouts of the circadian system will be critical for future development of non-invasive devices to monitor the circadian rhythmicity of humans. On the other hand, further study of the impact of metabolism on the circadian system can provide insights for personalized non-invasive, drug-free treatment for patients suffering dysfunction of circadian system.

Addendum 1: A building block-based beam-break (B5) locomotor activity monitoring system and its use in circadian biology research.

Qijun Tang[1], Sydney P. Williams[1] & Ali D. Güler[1,2,*]

[1]Department of Biology, University of Virginia, Charlottesville, VA 22904, USA

[2]Department of Neuroscience, School of Medicine, University of Virginia, Charlottesville, VA 22908, USA

Correspondence

*To whom correspondence should be sent:

Ali D. Güler

Departments of Biology and Neuroscience

University of Virginia

Charlottesville, VA 22904-4328

Email: aguler@virginia.edu

This methodology development work was published in July, 2022, in *BioTechniques*. DOI: 10.2144/btn-2022-0036, PMID: 35848801. [208].

a1.1 Abstract

Locomotor activity is one of the most commonly assayed animal behaviors. It is the gold standard for assessing behavioral circadian rhythmicity. Here, we develop a flexible and affordable locomotor activity monitoring system that does not interfere with the behavior of animals. We validate the reliability of the system in multiple circadian biology research scenarios. This device is customizable and can be used for many animal species.

a1.2 Main

Nearly all organisms on Earth possess a biological clock that is synchronized to the astronomical day to align physiological and behavioral responses to the optimal time of day [209]. Locomotor activity has been one of the most widely used rhythmic behaviors to study circadian clocks, beginning with the studies that led to the identification of the first circadian gene mutants in Drosophila and mice [2,210]. Rodents have been an invaluable laboratory model system to study circadian rhythmicity, and their locomotor activity is generally monitored by four different methods: 1) Wheel running activity; this is the most popular in rodent models [80], however, access to the running wheel can influence circadian activity rhythms of the animals [26]. 2) Biotelemetry implantation; this method can monitor multiple circadian rhythms simultaneously (e.g., locomotor activity, body temperature, and heart rate), however, it requires surgical implantation of a probe which induces adverse effects on the animals [211]. 3) Video recording; this is a less invasive technique and can provide a wide array of information about circadian

behaviors, however, much of the information is redundant and video analysis requires sophisticated analytical tools [212]. 4) Infrared (IR) beam-break; this strategy is emerging as an ideal non-invasive option that provides precise circadian locomotor activity monitoring over extended periods of time without the need for a complicated analysis pipeline. The amount of data collected using IR beam-break is small yet sufficient for the analysis of circadian behavioral rhythmicity. There are a number of commercially available IR beam-break systems. Some of these can be incorporated into more sophisticated animal behavior phenotyping systems such as metabolic monitoring or operant conditioning chambers. In this work, we developed an affordable multi-beam based locomotor activity monitoring system named B^5 (Building Block-Based Beam-Break, figure 1, table 1). The activity monitoring modules of B^5 are constructed with building blocks which allows for flexibility in the size and shape of the system (figure 1B) and can be easily integrated into existing animal behavior chambers as an economical upgrade.

a1.2.1 Data acquisition

Each B^5 activity monitoring system is composed of two major components, a control panel and four detection modules. These two components are connected to one another with ethernet cables (figure 1, table 1).

The system is run with a custom program (see Resource Availability section) that is powered by an Arduino board located in the control panel. In addition to the Arduino board, the control panel is constructed with three major components (figure 1A&C, table

1): 1) A microSD (secure digital) card module; the data can be collected and stored on the microSD card without the need for a computer. 2) A real-time clock module; the internal time of the Arduino board is reset every time it is powered off and on. Thus, the clock module is used to track the actual time of data entry which is necessary information in circadian biology research. 3) An LCD (liquid-crystal display) screen allows status monitoring of the system with the ability to adjust the brightness and contrast of the screen. Notably, the background light can be fully turned off for minimum light disruption in circadian biology studies.

Each control panel can connect up to 4 detection modules. Each detection module holds one animal cage, which allows for simultaneous recording of up to 4 individually housed animals with a single B^5 system (figure 1A-D). Each module is constructed with 4 pairs of IR emitters and receivers to form a 4-beam IR grid (figure 1B). The IR receiver is connected to a resistor to form a simple photodiode amplifier circuit which sends a high potential to the control panel when the light from the emitter is successfully detected (figure 1E-F). The potential sent to the control panel is reduced when the animal interrupts the IR beam between the emitter and the receiver (beam blocked, figure 1F). The resistance of the resistor that is serially connected to the IR receiver affects the sensitivity of the detection. By changing this resistor, B^5 easily can be adjusted to meet the sensitivity requirements in a variety of scenarios, such as differing arena dimensions, animal size, transparency of animal cage, etc.

A multi-beam grid is necessary to differentiate if the detected beam-break counts are a result of locomotor activity, or stereotypic behaviors such as scratching, rearing,

food/water consumption, or even breathing (figure 1G-I). Every time a beam is blocked, the position of the blocked beam is stored in memory and is compared with the next beam-break. If the next beam-break takes place on the same beam, the “total” beam-break count is increased by 1, whereas if a different beam is blocked, this event is logged as both “total” beam-break and “ambulatory” activity (figure 1G-I). The “total” and “ambulatory” beam-break data are both useful in different scenarios. When reporting an animal’s locomotor activity, the “ambulatory beam-break” count should be used. The “total beam-break” count can be used to estimate the animal’s sleep, and produces comparable results as the “gold standard” of sleep analysis, electroencephalography (EEG) [206,213].

This infrared detector setup (figure1 E-I) can be adapted for a wide range of behavior monitoring purposes in addition to locomotor activity. For example, the detector can be placed by a feeder or water portal to detect a subject’s food or water consumption. Alternatively, an array of detectors can be used to monitor movement in a complex or multi-compartment arena to track location preference.

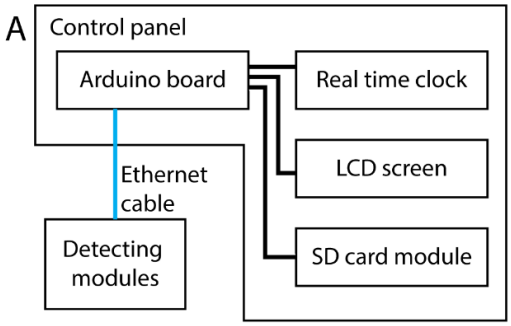

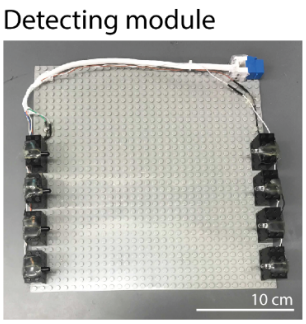

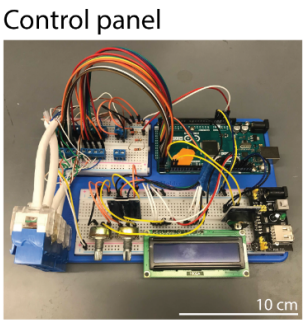

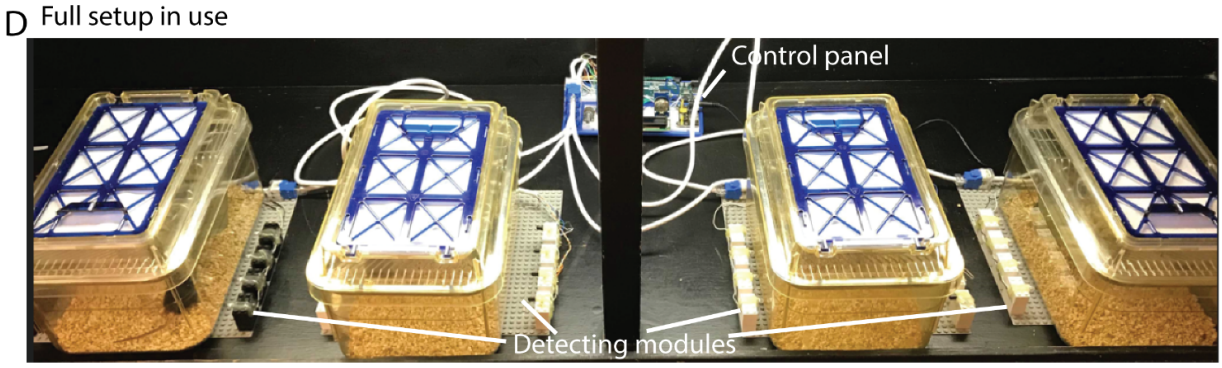

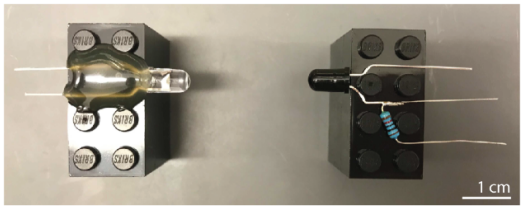

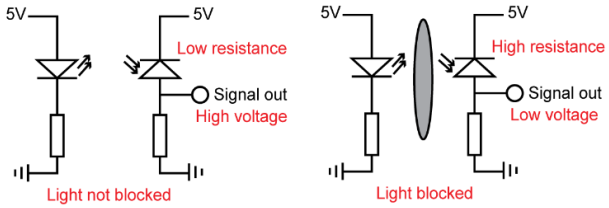

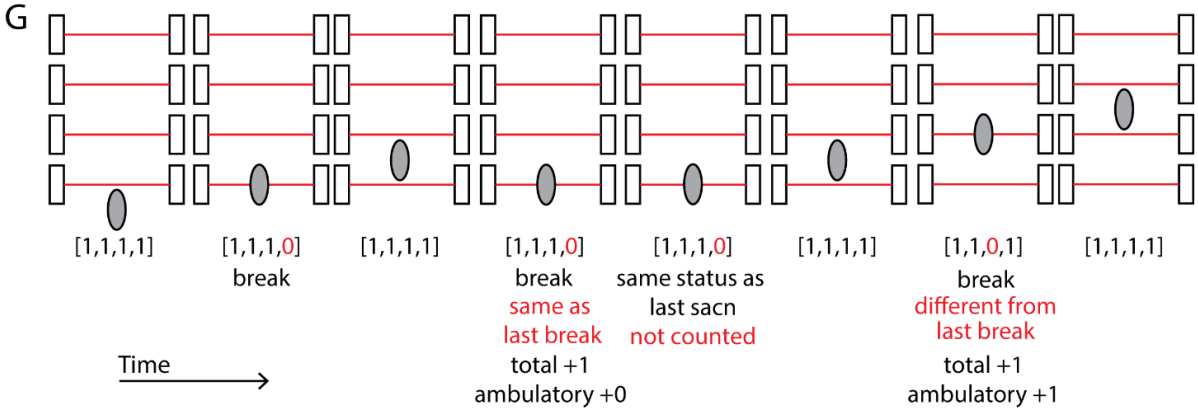

H

EXP_42.TXT - Notepad

File Edit Format View Help

```
Start time:05.11.2021,17:02:45,Friday
Intervals,Cage1-total,Cage1-amb,Cage2-total,Cage2-amb,Cage3-total,Cage3-amb,Cage4-total,Cage4-amb
1,1,1,8,1,0,0,5,2
2,0,0,8,2,0,0,8,6
3,0,0,0,0,0,0,3,2
4,0,0,2,2,0,0,1,1
5,0,0,5,1,0,0,2,1
6,0,0,0,0,0,0,5,1
7,0,0,0,0,0,0,3,1
8,0,0,7,4,0,0,3,2
9,0,0,11,1,0,0,1,1
10,1,0,0,0,0,0,0,0
11,0,0,2,1,0,0,8,6
12,0,0,4,3,0,0,4,2
13,0,0,5,0,0,0,0,0
14,0,0,5,2,0,0,0,0
15,0,0,3,0,0,0,0,0
```

I

	A	B	C	D	E	F	G	H	I
1	Start time:05.11.2021	17:02:45	Friday						
2	Intervals	Cage1-tot	Cage1-am	Cage2-tot	Cage2-am	Cage3-tot	Cage3-am	Cage4-tot	Cage4-amb
3	1	1	1	8	1	0	0	5	2
4	2	0	0	8	2	0	0	8	6
5	3	0	0	0	0	0	0	3	2
6	4	0	0	2	2	0	0	1	1
7	5	0	0	5	1	0	0	2	1
8	6	0	0	0	0	0	0	5	1
9	7	0	0	0	0	0	0	3	1
10	8	0	0	7	4	0	0	3	2
11	9	0	0	11	1	0	0	1	1
12	10	1	0	0	0	0	0	0	0
13	11	0	0	2	1	0	0	8	6
14	12	0	0	4	3	0	0	4	2
15	13	0	0	5	0	0	0	0	0

Figure 1. Overview and data acquisition logic of the system

A. Overview of the key components of B5. Each system is designed to have one control panel and four detection modules, which is capable of monitoring four individually housed animals simultaneously.
B. Image of one detection module of B5.
C. Image of the control panel of B5.
D. Image of the B5 system setup for recording locomotor activity of four individually housed mice simultaneously.
E. Image of one pair of IR emitter (left) and IR receiver (right).
F. Diagram illustrating the circuit that converts beam-break status to binary signal.
G. Diagram illustrating how to use the 4-beam grid to discriminate "total" and "ambulatory" activity
H. Example of the beginning part of the raw data (.txt file) recorded by the B5 system.
I. Example of the same data in (H), opened with Microsoft Excel.

a1.2.2 Validation of the system in circadian biology research

To demonstrate the effectiveness of our system in circadian biology research, we conducted various circadian biology assays on mice and used our system to monitor the locomotor activity (figure 2). First, we monitored light-dark entrained locomotor activity of mice. 4 adult male C57BL6/J mice were individually housed in transparent cages under a 12h:12h L:D cycle with ad libitum access to food and water. Each cage was put on one of the detection modules (figure 1). Two other cohorts of strain, age, and sex matched mice (4 mice each cohort) were individually housed and provided with ad libitum access to food and water for locomotor activity recording using a commercially available IR beam-break system (Columbus Instruments) or cages equipped with running wheels. After 5 days of recording, we observed nocturnal, entrained locomotor activity using the B^5 system (figure 2A). This result was comparable to behavioral data collected by the commercially available IR beam-break system or cages equipped with running wheels (figure 2A-D). Notably, both IR beam-break-based systems revealed

small bouts of locomotor activity during the daytime (rest phase of mice) (figure 2A-B), whereas there was negligible wheel running activity at this time (figure 2C).

We performed more sophisticated circadian assays to validate the ability of B^5 to reveal them. Light is the major environmental cue that provides the time-of-day information to the circadian timing system [8,162]. It is well documented that a brief light pulse during a rodent's nighttime will alter the intrinsic circadian timing of the animal. For example, a light pulse early in the dark phase (i.e., Zeitgeber time 14 [ZT14]) delays the phase of activity onset on the following day [80,162]. To test this response, we housed a cohort of 4 adult male C57BL6/J mice individually in a 12h:12h L:D cycle to record baseline activity. After 5 days, we delivered a 15-minute light pulse (100 mW/cm^2) at ZT 14 (two hours after lights off), and then released the mice to constant darkness to determine their circadian phase. On the following day, we observed the expected ~2-hour delay in the onsets of activity using the B^5 system (figure 2E-F).

In addition to light, the circadian system is also capable of adapting to salient events such as food availability. We performed a time-restricted feeding (TRF) assay on a cohort of 4 adult male C57BL6/J mice. It is well documented that when the food availability is restricted to the same time every day, animals anticipate the presentation of food. This food anticipatory activity (FAA) is expressed as increased locomotor activity prior to the scheduled food provision, even if food is provided during the rest phase of the animal [37]. After 5 days of baseline activity recording where the mice had ad libitum access to the food, we subjected mice to TRF where a limited amount of food

was scheduled to deliver at the middle of light phase (ZT6) for an additional 5 days. We successfully observed the FAA as expected using the B^5 system (figure 2G-H).

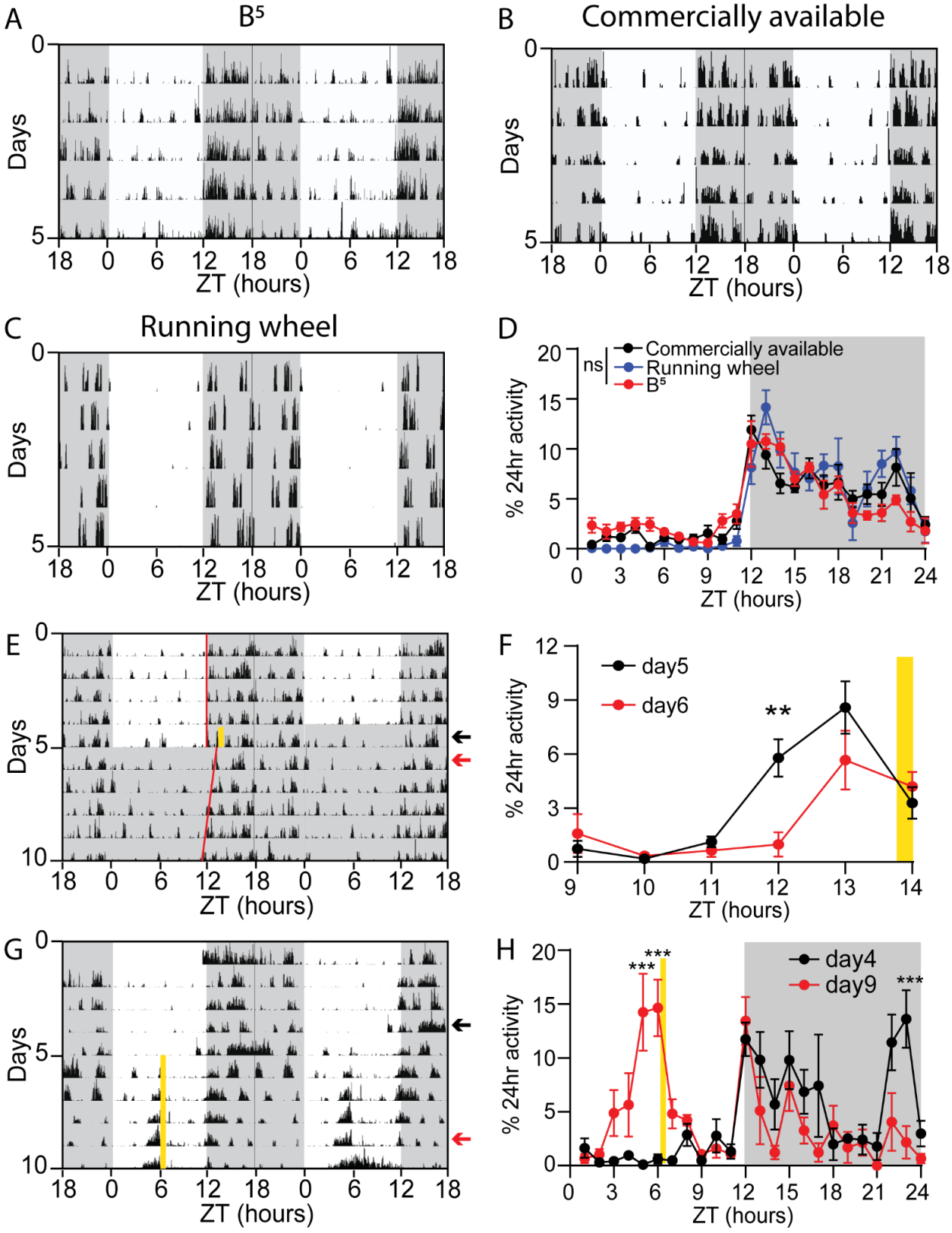
A
B⁵
Days
ZT (hours)
B
Commercially available
C
Running wheel
D
Commercially available
Running wheel
B⁵
ns
% 24hr activity
E
F
day5
day6
**
G
H
day4
day9
***

Figure 2. Validation of the system in circadian biology research

A. Representative actogram of an animal's locomotor activity recorded by B^5.

B. Representative actogram of an animal's locomotor activity recorded by a commercially available system.

C. Representative actogram of an animal's locomotor activity recorded by running wheel.

D. Five-day average of the activity data shown in figure A, B and C, normalized to percentage of total daily activity. Repeated measures two-way ANOVA; n=4 / group; $F_{method}(2,9)=2.22$, $p=0.1645$. Data represented as mean ± SEM. ns, not significant.

E. Representative actogram of light pulse induced phase delay, monitored by B^5. Time of light pulse is depicted as vertical yellow line. Color coded arrows indicate the days selected for quantification in (F).

F. ZT9-14 average activity at the day before (day5) and after (day6) light pulse. Time of light pulse on day5 is depicted as yellow shade. Repeated measure two-way ANOVA with Bonferroni post hoc comparison; n=4 / group; $F_{treatment*time}(5,30)=3.54$, $p=0.0124$. Data represented as mean ± SEM. **p<0.01.

G. Representative actogram of time-restricted feeding induced food anticipatory activity, monitored by B^5. Time of food delivery is depicted as vertical yellow line. Color coded arrows indicate the days selected for quantification in (H).

H. Average activity across 24-hours at day4 (free access to food) and day9 (4^{th} day on TRF) of the TRF experiment. Time of food delivery on day9 is depicted as vertical yellow line. Repeated measure two-way ANOVA with Bonferroni post hoc comparison; n=4 / group; $F_{treatment*time}(23,138)=5.04$, $p<0.001$. Data represented as mean ± SEM. ***$p<0.001$.

In A-F, the gray shaded area indicates the dark phase.

a1.3 Conclusion

We constructed an economical system, B^5, which monitors the locomotor activity of mice with minimum interference to an animal's regular behavior. The system successfully revealed a variety of expected circadian biology responses, including light and food entrainment. The results obtained using B^5 are comparable to widely used locomotor activity monitoring methods. One advantage of the B^5 system is that it is operated with 6-12 volts DC power. Although a plugged 6-volt AC/DC power adaptor was used for all the experiments described above, simple batteries can be used as the power supply. Coupled with the building block-based design, the system can function for long durations without investigator intervention in light-tight compartments for circadian biology research, or in the field for a wider range of research purposes. The simplicity of the concept and circuit of the IR beam blocking detector makes the B^5 system adaptable to meet a variety of behavior monitoring needs. The entire system is open-source and constructed with commercially available and affordable components (table 1). Our work

here makes high throughput animal behavior monitoring accessible to a broader range of scientists.

a1.4 Resource Availability

The custom Arduino program to power the B^5 is available on: https://github.com/qjtang12/BX5

a1.5 Materials and Methods

Mice.

All experiments were carried out in compliance with the Association for Assessment of Laboratory Animal Care policies (AALAC) and approved by the University of Virginia Animal Care and Use Committee (ACUC). Animals were housed on a 12-h light/dark cycle with food (PicoLab Rodent Diet 5053) and sterile water ad libitum unless otherwise indicated. All experiments were performed on male mice 12 weeks or older (adult). Wild-type C57BL6/J mouse is the only strain used in this work.

Before experiments, adult male C57BL6/J mice were individually housed in activity wheel-equipped cages (Nalgene, 144 in^2 [18 (L) x 8 (W) x 8 (H)]), or in transparent regular mouse home cages (60 in^2 [10 (L) x 6 (W) x 6 (H)]), within the IR beam interruption modules (Columbus Instruments [commercially available], or B^5 [this work]) in ventilated light-tight compartments (1446 in^2 [70.5 (L) x 20.5 (W) x 18 (H)]), under a 12h:12h LD cycle for at least 3 days for habituation. Fluorescent lights (100 mW/cm^2) were used in all the light-tight compartments for behavioral experiments. Corn cob

bedding was provided in all the animal cages. Environmental enrichment was not provided to avoid interruption of the locomotor activity monitoring systems.

Light-Dark entrainment using three different monitoring systems

After 3-day habituation period, the locomotor activity was recorded for 5 days. The wheel running activity and the Columbus Instruments IR beam interruption system data were collected at 6-minute intervals. The B^5 data was collected at 10-second intervals. Wheel running activity was monitored and analyzed with ClockLab collection and analysis system (Actimetrics). Data from the IR beam interruption systems (both Columbus Instruments and B^5 systems) were analyzed in Excel for quantification, or converted to ClockLab (Actimetrics) supported file format using a custom MATLAB (Mathworks) script for circadian analysis. The MATLAB script used for converting the raw data of B^5 to ClockLab supported file format is available along with the source code of the B^5 system at https://github.com/qjtang12/BX5 (see Resource Availability section for details). The collected data was binned hourly, and then normalized to 24-hour total activity for each day (ZT0-ZT24). This normalized hourly activity was averaged over 5 days for each animal. The averaged activity of all animals for each recording method was statistically compared.

Light-pulse induced phase shift

After 3-day habituation period, the locomotor activity at 10-second intervals was recorded for 5 days as the baseline for individually housed mice in the B^5 system. On the 5^{th} day, ~2 hours after the light had been off, the housing light (100 mW/cm^2) was

turned back on for 15 minutes as the light-pulse treatment. After the 15-minute light pulse, the animals were released to constant darkness. The locomotor activity was recorded for another 5 days. For the quantification of the effect of the light pulse, the data from day of light pulse and the following day were further analyzed. The collected data of these two days were binned hourly, and then normalized to 24-hour total activity for each day. The averaged activity for all animals in each of these two days was statistically compared.

Time restricted feeding (TRF).

After 3-day habituation period, the locomotor activity at 10-second intervals was recorded for 5 days as the baseline for individually housed mice in the B^5 system. On the 5^{th} day, mice were fasted at lights off (ZT12) along with a full cage change. Mice were then refed at ZT6 (6 hours after light on) for the next five days. On the first two days mice were fed 2g of food (PicoLab Rodent Diet 5053), and on all remaining days were fed 2.5g. For quantification of the effect of the TRF treatment, the data from a baseline day that the animals had ad libitum access to food, and 4^{th} day on TRF were further analyzed. The collected data of these two days were binned hourly, and then normalized to 24-hour total activity for each day. The averaged activity for all animals in each of these two days was statistically compared.

Data analysis and visualization

Wheel running activity was monitored and analyzed with the ClockLab collection and analysis system (Actimetrics). Data from the IR beam interruption systems (both

Columbus Instruments and B^5 systems) were analyzed in Excel for quantification, or converted to ClockLab (Actimetrics) supported file format using a custom MATLAB (Mathworks) script for circadian analysis as described above. See also the Actimetrics webpage for converting data to ClockLab compatible format: https://actimetrics.com/text-based-clocklab-data-format/

For data visualization, the actograms (Figure 2A-C, E, G) were produced by the ClockLab analysis software (Actimetrics). The line plots (Figure 2D, F, H) were produced by GraphPad Prism 8 software.

Statistical Analysis

To compare the effects of treatment or recording methodology over time, repeated-measures two-way ANOVA test was used. Following a significant effect in the ANOVA test, Bonferroni's post hoc comparison was used to determine differences between individual data points. Analyses were conducted using GraphPad Prism 8 statistical software for Windows. All data are presented as means ± standard error of the mean with $p < 0.05$ considered statistically significant.

Table 1: Core components used for the construction of the system

Key components used	**Manufacturer/Identification**
Arduino Mega 2560	REV3 [A000067]
IR photo emitter	XINGYHENG

IR photo receiver	XINGYHENG
microSD card module	HiLetgo; 3-01-0038-5PCS
Micro SD card	SanDisk; 16GB
LCD screen	HiLetgo; 3-01-0045
Potentiometers	HiLetgo; 3-02-0413
Real time clock	HiLetgo; 3-01-0435
6V/2A AC/DC power adaptor	Security-01; DK19-060-2000
5V breadboard power supply module	HiLetgo; 3-01-0435; 3-01-0051
Building blocks	Strictly Briks; 2x4 blocks
Building blocks (base plate)	Leke; 10” x 10” base plate
10k ohm resistors	EDGELEC; EFR-W0D50-A:MF [E5P011] 10K ohm
43 ohm resistors	EDGELEC; EFR-W0D50-A:MF [E5P002] 43 ohm
Breadboard	REXQualis
Breadboard holder	SunFounder
RJ45 jack for ethernet cable connection	AMPCOM

CAT6 ethernet cables	trueCABLE
Wires, hot glue, soldering iron	N/A

Addendum 2 : Unpublished results

a2.1 Effect of Elevated Drd1 Signaling in the SCN

Using on-slice electrophysiology, we demonstrated that elevating Drd1 signaling in the SCN by applying Drd1 agonist SKF-81297 suppresses the spontaneous firing of SCN cells at both day and night (Chapter 2 Figure 4E). I sought to further explore the effect of SKF-81297 on the circadian behavior of the SCN cells. Using the PER2::Luciferase mouse model, I was able to monitor the expression level of the circadian gene *Per2* by recording the bioluminescence, at a single-cell level (Figure 1A). Application of 5 mM SKF-81297, in the SCN explants regenerate a PER2 peak despite the circadian phase of individual cells (Figure 1B). This observation demonstrated the functionality of elevated Drd1 signaling on the circadian synchronization of SCN cells.

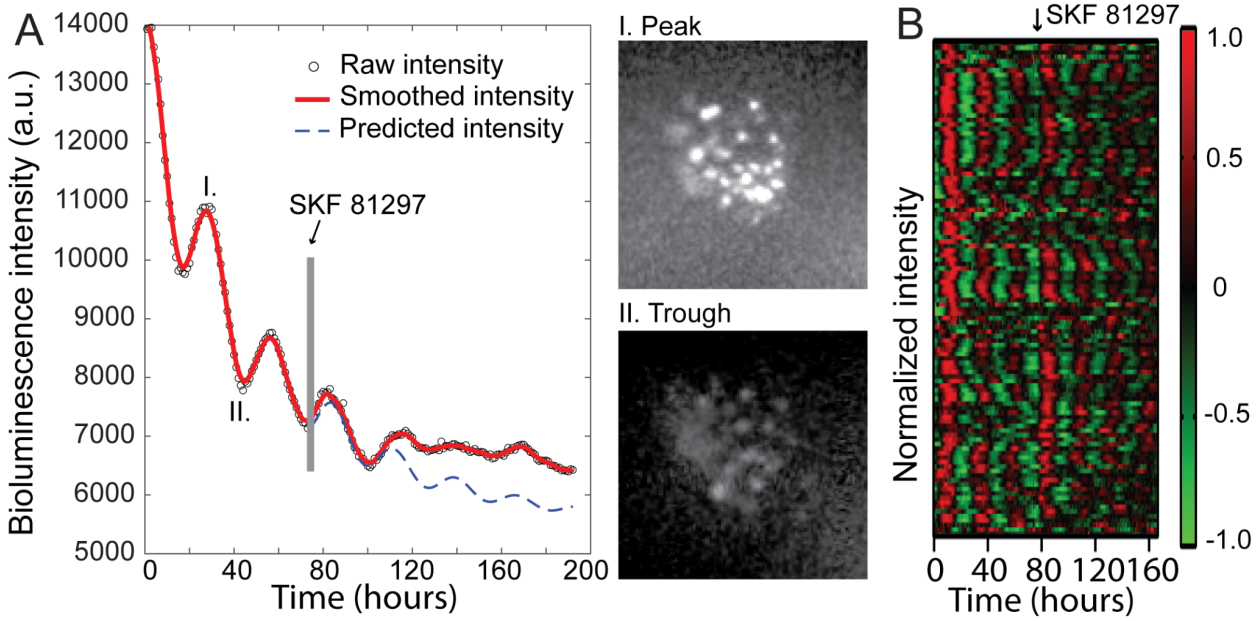

Figure 1. Elevated SCN-Drd1 signaling reset the circadian phase of SCN cells

A. Representative bioluminescence rhythm of an entire SCN explant pre- and post-SKF-81297 (5mM) application. Insets: SCN PER2::LUC bioluminescent images at peak (I.) and trough (II.) with single-cell resolution.
B. Heatmap of normalized single-cell PER2::LUC bioluminescence rhythms from a SCN explant treated with SKF 81297. Each row represents a cell. Only cells that remain rhythmic throughout the whole recording session (as determined by BD2 eJTK rhythmicity test [214]) are included in the analysis.

We demonstrated that DA tone was elevated in the SCN in response to HFD using HPLC on the tissue punches containing SCN (Chapter 2 Figure 4D). To provide more in vivo evidence that HFD is capable of inducing dopamine release in the SCN, I expressed the genetically encoded DA sensor dLight1.3b [204] in the SCN. In support of our hypothesis, I observed that consumption of high-fat diet (HFD) increases DA in the SCN (Figure 2A). While we demonstrated the ability of Drd1 agonist SKF-81297 to suppress the activity of SCN neurons (Chapter 2 Figure 4E), the *in vivo* effects of HFD on the SCN neuron activity is unclear. To monitor neuronal activity in the SCN neurons, I expressed the genetically encoded calcium sensor GCaMP7s [201] in the Drd1 neurons of the SCN and recorded circadian oscillations of calcium over days. The amplitude of the circadian cycling of calcium level in the SCN-Drd1 neurons was reduced following the provision of HFD. Conversely, time restricted feeding (TRF)-induced calorie deprivation increased this amplitude (Figure 2B).

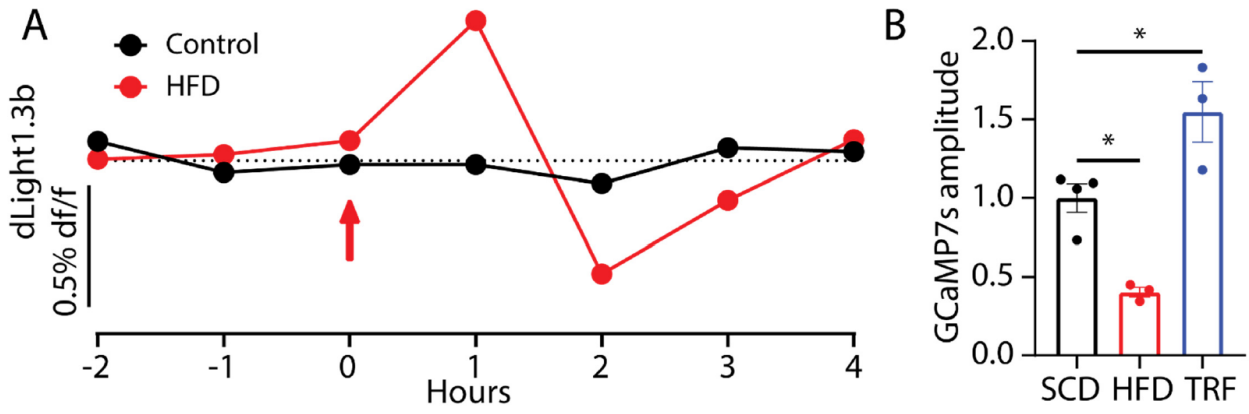

Figure 2. HFD induces DA release in the SCN and dempens the amplitude of neuron activity cycling.

A. DA fiber photometry recordings from the SCN of a freely-moving WT mouse injected with AAV1-hSyn-dLight1.3b in the SCN. The average dLight1.3b signal relative to the baseline (df/f) is reported for each depicted time point. A rewarding HFD pellet was delivered at zero time point (red arrow) during the HFD recording (red). The change in the DA level in response to the rewarding stimulus is compared to the no reward control condition (black).
B. Amplitude of the circadian calcium oscillations from the SCN of a freely-moving Drd1-Cre mouse injected with AAV1-hSyn-FLEX-GCaMP7s in the SCN. Fiber photometry recordings were performed during *ad libitum* provision of SCD or HFD. SCN intracellular calcium dynamics were also monitored during a hypocaloric regiment, TRF, which reduces the body weight by ~20% [37]. The long-term calcium monitoring was achieved by 10-minute bout recordings of isosbestic normalized GCaMP7s signal every hour across a minimum of 3 days for each condition [185]. The dataset is normalized to the average circadian amplitude of the SCD recordings.

a2.2 SCN Suppresses Food Intake in a Time-dependent Manner

In chapter 2, we hypothesize that HFD-driven elevation in the SCN DA levels translates to increased food consumption outside of the regular mealtimes by disinhibiting the downstream orexigenic centers. We demonstrated that the activation of G_s-coupled Drd1-signaling in the SCN inhibits the activity of the local neurons via GABAergic

neurotransmission (Chapter 2 Figure 4E-K)[206]. Since SCN-neurons are almost all GABAergic, the decreased SCN activity would be expected to disinhibit the downstream targets [151,152,215], therefore lead to overeating. To further validate the suspected inhibitory effect of SCN on feeding, I used chemogenetics strategy to activate SCN neurons, by selectively expressing hM3Dq in the Drd1 neurons of SCN. Approximately 60% of the SCN neurons express Drd1 and they are expressed across the entire SCN anatomically [78,169,199,216–218]. When the mice were fed SCD, SCN remained a high amplitude of neuron activity rhythm, which is more active during day than night (Figure 2B, 3A; Chapter 2 Figure 4E, S4F). When chemogenetically activating the SCN neurons using hM3Dq, there was more dynamic range to elevated the SCN activity during the night when the SCN is naturally less active. Therefore, activating SCN by hM3Dq at night but not day suppressed food intake (Figure 3B). When the mice were fed HFD, the amplitude of the SCN neuron activity was dampened, therefore rendering space for the hM3Dq to elevate the neuron activity. In line with this hypothesis, activating SCN by hM3Dq at both day and night was able to suppress the food intake.

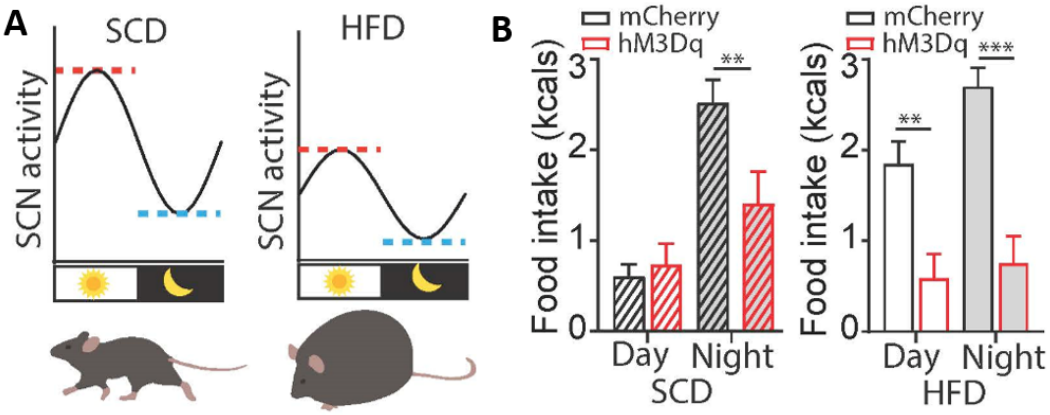

Figure 3. SCN Suppresses Food Intake in a Time-dependent Manner

A. High-fat diet (HFD) dampens SCN neuronal activity, which increases rest-phase food intake leading to obesity.
B. 3-hour food consumption following CNO administration in mice expressing hM3Dq or mCherry (control) in the SCN Drd1 neurons, with *ad libitu*m access to SCD (left) or HFD (right) during day or night.

Acknowledgement

I will regret my entire life if I accidentally miss someone here. Therefore, I am grateful for everybody, all my pets, all wild lifes and everything in my life so far, without whom I am not who I am at this point.

References

Bibliography

1. Tang, Q., Assali, D.R., Güler, A.D., and Steele, A.D. (2022). Dopamine systems and biological rhythms: Let's get a move on. Front. Integr. Neurosci. *16*, 957193.
2. Konopka, R.J., and Benzer, S. (1971). Clock mutants of Drosophila melanogaster. Proc Natl Acad Sci USA *68*, 2112–2116.
3. Roenneberg, T., and Merrow, M. (2005). Circadian clocks - the fall and rise of physiology. Nat. Rev. Mol. Cell Biol. *6*, 965–971.
4. Kohsaka, A., and Bass, J. (2007). A sense of time: how molecular clocks organize metabolism. Trends Endocrinol. Metab. *18*, 4–11.
5. Yamaguchi, S., Isejima, H., Matsuo, T., Okura, R., Yagita, K., Kobayashi, M., and Okamura, H. (2003). Synchronization of cellular clocks in the suprachiasmatic nucleus. Science *302*, 1408–1412.
6. Welsh, D.K., Yoo, S.-H., Liu, A.C., Takahashi, J.S., and Kay, S.A. (2004). Bioluminescence imaging of individual fibroblasts reveals persistent, independently phased circadian rhythms of clock gene expression. Curr. Biol. *14*, 2289–2295.
7. King, D.P., Zhao, Y., Sangoram, A.M., Wilsbacher, L.D., Tanaka, M., Antoch, M.P., Steeves, T.D., Vitaterna, M.H., Kornhauser, J.M., Lowrey, P.L., *et al.* (1997). Positional cloning of the mouse circadian clock gene. Cell *89*, 641–653.
8. Takahashi, J.S. (2017). Transcriptional architecture of the mammalian circadian clock. Nat. Rev. Genet. *18*, 164–179.
9. Ueda, H.R., Hayashi, S., Chen, W., Sano, M., Machida, M., Shigeyoshi, Y., Iino, M., and Hashimoto, S. (2005). System-level identification of transcriptional circuits underlying mammalian circadian clocks. Nat. Genet. *37*, 187–192.
10. Panda, S. (2016). Circadian physiology of metabolism. Science *354*, 1008–1015.
11. Panda, S., Antoch, M.P., Miller, B.H., Su, A.I., Schook, A.B., Straume, M., Schultz, P.G., Kay, S.A., Takahashi, J.S., and Hogenesch, J.B. (2002). Coordinated transcription of key pathways in the mouse by the circadian clock. Cell *109*, 307–320.
12. Abe, K., Kroning, J., Greer, M.A., and Critchlow, V. (1979). Effects of destruction of the suprachiasmatic nuclei on the circadian rhythms in plasma corticosterone, body temperature, feeding and plasma thyrotropin. Neuroendocrinology *29*, 119–131.

13. Bass, J., and Takahashi, J.S. (2010). Circadian integration of metabolism and energetics. Science *330*, 1349–1354.

14. Patton, D.F., and Mistlberger, R.E. (2013). Circadian adaptations to meal timing: neuroendocrine mechanisms. Front. Neurosci. *7*, 185.

15. Stephan, F.K., and Zucker, I. (1972). Circadian rhythms in drinking behavior and locomotor activity of rats are eliminated by hypothalamic lesions. Proc Natl Acad Sci USA *69*, 1583–1586.

16. Edgar, D.M., Dement, W.C., and Fuller, C.A. (1993). Effect of SCN lesions on sleep in squirrel monkeys: evidence for opponent processes in sleep-wake regulation. J. Neurosci. *13*, 1065–1079.

17. Lehman, M.N., Silver, R., Gladstone, W.R., Kahn, R.M., Gibson, M., and Bittman, E.L. (1987). Circadian rhythmicity restored by neural transplant. Immunocytochemical characterization of the graft and its integration with the host brain. J. Neurosci. *7*, 1626–1638.

18. Silver, R., LeSauter, J., Tresco, P.A., and Lehman, M.N. (1996). A diffusible coupling signal from the transplanted suprachiasmatic nucleus controlling circadian locomotor rhythms. Nature *382*, 810–813.

19. Buhr, E.D., Vemaraju, S., Diaz, N., Lang, R.A., and Van Gelder, R.N. (2019). Neuropsin (OPN5) Mediates Local Light-Dependent Induction of Circadian Clock Genes and Circadian Photoentrainment in Exposed Murine Skin. Curr. Biol. *29*, 3478-3487.e4.

20. Abe, M., Herzog, E.D., Yamazaki, S., Straume, M., Tei, H., Sakaki, Y., Menaker, M., and Block, G.D. (2002). Circadian rhythms in isolated brain regions. J. Neurosci. *22*, 350–356.

21. Yoo, S.-H., Yamazaki, S., Lowrey, P.L., Shimomura, K., Ko, C.H., Buhr, E.D., Siepka, S.M., Hong, H.-K., Oh, W.J., Yoo, O.J., *et al.* (2004). PERIOD2::LUCIFERASE real-time reporting of circadian dynamics reveals persistent circadian oscillations in mouse peripheral tissues. Proc Natl Acad Sci USA *101*, 5339–5346.

22. Challet, E. (2019). The circadian regulation of food intake. Nat. Rev. Endocrinol. *15*, 393–405.

23. Mendoza, J. (2019). Eating rewards the gears of the clock. Trends Endocrinol. Metab. *30*, 299–311.

24. Landry, G.J., Opiol, H., Marchant, E.G., Pavlovski, I., Mear, R.J., Hamson, D.K., and Mistlberger, R.E. (2012). Scheduled daily mating induces circadian anticipatory activity rhythms in the male rat. PLoS ONE *7*, e40895.

25. Richter, C.P. (1922). A behavioristic study of the activity of the rat. Comp. Psychol, Monog *1*, 1–54.

26. Edgar, D.M., and Dement, W.C. (1991). Regularly scheduled voluntary exercise synchronizes the mouse circadian clock. Am. J. Physiol. *261*, R928-33.

27. Mistlberger, R.E. (2011). Neurobiology of food anticipatory circadian rhythms. Physiol. Behav. *104*, 535–545.

28. Piggins, H.D., and Bechtold, D.A. (2015). Feeding time. eLife *4*.

29. Pendergast, J.S., and Yamazaki, S. (2018). The Mysterious Food-Entrainable Oscillator: Insights from Mutant and Engineered Mouse Models. J. Biol. Rhythms *33*, 458–474.

30. Stokkan, K.A., Yamazaki, S., Tei, H., Sakaki, Y., and Menaker, M. (2001). Entrainment of the circadian clock in the liver by feeding. Science *291*, 490–493.

31. Mistlberger, R.E., and Antle, M.C. (2011). Entrainment of circadian clocks in mammals by arousal and food. Essays Biochem. *49*, 119–136.

32. Davidson, A.J. (2009). Lesion studies targeting food-anticipatory activity. Eur. J. Neurosci. *30*, 1658–1664.

33. Gunapala, K.M., Gallardo, C.M., Hsu, C.T., and Steele, A.D. (2011). Single gene deletions of orexin, leptin, neuropeptide Y, and ghrelin do not appreciably alter food anticipatory activity in mice. PLoS ONE *6*, e18377.

34. Mendoza, J., Albrecht, U., and Challet, E. (2010). Behavioural food anticipation in clock genes deficient mice: confirming old phenotypes, describing new phenotypes. Genes Brain Behav. *9*, 467–477.

35. Acosta-Galvan, G., Yi, C.-X., van der Vliet, J., Jhamandas, J.H., Panula, P., Angeles-Castellanos, M., Del Carmen Basualdo, M., Escobar, C., and Buijs, R.M. (2011). Interaction between hypothalamic dorsomedial nucleus and the suprachiasmatic nucleus determines intensity of food anticipatory behavior. Proc Natl Acad Sci USA *108*, 5813–5818.

36. Mieda, M., Williams, S.C., Richardson, J.A., Tanaka, K., and Yanagisawa, M. (2006). The dorsomedial hypothalamic nucleus as a putative food-entrainable circadian pacemaker. Proc Natl Acad Sci USA *103*, 12150–12155.

37. Podyma, B., Johnson, D.-A., Sipe, L., Remcho, T.P., Battin, K., Liu, Y., Yoon, S.O., Deppmann, C.D., and Güler, A.D. (2020). The p75 neurotrophin receptor in AgRP neurons is necessary for homeostatic feeding and food anticipation. eLife *9*.

38. Liu, Y.-Y., Liu, T.-Y., Qu, W.-M., Hong, Z.-Y., Urade, Y., and Huang, Z.-L. (2012). Dopamine is involved in food-anticipatory activity in mice. J. Biol. Rhythms *27*,

398–409.

39. Gallardo, C.M., Darvas, M., Oviatt, M., Chang, C.H., Michalik, M., Huddy, T.F., Meyer, E.E., Shuster, S.A., Aguayo, A., Hill, E.M., *et al.* (2014). Dopamine receptor 1 neurons in the dorsal striatum regulate food anticipatory circadian activity rhythms in mice. eLife *3*, e03781.
40. Takasu, N.N., Kurosawa, G., Tokuda, I.T., Mochizuki, A., Todo, T., and Nakamura, W. (2012). Circadian regulation of food-anticipatory activity in molecular clock-deficient mice. PLoS ONE *7*, e48892.
41. Stephan, F.K., Swann, J.M., and Sisk, C.L. (1979). Anticipation of 24-hr feeding schedules in rats with lesions of the suprachiasmatic nucleus. Behav. Neural Biol. *25*, 346–363.
42. Krieger, D.T., Hauser, H., and Krey, L.C. (1977). Suprachiasmatic nuclear lesions do not abolish food-shifted circadian adrenal and temperature rhythmicity. Science *197*, 398–399.
43. Mistlberger, R.E. (2020). Food as circadian time cue for appetitive behavior. [version 1; peer review: 5 approved]. F1000Res. *9*.
44. Angeles-Castellanos, M., Salgado-Delgado, R., Rodriguez, K., Buijs, R.M., and Escobar, C. (2010). The suprachiasmatic nucleus participates in food entrainment: a lesion study. Neuroscience *165*, 1115–1126.
45. Fernandez, D.C., Komal, R., Langel, J., Ma, J., Duy, P.Q., Penzo, M.A., Zhao, H., and Hattar, S. (2020). Retinal innervation tunes circuits that drive nonphotic entrainment to food. Nature *581*, 194–198.
46. Nishide, S., Suzuki, Y., Ono, D., Honma, S., and Honma, K.-I. (2021). The Food-entrainable Oscillator Is a Complex of Non-SCN Activity Bout Oscillators Uncoupled From the SCN Circadian Pacemaker. J. Biol. Rhythms *36*, 575–588.
47. Petersen, C.C., Cao, F., Stinchcombe, A.R., and Mistlberger, R.E. (2022). Multiple entrained oscillator model of food anticipatory circadian rhythms. Sci. Rep. *12*, 9306.
48. Storch, K.-F., and Weitz, C.J. (2009). Daily rhythms of food-anticipatory behavioral activity do not require the known circadian clock. Proc Natl Acad Sci USA *106*, 6808–6813.
49. Pendergast, J.S., Wendroth, R.H., Stenner, R.C., Keil, C.D., and Yamazaki, S. (2017). mPeriod2 Brdm1 and other single Period mutant mice have normal food anticipatory activity. Sci. Rep. *7*, 15510.
50. Delezie, J., Dumont, S., Sandu, C., Reibel, S., Pevet, P., and Challet, E. (2016).

Rev-erbα in the brain is essential for circadian food entrainment. Sci. Rep. *6*, 29386.

51. Chavan, R., Feillet, C., Costa, S.S.F., Delorme, J.E., Okabe, T., Ripperger, J.A., and Albrecht, U. (2016). Liver-derived ketone bodies are necessary for food anticipation. Nat. Commun. *7*, 10580.

52. Liu, C.M., and Kanoski, S.E. (2018). Homeostatic and non-homeostatic controls of feeding behavior: Distinct vs. common neural systems. Physiol. Behav. *193*, 223–231.

53. Ferrario, C.R., Labouèbe, G., Liu, S., Nieh, E.H., Routh, V.H., Xu, S., and O'Connor, E.C. (2016). Homeostasis meets motivation in the battle to control food intake. J. Neurosci. *36*, 11469–11481.

54. Betley, J.N., Cao, Z.F.H., Ritola, K.D., and Sternson, S.M. (2013). Parallel, redundant circuit organization for homeostatic control of feeding behavior. Cell *155*, 1337–1350.

55. Betley, J.N., Xu, S., Cao, Z.F.H., Gong, R., Magnus, C.J., Yu, Y., and Sternson, S.M. (2015). Neurons for hunger and thirst transmit a negative-valence teaching signal. Nature *521*, 180–185.

56. Krashes, M.J., Koda, S., Ye, C., Rogan, S.C., Adams, A.C., Cusher, D.S., Maratos-Flier, E., Roth, B.L., and Lowell, B.B. (2011). Rapid, reversible activation of AgRP neurons drives feeding behavior in mice. J. Clin. Invest. *121*, 1424–1428.

57. Aponte, Y., Atasoy, D., and Sternson, S.M. (2011). AGRP neurons are sufficient to orchestrate feeding behavior rapidly and without training. Nat. Neurosci. *14*, 351–355.

58. Zhan, C., Zhou, J., Feng, Q., Zhang, J.-E., Lin, S., Bao, J., Wu, P., and Luo, M. (2013). Acute and long-term suppression of feeding behavior by POMC neurons in the brainstem and hypothalamus, respectively. J. Neurosci. *33*, 3624–3632.

59. Steculorum, S.M., Ruud, J., Karakasilioti, I., Backes, H., Engström Ruud, L., Timper, K., Hess, M.E., Tsaousidou, E., Mauer, J., Vogt, M.C., *et al.* (2016). Agrp neurons control systemic insulin sensitivity via myostatin expression in brown adipose tissue. Cell *165*, 125–138.

60. Kojima, M., Hosoda, H., Date, Y., Nakazato, M., Matsuo, H., and Kangawa, K. (1999). Ghrelin is a growth-hormone-releasing acylated peptide from stomach. Nature *402*, 656–660.

61. Pan, W.W., and Myers, M.G. (2018). Leptin and the maintenance of elevated body weight. Nat. Rev. Neurosci. *19*, 95–105.

62. Kohsaka, A., Laposky, A.D., Ramsey, K.M., Estrada, C., Joshu, C., Kobayashi, Y., Turek, F.W., and Bass, J. (2007). High-fat diet disrupts behavioral and molecular circadian rhythms in mice. Cell Metab. *6*, 414–421.

63. Saper, C.B., Chou, T.C., and Elmquist, J.K. (2002). The need to feed: homeostatic and hedonic control of eating. Neuron *36*, 199–211.

64. Mohebi, A., Pettibone, J.R., Hamid, A.A., Wong, J.-M.T., Vinson, L.T., Patriarchi, T., Tian, L., Kennedy, R.T., and Berke, J.D. (2019). Dissociable dopamine dynamics for learning and motivation. Nature *570*, 65–70.

65. Denis, R.G.P., Joly-Amado, A., Webber, E., Langlet, F., Schaeffer, M., Padilla, S.L., Cansell, C., Dehouck, B., Castel, J., Delbès, A.-S., *et al.* (2015). Palatability can drive feeding independent of agrp neurons. Cell Metab. *22*, 646–657.

66. Güler, A.D., Rainwater, A., Parker, J.G., Jones, G.L., Argilli, E., Arenkiel, B.R., Ehlers, M.D., Bonci, A., Zweifel, L.S., and Palmiter, R.D. (2012). Transient activation of specific neurons in mice by selective expression of the capsaicin receptor. Nat. Commun. *3*, 746.

67. King, C.M., and Hentges, S.T. (2011). Relative number and distribution of murine hypothalamic proopiomelanocortin neurons innervating distinct target sites. PLoS ONE *6*, e25864.

68. Lim, B.K., Huang, K.W., Grueter, B.A., Rothwell, P.E., and Malenka, R.C. (2012). Anhedonia requires MC4R-mediated synaptic adaptations in nucleus accumbens. Nature *487*, 183–189.

69. Alhadeff, A.L., Goldstein, N., Park, O., Klima, M.L., Vargas, A., and Betley, J.N. (2019). Natural and Drug Rewards Engage Distinct Pathways that Converge on Coordinated Hypothalamic and Reward Circuits. Neuron *103*, 891-908.e6.

70. Dibner, C., Schibler, U., and Albrecht, U. (2010). The mammalian circadian timing system: organization and coordination of central and peripheral clocks. Annu. Rev. Physiol. *72*, 517–549.

71. Morin, L.P. (2007). SCN organization reconsidered. J. Biol. Rhythms *22*, 3–13.

72. Buijs, F.N., Guzmán-Ruiz, M., León-Mercado, L., Basualdo, M.C., Escobar, C., Kalsbeek, A., and Buijs, R.M. (2017). Suprachiasmatic Nucleus Interaction with the Arcuate Nucleus; Essential for Organizing Physiological Rhythms. eNeuro *4*.

73. Challet, E. (2015). Keeping circadian time with hormones. Diabetes Obes. Metab. *17 Suppl 1*, 76–83.

74. Nagai, K., Nishio, T., Nakagawa, H., Nakamura, S., and Fukuda, Y. (1978). Effect of bilateral lesions of the suprachiasmatic nuclei on the circadian rhythm of

food-intake. Brain Res. *142*, 384–389.

75. Wise, R.A. (2004). Dopamine, learning and motivation. Nat. Rev. Neurosci. *5*, 483–494.

76. Wise, R.A. (2006). Role of brain dopamine in food reward and reinforcement. Philos. Trans. R. Soc. Lond. B Biol. Sci. *361*, 1149–1158.

77. Gerfen, C.R., and Surmeier, D.J. (2011). Modulation of striatal projection systems by dopamine. Annu. Rev. Neurosci. *34*, 441–466.

78. Smyllie, N.J., Chesham, J.E., Hamnett, R., Maywood, E.S., and Hastings, M.H. (2016). Temporally chimeric mice reveal flexibility of circadian period-setting in the suprachiasmatic nucleus. Proc Natl Acad Sci USA *113*, 3657–3662.

79. Ferguson, S.A., Rowe, S.A., Krupa, M., and Kennaway, D.J. (2000). Prenatal exposure to the dopamine agonist SKF-38393 disrupts the timing of the initial response of the suprachiasmatic nucleus to light. Brain Res. *858*, 284–289.

80. Grippo, R.M., Purohit, A.M., Zhang, Q., Zweifel, L.S., and Güler, A.D. (2017). Direct midbrain dopamine input to the suprachiasmatic nucleus accelerates circadian entrainment. Curr. Biol. *27*, 2465-2475.e3.

81. Escobar, C., Espitia-Bautista, E., Guzmán-Ruiz, M.A., Guerrero-Vargas, N.N., Hernández-Navarrete, M.Á., Ángeles-Castellanos, M., Morales-Pérez, B., and Buijs, R.M. (2020). Chocolate for breakfast prevents circadian desynchrony in experimental models of jet-lag and shift-work. Sci. Rep. *10*, 6243.

82. Gallardo, C.M., Gunapala, K.M., King, O.D., and Steele, A.D. (2012). Daily scheduled high fat meals moderately entrain behavioral anticipatory activity, body temperature, and hypothalamic c-Fos activation. PLoS ONE *7*, e41161.

83. Hsu, C.T., Patton, D.F., Mistlberger, R.E., and Steele, A.D. (2010). Palatable meal anticipation in mice. PLoS ONE *5*.

84. Blum, I.D., Zhu, L., Moquin, L., Kokoeva, M.V., Gratton, A., Giros, B., and Storch, K.-F. (2014). A highly tunable dopaminergic oscillator generates ultradian rhythms of behavioral arousal. eLife *3*.

85. Tataroglu, O., Davidson, A.J., Benvenuto, L.J., and Menaker, M. (2006). The methamphetamine-sensitive circadian oscillator (MASCO) in mice. J. Biol. Rhythms *21*, 185–194.

86. Honma, K., Honma, S., and Hiroshige, T. (1987). Activity rhythms in the circadian domain appear in suprachiasmatic nuclei lesioned rats given methamphetamine. Physiol. Behav. *40*, 767–774.

87. Adult Obesity Causes & Consequences | Overweight & Obesity | CDC Available

at: https://www.cdc.gov/obesity/adult/causes.html [Accessed December 6, 2019].

88. America's Obesity Crisis: The Health and Economic Costs of Excess Weight | Milken Institute Available at: http://milkeninstitute.org/reports/americas-obesity-crisis-health-and-economic-costs-excess-weight [Accessed December 6, 2019].

89. Hurt, R.T., Kulisek, C., Buchanan, L.A., and McClave, S.A. (2010). The obesity epidemic: challenges, health initiatives, and implications for gastroenterologists. Gastroenterol Hepatol (N Y) *6*, 780–792.

90. Flegal, K.M., Kruszon-Moran, D., Carroll, M.D., Fryar, C.D., and Ogden, C.L. (2016). Trends in obesity among adults in the united states, 2005 to 2014. JAMA *315*, 2284–2291.

91. Eckel, R.H., Kahn, S.E., Ferrannini, E., Goldfine, A.B., Nathan, D.M., Schwartz, M.W., Smith, R.J., Smith, S.R., Endocrine Society, American Diabetes Association, *et al.* (2011). Obesity and type 2 diabetes: what can be unified and what needs to be individualized? Diabetes Care *34*, 1424–1430.

92. Guh, D.P., Zhang, W., Bansback, N., Amarsi, Z., Birmingham, C.L., and Anis, A.H. (2009). The incidence of co-morbidities related to obesity and overweight: a systematic review and meta-analysis. BMC Public Health *9*, 88.

93. de Mutsert, R., Sun, Q., Willett, W.C., Hu, F.B., and van Dam, R.M. (2014). Overweight in early adulthood, adult weight change, and risk of type 2 diabetes, cardiovascular diseases, and certain cancers in men: a cohort study. Am. J. Epidemiol. *179*, 1353–1365.

94. Attia, E. (2010). Anorexia nervosa: current status and future directions. Annu. Rev. Med. *61*, 425–435.

95. Treasure, J., Zipfel, S., Micali, N., Wade, T., Stice, E., Claudino, A., Schmidt, U., Frank, G.K., Bulik, C.M., and Wentz, E. (2015). Anorexia nervosa. Nat. Rev. Dis. Primers *1*, 15074.

96. Garaulet, M., Gómez-Abellán, P., Alburquerque-Béjar, J.J., Lee, Y.C., Ordovás, J.M., and Scheer, F.A.J.L. (2013). Timing of food intake predicts weight loss effectiveness. Int J Obes (Lond) *37*, 604–611.

97. Sutton, E.F., Beyl, R., Early, K.S., Cefalu, W.T., Ravussin, E., and Peterson, C.M. (2018). Early Time-Restricted Feeding Improves Insulin Sensitivity, Blood Pressure, and Oxidative Stress Even without Weight Loss in Men with Prediabetes. Cell Metab. *27*, 1212-1221.e3.

98. Hatori, M., Vollmers, C., Zarrinpar, A., DiTacchio, L., Bushong, E.A., Gill, S., Leblanc, M., Chaix, A., Joens, M., Fitzpatrick, J.A.J., *et al.* (2012). Time-restricted

feeding without reducing caloric intake prevents metabolic diseases in mice fed a high-fat diet. Cell Metab. *15*, 848–860.

99. Acosta-Rodríguez, V., Rijo-Ferreira, F., Izumo, M., Xu, P., Wight-Carter, M., Green, C.B., and Takahashi, J.S. (2022). Circadian alignment of early onset caloric restriction promotes longevity in male C57BL/6J mice. Science *376*, 1192–1202.
100. Di Lorenzo, L., De Pergola, G., Zocchetti, C., L'Abbate, N., Basso, A., Pannacciulli, N., Cignarelli, M., Giorgino, R., and Soleo, L. (2003). Effect of shift work on body mass index: results of a study performed in 319 glucose-tolerant men working in a Southern Italian industry. Int. J. Obes. Relat. Metab. Disord. *27*, 1353–1358.
101. Arble, D.M., Bass, J., Laposky, A.D., Vitaterna, M.H., and Turek, F.W. (2009). Circadian timing of food intake contributes to weight gain. Obesity (Silver Spring) *17*, 2100–2102.
102. Chaix, A., Lin, T., Le, H.D., Chang, M.W., and Panda, S. (2019). Time-Restricted Feeding Prevents Obesity and Metabolic Syndrome in Mice Lacking a Circadian Clock. Cell Metab. *29*, 303-319.e4.
103. Turek, F.W., Joshu, C., Kohsaka, A., Lin, E., Ivanova, G., McDearmon, E., Laposky, A., Losee-Olson, S., Easton, A., Jensen, D.R., *et al.* (2005). Obesity and metabolic syndrome in circadian Clock mutant mice. Science *308*, 1043–1045.
104. Fonken, L.K., Aubrecht, T.G., Meléndez-Fernández, O.H., Weil, Z.M., and Nelson, R.J. (2013). Dim light at night disrupts molecular circadian rhythms and increases body weight. J. Biol. Rhythms *28*, 262–271.
105. Fonken, L.K., Workman, J.L., Walton, J.C., Weil, Z.M., Morris, J.S., Haim, A., and Nelson, R.J. (2010). Light at night increases body mass by shifting the time of food intake. Proc Natl Acad Sci USA *107*, 18664–18669.
106. Webb, V.L., and Wadden, T.A. (2017). Intensive lifestyle intervention for obesity: principles, practices, and results. Gastroenterology *152*, 1752–1764.
107. Del Corral, P., Bryan, D.R., Garvey, W.T., Gower, B.A., and Hunter, G.R. (2011). Dietary adherence during weight loss predicts weight regain. Obesity (Silver Spring) *19*, 1177–1181.
108. Del Corral, P., Chandler-Laney, P.C., Casazza, K., Gower, B.A., and Hunter, G.R. (2009). Effect of dietary adherence with or without exercise on weight loss: a mechanistic approach to a global problem. J. Clin. Endocrinol. Metab. *94*, 1602–1607.
109. Hall, K.D. (2018). Did the food environment cause the obesity epidemic? Obesity (Silver Spring) *26*, 11–13.

110. Hall, K.D., Bemis, T., Brychta, R., Chen, K.Y., Courville, A., Crayner, E.J., Goodwin, S., Guo, J., Howard, L., Knuth, N.D., *et al.* (2015). Calorie for Calorie, Dietary Fat Restriction Results in More Body Fat Loss than Carbohydrate Restriction in People with Obesity. Cell Metab. *22*, 427–436.

111. O'Neal, T.J., Friend, D.M., Guo, J., Hall, K.D., and Kravitz, A.V. (2017). Increases in physical activity result in diminishing increments in daily energy expenditure in mice. Curr. Biol. *27*, 423–430.

112. Chaix, A., Zarrinpar, A., Miu, P., and Panda, S. (2014). Time-restricted feeding is a preventative and therapeutic intervention against diverse nutritional challenges. Cell Metab. *20*, 991–1005.

113. Blancas-Velazquez, A., Mendoza, J., Garcia, A.N., and la Fleur, S.E. (2017). Diet-Induced Obesity and Circadian Disruption of Feeding Behavior. Front. Neurosci. *11*, 23.

114. Arble, D.M., Ramsey, K.M., Bass, J., and Turek, F.W. (2010). Circadian disruption and metabolic disease: findings from animal models. Best Pract. Res. Clin. Endocrinol. Metab. *24*, 785–800.

115. Zhou, Q.Y., and Palmiter, R.D. (1995). Dopamine-deficient mice are severely hypoactive, adipsic, and aphagic. Cell *83*, 1197–1209.

116. Missale, C., Nash, S.R., Robinson, S.W., Jaber, M., and Caron, M.G. (1998). Dopamine receptors: from structure to function. Physiol. Rev. *78*, 189–225.

117. Beaulieu, J.-M., and Gainetdinov, R.R. (2011). The physiology, signaling, and pharmacology of dopamine receptors. Pharmacol. Rev. *63*, 182–217.

118. Johnson, P.M., and Kenny, P.J. (2010). Dopamine D2 receptors in addiction-like reward dysfunction and compulsive eating in obese rats. Nat. Neurosci. *13*, 635–641.

119. Land, B.B., Narayanan, N.S., Liu, R.-J., Gianessi, C.A., Brayton, C.E., Grimaldi, D.M., Sarhan, M., Guarnieri, D.J., Deisseroth, K., Aghajanian, G.K., *et al.* (2014). Medial prefrontal D1 dopamine neurons control food intake. Nat. Neurosci. *17*, 248–253.

120. Alsiö, J., Olszewski, P.K., Norbäck, A.H., Gunnarsson, Z.E.A., Levine, A.S., Pickering, C., and Schiöth, H.B. (2010). Dopamine D1 receptor gene expression decreases in the nucleus accumbens upon long-term exposure to palatable food and differs depending on diet-induced obesity phenotype in rats. Neuroscience *171*, 779–787.

121. Carlin, J., Hill-Smith, T.E., Lucki, I., and Reyes, T.M. (2013). Reversal of dopamine system dysfunction in response to high-fat diet. Obesity (Silver Spring) *21*,

2513–2521.

122. Terry, P., and Katz, J.L. (1994). A comparison of the effects of the D1 receptor antagonists SCH 23390 and SCH 39166 on suppression of feeding behavior by the D1 agonist SKF38393. Psychopharmacology (Berl) *113*, 328–333.

123. Astrup, A., Greenway, F.L., Ling, W., Pedicone, L., Lachowicz, J., Strader, C.D., Kwan, R., and Ecopipam Obesity Study Group (2007). Randomized controlled trials of the D1/D5 antagonist ecopipam for weight loss in obese subjects. Obesity (Silver Spring) *15*, 1717–1731.

124. Winzell, M.S., and Ahrén, B. (2004). The high-fat diet-fed mouse: a model for studying mechanisms and treatment of impaired glucose tolerance and type 2 diabetes. Diabetes *53 Suppl 3*, S215-9.

125. Hariri, N., and Thibault, L. (2010). High-fat diet-induced obesity in animal models. Nutr. Res. Rev. *23*, 270–299.

126. Heusner, C.L., Beutler, L.R., Houser, C.R., and Palmiter, R.D. (2008). Deletion of GAD67 in dopamine receptor-1 expressing cells causes specific motor deficits. Genesis *46*, 357–367.

127. Drago, J., Gerfen, C.R., Lachowicz, J.E., Steiner, H., Hollon, T.R., Love, P.E., Ooi, G.T., Grinberg, A., Lee, E.J., and Huang, S.P. (1994). Altered striatal function in a mutant mouse lacking D1A dopamine receptors. Proc Natl Acad Sci USA *91*, 12564–12568.

128. Espinosa-Carrasco, J., Burokas, A., Fructuoso, M., Erb, I., Martín-García, E., Gutiérrez-Martos, M., Notredame, C., Maldonado, R., and Dierssen, M. (2018). Time-course and dynamics of obesity-related behavioral changes induced by energy-dense foods in mice. Addict. Biol. *23*, 531–543.

129. Mrosovsky, N. (1999). Masking: history, definitions, and measurement. Chronobiol. Int. *16*, 415–429.

130. Gore, B.B., and Zweifel, L.S. (2013). Genetic reconstruction of dopamine D1 receptor signaling in the nucleus accumbens facilitates natural and drug reward responses. J. Neurosci. *33*, 8640–8649.

131. Riera, C.E., Tsaousidou, E., Halloran, J., Follett, P., Hahn, O., Pereira, M.M.A., Ruud, L.E., Alber, J., Tharp, K., Anderson, C.M., *et al.* (2017). The sense of smell impacts metabolic health and obesity. Cell Metab. *26*, 198-211.e5.

132. Stenvers, D.J., Scheer, F.A.J.L., Schrauwen, P., la Fleur, S.E., and Kalsbeek, A. (2019). Circadian clocks and insulin resistance. Nat. Rev. Endocrinol. *15*, 75–89.

133. Pendergast, J.S., Branecky, K.L., Yang, W., Ellacott, K.L.J., Niswender, K.D., and

Yamazaki, S. (2013). High-fat diet acutely affects circadian organisation and eating behavior. Eur. J. Neurosci. *37*, 1350–1356.

134. Kraemer, F.B., and Shen, W.-J. (2002). Hormone-sensitive lipase: control of intracellular tri-(di-)acylglycerol and cholesteryl ester hydrolysis. J. Lipid Res. *43*, 1585–1594.

135. Akasheh, R.T., Pini, M., Pang, J., and Fantuzzi, G. (2013). Increased adiposity in annexin A1-deficient mice. PLoS ONE *8*, e82608.

136. Luo, Y.-J., Li, Y.-D., Wang, L., Yang, S.-R., Yuan, X.-S., Wang, J., Cherasse, Y., Lazarus, M., Chen, J.-F., Qu, W.-M., *et al.* (2018). Nucleus accumbens controls wakefulness by a subpopulation of neurons expressing dopamine D1 receptors. Nat. Commun. *9*, 1576.

137. Mills, E.L., Pierce, K.A., Jedrychowski, M.P., Garrity, R., Winther, S., Vidoni, S., Yoneshiro, T., Spinelli, J.B., Lu, G.Z., Kazak, L., *et al.* (2018). Accumulation of succinate controls activation of adipose tissue thermogenesis. Nature *560*, 102–106.

138. Wan, M., Easton, R.M., Gleason, C.E., Monks, B.R., Ueki, K., Kahn, C.R., and Birnbaum, M.J. (2012). Loss of Akt1 in mice increases energy expenditure and protects against diet-induced obesity. Mol. Cell. Biol. *32*, 96–106.

139. Kopelman, P.G. (2000). Obesity as a medical problem. Nature *404*, 635–643.

140. Steppan, C.M., Bailey, S.T., Bhat, S., Brown, E.J., Banerjee, R.R., Wright, C.M., Patel, H.R., Ahima, R.S., and Lazar, M.A. (2001). The hormone resistin links obesity to diabetes. Nature *409*, 307–312.

141. Kahn, S.E., Hull, R.L., and Utzschneider, K.M. (2006). Mechanisms linking obesity to insulin resistance and type 2 diabetes. Nature *444*, 840–846.

142. Stamatakis, A.M., Van Swieten, M., Basiri, M.L., Blair, G.A., Kantak, P., and Stuber, G.D. (2016). Lateral hypothalamic area glutamatergic neurons and their projections to the lateral habenula regulate feeding and reward. J. Neurosci. *36*, 302–311.

143. Rossi, M.A., and Stuber, G.D. (2018). Overlapping brain circuits for homeostatic and hedonic feeding. Cell Metab. *27*, 42–56.

144. Sariñana, J., and Tonegawa, S. (2016). Differentiation of forebrain and hippocampal dopamine 1-class receptors, D1R and D5R, in spatial learning and memory. Hippocampus *26*, 76–86.

145. Wang, X., Zhang, C., Szábo, G., and Sun, Q.-Q. (2013). Distribution of CaMKIIα expression in the brain in vivo, studied by CaMKIIα-GFP mice. Brain Res. *1518*,

9–25.

146. Vong, L., Ye, C., Yang, Z., Choi, B., Chua, S., and Lowell, B.B. (2011). Leptin action on GABAergic neurons prevents obesity and reduces inhibitory tone to POMC neurons. Neuron *71*, 142–154.

147. Davis, J.F., Tracy, A.L., Schurdak, J.D., Tschöp, M.H., Lipton, J.W., Clegg, D.J., and Benoit, S.C. (2008). Exposure to elevated levels of dietary fat attenuates psychostimulant reward and mesolimbic dopamine turnover in the rat. Behav. Neurosci. *122*, 1257–1263.

148. Mendoza, J., Angeles-Castellanos, M., and Escobar, C. (2005). A daily palatable meal without food deprivation entrains the suprachiasmatic nucleus of rats. Eur. J. Neurosci. *22*, 2855–2862.

149. Mendoza, J., Pévet, P., and Challet, E. (2008). High-fat feeding alters the clock synchronization to light. J Physiol (Lond) *586*, 5901–5910.

150. Mendoza, J., Clesse, D., Pévet, P., and Challet, E. (2010). Food-reward signalling in the suprachiasmatic clock. J. Neurochem. *112*, 1489–1499.

151. Okamura, H., Bérod, A., Julien, J.F., Geffard, M., Kitahama, K., Mallet, J., and Bobillier, P. (1989). Demonstration of GABAergic cell bodies in the suprachiasmatic nucleus: in situ hybridization of glutamic acid decarboxylase (GAD) mRNA and immunocytochemistry of GAD and GABA. Neurosci. Lett. *102*, 131–136.

152. Moore, R.Y., and Speh, J.C. (1993). GABA is the principal neurotransmitter of the circadian system. Neurosci. Lett. *150*, 112–116.

153. McNulty, S., Schurov, I.L., Sloper, P.J., and Hastings, M.H. (1998). Stimuli which entrain the circadian clock of the neonatal Syrian hamster in vivo regulate the phosphorylation of the transcription factor CREB in the suprachiasmatic nucleus in vitro. Eur. J. Neurosci. *10*, 1063–1072.

154. Gill, S., and Panda, S. (2015). A Smartphone App Reveals Erratic Diurnal Eating Patterns in Humans that Can Be Modulated for Health Benefits. Cell Metab. *22*, 789–798.

155. Gabel, K., Hoddy, K.K., Haggerty, N., Song, J., Kroeger, C.M., Trepanowski, J.F., Panda, S., and Varady, K.A. (2018). Effects of 8-hour time restricted feeding on body weight and metabolic disease risk factors in obese adults: A pilot study. Nutr. Healthy Aging *4*, 345–353.

156. Berridge, K.C., and Robinson, T.E. (1998). What is the role of dopamine in reward: hedonic impact, reward learning, or incentive salience? Brain Res. Brain Res. Rev. *28*, 309–369.

157. Gabriel, B.M., and Zierath, J.R. (2019). Circadian rhythms and exercise - re-setting the clock in metabolic disease. Nat. Rev. Endocrinol. *15*, 197–206.

158. Pendergast, J.S., Branecky, K.L., Huang, R., Niswender, K.D., and Yamazaki, S. (2014). Wheel-running activity modulates circadian organization and the daily rhythm of eating behavior. Front. Psychol. *5*, 177.

159. Landgraf, D., Joiner, W.J., McCarthy, M.J., Kiessling, S., Barandas, R., Young, J.W., Cermakian, N., and Welsh, D.K. (2016). The mood stabilizer valproic acid opposes the effects of dopamine on circadian rhythms. Neuropharmacology *107*, 262–270.

160. Wisor, J.P., Nishino, S., Sora, I., Uhl, G.H., Mignot, E., and Edgar, D.M. (2001). Dopaminergic role in stimulant-induced wakefulness. J. Neurosci. *21*, 1787–1794.

161. Eban-Rothschild, A., Rothschild, G., Giardino, W.J., Jones, J.R., and de Lecea, L. (2016). VTA dopaminergic neurons regulate ethologically relevant sleep-wake behaviors. Nat. Neurosci. *19*, 1356–1366.

162. Grippo, R.M., and Güler, A.D. (2019). Dopamine signaling in circadian photoentrainment: consequences of desynchrony. Yale J. Biol. Med. *92*, 271–281.

163. Kalsbeek, A., Palm, I.F., La Fleur, S.E., Scheer, F.A.J.L., Perreau-Lenz, S., Ruiter, M., Kreier, F., Cailotto, C., and Buijs, R.M. (2006). SCN outputs and the hypothalamic balance of life. J. Biol. Rhythms *21*, 458–469.

164. Moore, R.Y. (1995). Organization of the mammalian circadian system. Ciba Found. Symp. *183*, 88–99; discussion 100.

165. Schaap, J., Pennartz, C.M.A., and Meijer, J.H. (2003). Electrophysiology of the circadian pacemaker in mammals. Chronobiol. Int. *20*, 171–188.

166. Ellacott, K.L.J., Morton, G.J., Woods, S.C., Tso, P., and Schwartz, M.W. (2010). Assessment of feeding behavior in laboratory mice. Cell Metab. *12*, 10–17.

167. Sumová, A., Trávnícková, Z., and Illnerová, H. (2000). Spontaneous c-Fos rhythm in the rat suprachiasmatic nucleus: location and effect of photoperiod. Am. J. Physiol. Regul. Integr. Comp. Physiol. *279*, R2262-9.

168. Fonken, L.K., Lieberman, R.A., Weil, Z.M., and Nelson, R.J. (2013). Dim light at night exaggerates weight gain and inflammation associated with a high-fat diet in male mice. Endocrinology *154*, 3817–3825.

169. Lee, I.T., Chang, A.S., Manandhar, M., Shan, Y., Fan, J., Izumo, M., Ikeda, Y., Motoike, T., Dixon, S., Seinfeld, J.E., *et al.* (2015). Neuromedin s-producing neurons act as essential pacemakers in the suprachiasmatic nucleus to couple clock neurons and dictate circadian rhythms. Neuron *85*, 1086–1102.

170. Smyllie, N.J., Pilorz, V., Boyd, J., Meng, Q.-J., Saer, B., Chesham, J.E., Maywood, E.S., Krogager, T.P., Spiller, D.G., Boot-Handford, R., *et al.* (2016). Visualizing and quantifying intracellular behavior and abundance of the core circadian clock protein PERIOD2. Curr. Biol. *26*, 1880–1886.

171. Zarrinpar, A., Chaix, A., and Panda, S. (2016). Daily eating patterns and their impact on health and disease. Trends Endocrinol. Metab. *27*, 69–83.

172. Mistlberger, R.E., and Skene, D.J. (2005). Nonphotic entrainment in humans? J. Biol. Rhythms *20*, 339–352.

173. Lewis, P., Oster, H., Korf, H.W., Foster, R.G., and Erren, T.C. (2020). Food as a circadian time cue - evidence from human studies. Nat. Rev. Endocrinol. *16*, 213–223.

174. Xie, Z., Sun, Y., Ye, Y., Hu, D., Zhang, H., He, Z., Zhao, H., Yang, H., and Mao, Y. (2022). Randomized controlled trial for time-restricted eating in healthy volunteers without obesity. Nat. Commun. *13*, 1003.

175. Kalsbeek, A., Fliers, E., Romijn, J.A., La Fleur, S.E., Wortel, J., Bakker, O., Endert, E., and Buijs, R.M. (2001). The suprachiasmatic nucleus generates the diurnal changes in plasma leptin levels. Endocrinology *142*, 2677–2685.

176. Schoeller, D.A., Cella, L.K., Sinha, M.K., and Caro, J.F. (1997). Entrainment of the diurnal rhythm of plasma leptin to meal timing. J. Clin. Invest. *100*, 1882–1887.

177. Arble, D.M., Vitaterna, M.H., and Turek, F.W. (2011). Rhythmic leptin is required for weight gain from circadian desynchronized feeding in the mouse. PLoS ONE *6*, e25079.

178. Prosser, R.A., and Bergeron, H.E. (2003). Leptin phase-advances the rat suprachiasmatic circadian clock in vitro. Neurosci. Lett. *336*, 139–142.

179. Fernandes, M.F.A., Matthys, D., Hryhorczuk, C., Sharma, S., Mogra, S., Alquier, T., and Fulton, S. (2015). Leptin suppresses the rewarding effects of running via STAT3 signaling in dopamine neurons. Cell Metab. *22*, 741–749.

180. Scott, M.M., Lachey, J.L., Sternson, S.M., Lee, C.E., Elias, C.F., Friedman, J.M., and Elmquist, J.K. (2009). Leptin targets in the mouse brain. J. Comp. Neurol. *514*, 518–532.

181. Guan, X.M., Hess, J.F., Yu, H., Hey, P.J., and van der Ploeg, L.H. (1997). Differential expression of mRNA for leptin receptor isoforms in the rat brain. Mol. Cell. Endocrinol. *133*, 1–7.

182. Chou, T.C., Scammell, T.E., Gooley, J.J., Gaus, S.E., Saper, C.B., and Lu, J. (2003). Critical role of dorsomedial hypothalamic nucleus in a wide range of

behavioral circadian rhythms. J. Neurosci. *23*, 10691–10702.

183. Faber, C.L., Deem, J.D., Phan, B.A., Doan, T.P., Ogimoto, K., Mirzadeh, Z., Schwartz, M.W., and Morton, G.J. (2021). Leptin receptor neurons in the dorsomedial hypothalamus regulate diurnal patterns of feeding, locomotion, and metabolism. eLife *10*.

184. Verwey, M., Khoja, Z., Stewart, J., and Amir, S. (2007). Differential regulation of the expression of Period2 protein in the limbic forebrain and dorsomedial hypothalamus by daily limited access to highly palatable food in food-deprived and free-fed rats. Neuroscience *147*, 277–285.

185. Jones, J.R., Simon, T., Lones, L., and Herzog, E.D. (2018). SCN VIP Neurons Are Essential for Normal Light-Mediated Resetting of the Circadian System. J. Neurosci. *38*, 7986–7995.

186. Garfield, A.S., Shah, B.P., Burgess, C.R., Li, M.M., Li, C., Steger, J.S., Madara, J.C., Campbell, J.N., Kroeger, D., Scammell, T.E., *et al.* (2016). Dynamic GABAergic afferent modulation of AgRP neurons. Nat. Neurosci. *19*, 1628–1635.

187. Rezai-Zadeh, K., Yu, S., Jiang, Y., Laque, A., Schwartzenburg, C., Morrison, C.D., Derbenev, A.V., Zsombok, A., and Münzberg, H. (2014). Leptin receptor neurons in the dorsomedial hypothalamus are key regulators of energy expenditure and body weight, but not food intake. Mol. Metab. *3*, 681–693.

188. Klapoetke, N.C., Murata, Y., Kim, S.S., Pulver, S.R., Birdsey-Benson, A., Cho, Y.K., Morimoto, T.K., Chuong, A.S., Carpenter, E.J., Tian, Z., *et al.* (2014). Independent optical excitation of distinct neural populations. Nat. Methods *11*, 338–346.

189. Mendoza, J., Lopez-Lopez, C., Revel, F.G., Jeanneau, K., Delerue, F., Prinssen, E., Challet, E., Moreau, J.L., and Grundschober, C. (2011). Dimorphic effects of leptin on the circadian and hypocretinergic systems of mice. J. Neuroendocrinol. *23*, 28–38.

190. Ribeiro, A.C., Ceccarini, G., Dupré, C., Friedman, J.M., Pfaff, D.W., and Mark, A.L. (2011). Contrasting effects of leptin on food anticipatory and total locomotor activity. PLoS ONE *6*, e23364.

191. Zhang, Y., Kerman, I.A., Laque, A., Nguyen, P., Faouzi, M., Louis, G.W., Jones, J.C., Rhodes, C., and Münzberg, H. (2011). Leptin-receptor-expressing neurons in the dorsomedial hypothalamus and median preoptic area regulate sympathetic brown adipose tissue circuits. J. Neurosci. *31*, 1873–1884.

192. Enriori, P.J., Sinnayah, P., Simonds, S.E., Garcia Rudaz, C., and Cowley, M.A. (2011). Leptin action in the dorsomedial hypothalamus increases sympathetic tone

to brown adipose tissue in spite of systemic leptin resistance. J. Neurosci. *31*, 12189–12197.

193. Tan, K., Knight, Z.A., and Friedman, J.M. (2014). Ablation of AgRP neurons impairs adaption to restricted feeding. Mol. Metab. *3*, 694–704.

194. Moriya, T., Aida, R., Kudo, T., Akiyama, M., Doi, M., Hayasaka, N., Nakahata, N., Mistlberger, R., Okamura, H., and Shibata, S. (2009). The dorsomedial hypothalamic nucleus is not necessary for food-anticipatory circadian rhythms of behavior, temperature or clock gene expression in mice. Eur. J. Neurosci. *29*, 1447–1460.

195. Landry, G.J., Simon, M.M., Webb, I.C., and Mistlberger, R.E. (2006). Persistence of a behavioral food-anticipatory circadian rhythm following dorsomedial hypothalamic ablation in rats. Am. J. Physiol. Regul. Integr. Comp. Physiol. *290*, R1527-34.

196. Landry, G.J., Yamakawa, G.R., Webb, I.C., Mear, R.J., and Mistlberger, R.E. (2007). The dorsomedial hypothalamic nucleus is not necessary for the expression of circadian food-anticipatory activity in rats. J. Biol. Rhythms *22*, 467–478.

197. Stephan, F.K., Swann, J.M., and Sisk, C.L. (1979). Entrainment of circadian rhythms by feeding schedules in rats with suprachiasmatic lesions. Behav. Neural Biol. *25*, 545–554.

198. Stoleru, D., Peng, Y., Agosto, J., and Rosbash, M. (2004). Coupled oscillators control morning and evening locomotor behaviour of Drosophila. Nature *431*, 862–868.

199. Todd, W.D., Venner, A., Anaclet, C., Broadhurst, R.Y., De Luca, R., Bandaru, S.S., Issokson, L., Hablitz, L.M., Cravetchi, O., Arrigoni, E., *et al.* (2020). Suprachiasmatic VIP neurons are required for normal circadian rhythmicity and comprised of molecularly distinct subpopulations. Nat. Commun. *11*, 4410.

200. Leshan, R.L., Björnholm, M., Münzberg, H., and Myers, M.G. (2006). Leptin receptor signaling and action in the central nervous system. Obesity (Silver Spring) *14 Suppl 5*, 208S-212S.

201. Dana, H., Sun, Y., Mohar, B., Hulse, B.K., Kerlin, A.M., Hasseman, J.P., Tsegaye, G., Tsang, A., Wong, A., Patel, R., *et al.* (2019). High-performance calcium sensors for imaging activity in neuronal populations and microcompartments. Nat. Methods *16*, 649–657.

202. Kim, S., and McMahon, D.G. (2021). Light sets the brain's daily clock by regional quickening and slowing of the molecular clockworks at dawn and dusk. eLife *10*.

203. Kakava-Georgiadou, N., Severens, J.F., Jørgensen, A.M., Garner, K.M., Luijendijk,

M.C.M., Drkelic, V., van Dijk, R., Pers, T.H., Basak, O., and Adan, R.A.H. (2020). Single-cell analysis reveals cellular heterogeneity and molecular determinants of hypothalamic leptin-receptor cells. BioRxiv.

204. Patriarchi, T., Cho, J.R., Merten, K., Howe, M.W., Marley, A., Xiong, W.-H., Folk, R.W., Broussard, G.J., Liang, R., Jang, M.J., *et al.* (2018). Ultrafast neuronal imaging of dopamine dynamics with designed genetically encoded sensors. Science *360*.
205. Sun, F., Zeng, J., Jing, M., Zhou, J., Feng, J., Owen, S.F., Luo, Y., Li, F., Wang, H., Yamaguchi, T., *et al.* (2018). A genetically encoded fluorescent sensor enables rapid and specific detection of dopamine in flies, fish, and mice. Cell *174*, 481-496.e19.
206. Grippo, R.M., Tang, Q., Zhang, Q., Chadwick, S.R., Gao, Y., Altherr, E.B., Sipe, L., Purohit, A.M., Purohit, N.M., Sunkara, M.D., *et al.* (2020). Dopamine Signaling in the Suprachiasmatic Nucleus Enables Weight Gain Associated with Hedonic Feeding. Curr. Biol. *30*, 196-208.e8.
207. Morton, G.J., Blevins, J.E., Kim, F., Matsen, M., and Figlewicz, D.P. (2009). The action of leptin in the ventral tegmental area to decrease food intake is dependent on Jak-2 signaling. Am. J. Physiol. Endocrinol. Metab. *297*, E202-10.
208. Tang, Q., P Williams, S., and D Güler, A. (2022). A building block-based beam-break (B5) locomotor activity monitoring system and its use in circadian biology research. BioTechniques.
209. Mohawk, J.A., Green, C.B., and Takahashi, J.S. (2012). Central and peripheral circadian clocks in mammals. Annu. Rev. Neurosci. *35*, 445–462.
210. Vitaterna, M.H., King, D.P., Chang, A.M., Kornhauser, J.M., Lowrey, P.L., McDonald, J.D., Dove, W.F., Pinto, L.H., Turek, F.W., and Takahashi, J.S. (1994). Mutagenesis and mapping of a mouse gene, Clock, essential for circadian behavior. Science *264*, 719–725.
211. Leon, L.R., Walker, L.D., DuBose, D.A., and Stephenson, L.A. (2004). Biotelemetry transmitter implantation in rodents: impact on growth and circadian rhythms. Am. J. Physiol. Regul. Integr. Comp. Physiol. *286*, R967-74.
212. Assali, D.R., Sidikpramana, M., Villa, A.P., Falkenstein, J., and Steele, A.D. (2021). Type 1 dopamine receptor (D1R)-independent circadian food anticipatory activity in mice. PLoS ONE *16*, e0242897.
213. Pack, A.I., Galante, R.J., Maislin, G., Cater, J., Metaxas, D., Lu, S., Zhang, L., Von Smith, R., Kay, T., Lian, J., *et al.* (2007). Novel method for high-throughput phenotyping of sleep in mice. Physiol. Genomics *28*, 232–238.

214. Hutchison, A.L., Maienschein-Cline, M., Chiang, A.H., Tabei, S.M.A., Gudjonson, H., Bahroos, N., Allada, R., and Dinner, A.R. (2015). Improved statistical methods enable greater sensitivity in rhythm detection for genome-wide data. PLoS Comput. Biol. *11*, e1004094.

215. Moore, R.Y., Speh, J.C., and Leak, R.K. (2002). Suprachiasmatic nucleus organization. Cell Tissue Res. *309*, 89–98.

216. Santoso, P., Nakata, M., Ueta, Y., and Yada, T. (2018). Suprachiasmatic vasopressin to paraventricular oxytocin neurocircuit in the hypothalamus relays light reception to inhibit feeding behavior. Am. J. Physiol. Endocrinol. Metab. *315*, E478–E488.

217. Porcu, A., Booreddy, S., Welsh, D.K., and Dulcis, D. (2020). Photoperiod-Induced Neurotransmitter Switching in the Circadian Pacemaker Regulates Hypothalamic Dopamine Expression. BioRxiv.

218. Shan, Y., Abel, J.H., Li, Y., Izumo, M., Cox, K.H., Jeong, B., Yoo, S.-H., Olson, D.P., Doyle, F.J., and Takahashi, J.S. (2020). Dual-Color Single-Cell Imaging of the Suprachiasmatic Nucleus Reveals a Circadian Role in Network Synchrony. Neuron *108*, 164-179.e7.